

Augmenting a Microbial Selective Plugging Technique with Polymer  
Flooding to Increase the Efficiency of Oil Recovery  
-A Search for Synergy

Final Report

Project Start Date:  
1 June 1999

Project End Date:  
31 May 2002

By  
Lewis R. Brown  
Charles U. Pittman, Jr.  
F. Leo Lynch  
A. Alex Vadie  
W. Todd French

June 2002

DE-AC26-99BC15210

Prepared by  
Mississippi State University  
P.O. Drawer GY  
Mississippi State, Mississippi 39762

## **DISCLAIMER**

This report was prepared as an account of work sponsored by an agency of the United States Government. Neither the United States Government nor any agency thereof, nor any of their employees, make any warrant, expressed or implied, or assumes any legal liability or responsibility disclosed, or represents that its use would not infringe privately owned rights. Reference herein to any specific commercial product, process, or service by trade name, trademark, manufacturer, or otherwise does not necessarily constitute or imply its endorsement, recommendation, or favoring by the United States Government or any agency thereof. The views and opinions of authors expressed herein do not necessarily state or reflect those of the United States Government.

## ABSTRACT

Nine polymers [two Cr<sup>3+</sup> gelling partially hydrolyzed poly(acrylamides), four viscosity enhancing 25% hydrolyzed poly(acrylamides) of high molecular weight, one xanthan polymer, one biologically-produced gelling polymer of proprietary structure, and a special polymer of moderate molecular weight designed to have a high critical extension viscosity] were characterized (molecular weight, viscosities in water and brine solutions, intrinsic viscosities) and they were shown to be noninhibitory to a variety of oil-degrading microorganisms. Furthermore, they would not serve as a carbon and energy source for these same microorganisms.

Polymer flooding was shown to increase aerial sweep efficiency in crushed Berea sandstone/clay/oil sandpacks using simulated injection water containing <sup>56</sup>Mn as the radioactive tracer. Phosphate and nitrate additions also altered sweep pathways by stimulating microbial growth which facilitated local plugging.

Studies using Berea sandstone cores demonstrated that high molecular weight 25% hydrolyzed poly(acrylamides) adsorbed on the internal surfaces until an equilibrium layer had formed and further polymer traversed the cores without further adsorption. Shear degradation of these polymers occurred during flow through the cores according to viscosity studies.

No evidence was obtained for polymer flooding/MEOR synergy to produce more oil recovery from live cores obtained from North Blowhorn Creek Oil Field. While polymer flooding slows the flow rate through cores and redistributes water flow in cores, its effect is short lived. As soon as the polymer pulse passes through the core the flow rate again increases. The period required for effective MEOR is much longer. Thus, microbial growth and its modification of sweep efficiency require a long time frame and this does not match that of polymer flood pulses. Only continuous polymer flooding could match up these time frames but this would require greater polymer consumption. Long pulses or continuous polymer floods would sharply increase costs. Furthermore, evidence of polymer adsorption within cores suggests that adsorption will seriously deplete the polymer's solution concentration as the distance from the wellbore increases. Shear degradation of the polymer may also reduce its effectiveness.

Magnetic resonance imaging of cores was used successfully to determine the oil saturation level in cores and the special distribution of oil and water inside the cores using a combination of inversion recovery ( $T_1$ ) relaxation time distribution experiments and  $T_2$  profiles. Experiments were conducted at pixel resolution sizes of  $0.47 \text{ mm}^2$ . Difficulties included broad line widths and highly variable proton relaxation times which were dependent on the core's rock type and the fact both water and oil give  $^1\text{H}$  adsorption.  $\text{D}_2\text{O}$  experiments were employed to see oil in the absence of  $\text{H}_2\text{O}$ .

Investigations using electron microscopy revealed that the indigenous microflora in North Blowhorn Creek Oil Field produce considerable quantities of polymer. In fact, this biopolymer may be the major physical cause for flow redistribution. Further, it was found that the treatment of samples for electron microscopic examinations significantly influenced the images obtained. In some cases the treatment resulted in images of polymer appearing as nannobacteria. The results demonstrated the need to prepare specimens in at least two different ways in order to obtain an accurate assessment of the microbial role in MEOR.

From this study, it was concluded that polymer flooding and MEOR are not synergistic, particularly from an economic standpoint. Evidence was obtained that microbial permeability profile modification could be made more effective by increasing the *in situ* production of polymer by the indigenous microflora.

## TABLE OF CONTENTS

ABSTRACT .....	v
LIST OF TABLES .....	vii
LIST OF FIGURES .....	viii
INTRODUCTION.....	1
<u>Objective</u> .....	1
EXECUTIVE SUMMARY .....	2
EXPERIMENTAL .....	5
RESULTS AND DISCUSSION.....	7
Task 1. Select, Characterize, and Test Various Polymers for Their Impact on the Microflora Indigenous to Petroleum Reservoirs in Terms of Their Inhibitory Capabilities and Their Biodegradability. ....	7
<u>Chemical Characterization</u> .....	7
<u>Microbiological Evaluation of Polymers</u> .....	11
<u>Test for Inhibitory Properties of Polymers</u> .....	12
<u>Tests for the Ability of Polymers to Support Microbial Growth</u> .....	13
Task 2. Determine the Ability of Selected Polymers to Increase the Aerial Extent (Aerial Sweep Efficiency) of Stratal Material Colonized by Microorganisms in Sandpacks.....	14
<u>Description of Sandpacks</u> .....	14
<u>Results of Sandpack Experiments</u> .....	16
Task 3. Determine the Ability of Selected Polymer Flooding Protocols in Combination With Microbial Selective Plugging Techniques to Increase Oil Recovery From Berea Sandstone Core Plugs Prepared to Mimic a Depleted Oil Sand.....	20
<u>Studies of Alcoflood 1285 (Mol wt~20,000,000) Water Solutions in Berea         Cores</u> .....	20
<u>Core Flood Experiments</u> .....	22
<u>Initial Magnetic Resonance Imaging Studies Using Berea         Sandstone Cores</u> .....	25
<u>Further Nuclear Magnetic Resonance Imaging Analysis of Berea         Sandstone Cores and North Blowhorn Creek Cores</u> .....	31
<u>Results of NMR Imaging Experiments</u> .....	31

Task 4. Determine the Ability of Microbial Selective Plugging Technique in Combination With Selected Polymer Flooding Protocols to Increase Oil Recovery From Live Cores Obtained From Newly Drilled Wells.....	40
<u>Coreflood Experiments Using Live Cores</u> .....	40
<u>Investigation of the Polymer (NaAMB)</u> .....	45
<u>Extensional Viscosity Studies</u> .....	47
<u>Role of Extensional Viscosity in Polymer Flooding for Mobility Control</u> .....	49
<u>Experiments on the Polymer NaAMB</u> .....	56
<u>Studies Using the Electron Microscope</u> .....	62
Task 5. Prepare a Cost/Benefit Evaluation of Adding a Polymer- Flooding Procedure to a Microbial Enhanced Oil Recovery Process Using a Selective Plugging Technique.....	74
<u>The Economic Aspects of MEOR and Polymer-MEOR</u> .....	74
CONCLUSIONS.....	79
REFERENCES.....	81
ACKNOWLEDGEMENTS.....	83

## LIST OF TABLES

Table I:	Viscosities of Brine and Polymer Solutions and Viscosities of Polymer Solutions After Pumping Through a Berea Core.....	21
Table II:	The Relative Amount of Fluids in the Samples .....	39
Table III:	Viscosity Measurements on NaAMB (Mol wt $1.25 \cdot 10^6$ ) Determined at 30.3°C in Standard Injection Brine Solutions.....	46
Table IV:	Flow Rates and Pressure Drops over Core A During Injection Water/Water NaAMB/Injection Waterflooding.....	47
Table V:	Viscosity Measurements on RH-1 (Mol wt $1.25 \cdot 10^6$ ) Determined at 30.3 °C in Standard Injection Brine Solutions.....	48
Table VI:	Comparison of MEOR Methods.....	77

## LIST OF FIGURES

Figure 1.	Photograph of a completely assembled sandpack.....	15
Figure 2.	Schematic of sandpack. ....	15
Figure 3.	Photograph of the setup for water-flooding the sandpicks. ....	16
Figure 4.	Test using Alcoflood 1285 showing only a slight impact of polymer flooding on the pathway of injection water through the sandpack. ....	17
Figure 5.	Test using Alcoflood 1285 showing diversion of the pathway of injection water through the sandpack caused by the injection of polymer. ....	17
Figure 6.	Test using Alcoflood 1285 showing impact of polymer flooding followed by nutrient additions. ....	18
Figure 7.	Test using crosslinking polymer Alcoflood 254S showing impact of polymer flooding followed by nutrient additions. ....	19
Figure 8.	Test using Flocon 4800 showing impact of polymer flooding followed by nutrient additions. ....	19
Figure 9.	Diagrammatic sketch of the core testing assembly. ....	23
Figure 10.	Flow rate for Berea sandstone core when nutrients are added before polymer. ....	24
Figure 11.	Flow rate for Berea sandstone core when polymer is added before nutrients.....	24
Figure 12.	NMR spectrum of oil-depleted Berea Core 1 containing residual North Blowhorn Creek Oil (API gravity 28-35.2). ....	27
Figure 13.	1-D profile of oil-depleted Berea Core 1 containing residual North Blowhorn Creek Oil (API gravity 28-35.2). The pixel size is 0.47 mm. ....	27
Figure 14.	1-D profile of oil-depleted Berea Core 2 containing residual North Blowhorn Creek Oil (API gravity 28-35.2) after an aqueous polymer flooding treatment with Alcoflood 1285. The pixel size is 0.47 mm. ....	28
Figure 15.	2-D image of oil-depleted Berea Core 1 containing residual North Blowhorn Creek Oil (API gravity 28-35.2). ....	28
Figure 16.	2-D image of oil-depleted Berea Core 2 containing residual North Blowhorn Creek Oil (API gravity 28-35.2) after an aqueous polymer flooding treatment with Alcoflood 1285.....	29
Figure 17.	Inversion-recovery $T_1$ data for the core samples and oil. ....	29
Figure 18.	$T_1$ distributions for the core samples and oil. ....	30
Figure 19.	NMR images of four cores. ....	32
Figure 20.	One-dimensional $T_2$ Profile: apparent oil volume per sample length. ....	34
Figure 21.	Core 1 and Core 4 relaxation distribution figures. ....	34
Figure 22.	The effects of microbial activity on flow rates for D4 Cut #8 Core 1 over time. This was a depleted oil core from the North Blowhorn Creek Oil Field that was treated with $KNO_3$ and $Na_2HPO_4$ in the injection water. ....	35
Figure 23.	The effects of Alcoflood 1285 treatment on flow rates over time. D4 cut #8 Sleeve 2 was used. ....	35
Figure 24.	Sleeve One: Two-dimensional profiles. ....	36

Figure 25.	Sleeve Two: Two-dimensional profiles.....	37
Figure 26.	One-dimensional profiles. ....	38
Figure 27.	Inversion recovery: $T_1$ relaxation distributions. ....	38
Figure 28.	The effects of microbial activity on the flow rate using D4 Cut #15 Core 1.....	41
Figure 29.	The effects of polymer flooding (Alcoflood 1285) on the flow rate using D4 Cut #15 Core 2. ....	41
Figure 30.	The effects of microbial activity on the flow rate of injection water through core D4 Cut #10 Core 1 over time.....	42
Figure 31.	The effects of Alcoflood 1285 treatment and microbial activity on the flow rate of injection water through core D4 Cut #10 Core 2 over time. ....	43
Figure 32.	The effects of Flocon 4800 treatment and microbial activity on the flow rate of injection water through core D4 Cut #9 Core 1 over time. ....	44
Figure 33.	The effects of microbial activity on the flow rate of injection water through core D4 Cut #9 Core 2 over time.....	44
Figure 34.	Synthetic equation. ....	46
Figure 35.	Onset of extensional viscosity. ....	51
Figure 36.	Determining the flow rate at which the extensional viscosity begins to contribute. ....	53
Figure 37.	Specific viscosity vs. concentration for polymer Alcoflood 1285 in standard brine solution.....	55
Figure 38.	Specific viscosity vs. concentration of the polymer NaAMB in standard brine solution. ....	56
Figure 39.	NaAMB (5 ppm) without prepumping. ....	57
Figure 40.	NaAMB (5 ppm) after prepumping of 10 core volumes of polymer solution through core. ....	57
Figure 41.	NaAMB (2.5 ppm) after prepumping. ....	58
Figure 42.	NaAMB (1.0 ppm) after prepumping. ....	58
Figure 43.	NaAMB (0.5 ppm) after prepumping. ....	59
Figure 44.	NaAMB (5 ppm) after prepumping after all the above experiments had been done on the same core. ....	59
Figure 45.	NaAMB (50 ppm) after prepumping Alcoflood 1285 polymer.....	60
Figure 46.	Pure brine solution after prepumping. ....	60
Figure 47.	Alcoflood 1285 (15 ppm) after prepumping.....	61
Figure 48.	Different concentrations of Alcoflood 1285 polymer solutions. ....	61
Figure 49.	EPS biofilm slime covers both rock matrix and the deformed cylindrical bacteria in air-dried sample.....	63
Figure 50.	EPS biofilm slime (S) occurs as a more or less continuous coat over both rock and distorted bacteria (B). Sample fixed in 10% glutaraldehyde. ....	63
Figure 51.	Abundant undeformed bacteria devoid of EPS slime. Ethanol and HMDS dehydration sample. ....	64
Figure 52.	Well-preserved bacterial body covered with tattered remnant-strings of EPS. Glutaraldehyde fixation, ethanol and acetone dehydration, and critical point dried sample.....	65
Figure 53.	Grain-coating morphologies of EPS biofilm. ....	66
Figure 54.	EPS biofilm completely covering bacterial bodies and mineral grains. ....	66

Figure 55.	EPS slime meniscus partially occluding porosity. ....	67
Figure 56.	Sandstone porosity partially filled with EPS biofilm. ....	68
Figure 57.	Large (> 1 $\mu\text{m}$ ) and small (< 1 $\mu\text{m}$ ) ovoid and spherical bacteria and bacterial textures grown in less than one wk. ....	69
Figure 58.	Bacterium surrounded by thin “halo” of EPS.....	69
Figure 59.	Thick and clotted EPS biofilm developed in two wk growth.....	70
Figure 60.	EPS slime (outlined) completely filling porosity between sandstone grains (G). ....	70
Figure 61.	Purported nanobacteria drape between mineral crystal grains in weathered rock from Italy.....	71
Figure 62.	Nanobacteria on mineral surfaces in the Allende Meteorite, which fell to Earth in 1968.....	72
Figure 63.	Chain and filament-like morphology of EPS slime produced by dehydration preservation resembles purported nanobacteria.....	73
Figure 64.	High-magnification image of “nanobacterial textures” produced by dehydration of EPS biofilm. ....	73

## INTRODUCTION

In the U. S., the reliance on foreign oil imports is of increasing concern since it accounts for about 60% of the total demand. The economically recoverable oil reserves in this country are 27 billion barrels, which amounts to only about a 50-month supply. There are however, approximately 348 billion barrels of known reserves in this country that cannot be produced economically with presently employed technology. When primary production, *i.e.* production using the reservoirs own energy, becomes uneconomical, secondary and tertiary methods must be employed. Included among these methods are waterflooding, polymer flooding, CO<sub>2</sub> or N<sub>2</sub> flooding, and microbial enhanced oil recovery (MEOR). Currently, waterflooding is responsible for over 50% of all oil recoveries in the world oil fields. When waterflooding becomes uneconomical, 1/2 to 2/3 of the original oil in place is still left in the ground.

Work conducted under a recently completed Department of Energy contract demonstrated the effectiveness of a microbial permeability profile modification (MPPM) technology in recovering more oil from a nearly depleted oil reservoir (Brown, Vadie, and Stephens, 2002). This microbial enhanced oil recovery method is less costly than other secondary or tertiary recovery methods in terms of cost per barrel of incremental oil recovered other than waterflooding alone. In essence, this MPPM technology diverts injection water from the larger channels in the reservoir to previously unswept areas resulting in an increased efficiency of the waterflood operation.

Another secondary oil recovery method, waterflooding with polymers, accomplishes the same result as the MPPM but works much faster although it is considerably more expensive and its effectiveness is short-lived. MPPM, on the other hand, is less expensive and longer lasting but takes more time to become effective. The question arose as to whether coupling polymer flooding with MPPM would result in a cost-effective synergy. This project addresses this question.

### Objective

The objective of this project is to determine if the effectiveness of a microbial permeability profile modification technique can be improved through polymer flooding.

## EXECUTIVE SUMMARY

The objective of this project was to determine if the effectiveness of a microbial permeability profile modification technique could be improved through polymer flooding.

- Task 1. Select, Characterize, and Test Various Polymers for Their Impact on the Microflora Indigenous to Petroleum Reservoirs in Terms of Their Inhibitory Capabilities and Their Biodegradability.
- Task 2. Determine the Ability of Selected Polymers to Increase the Aerial Extent (Aerial Sweep Efficiency) of Stratal Material Colonized by Microorganisms in Sandpacks.
- Task 3. Determine the Ability of Selected Polymer Flooding Protocols in Combination With Microbial Selective Plugging Techniques to Increase Oil Recovery From Berea Sandstone Core Plugs Prepared to Mimic a Depleted Oil Sand.
- Task 4. Determine the Ability of Microbial Selective Plugging Technique in Combination With Selected Polymer Flooding Protocols to Increase Oil Recovery From Live Cores Obtained From Newly Drilled Wells.
- Task 5. Prepare a Cost/Benefit Evaluation of Adding a Polymer-Flooding Procedure to a Microbial Enhanced Oil Recovery Process Using a Selective Plugging Technique.

Nine polymers [two Cr<sup>3+</sup> gelling partially hydrolyzed poly(acrylamides), four viscosity enhancing 25% hydrolyzed poly(acrylamides) of high molecular weight, one xanthan polymer, one biologically-produced gelling polymer of proprietary structure, and a special polymer of moderate molecular weight designed to have a high critical extension viscosity] were characterized (molecular weight, viscosities in water and brine solutions, intrinsic viscosities) and they were shown to be noninhibitory to a variety of oil-degrading microorganisms. Furthermore, they would not serve as a carbon and energy source for these same microorganisms.

Polymer flooding was shown to increase aerial sweep efficiency in crushed Berea sandstone/clay/oil sandpacks using simulated injection water containing <sup>56</sup>Mn as the radioactive tracer. Phosphate and nitrate additions also altered sweep pathways by stimulating microbial growth which facilitated local plugging.

Studies using Berea sandstone cores demonstrated that high molecular weight 25% hydrolyzed poly(acrylamides) adsorbed on the internal surfaces until an equilibrium layer had formed and further polymer traversed the cores without further adsorption. Shear degradation of these polymers occurred during flow through the cores according to viscosity studies.

No evidence was obtained for polymer flooding/MEOR synergy to produce more oil recovery from live cores obtained from North Blowhorn Creek Oil Field. While polymer flooding slows the flow rate through cores and redistributes water flow in cores, its effect is short lived. As soon as the polymer pulse passes through the core the flow rate again increases. The period required for effective MEOR is much longer. Thus, microbial growth and its modification of sweep efficiency require a long time frame and this does not match that of polymer flood pulses. Only continuous polymer flooding could match up these time frames but this would require greater polymer consumption. Long pulses or continuous polymer floods would sharply increase costs. Furthermore, evidence of polymer adsorption within cores suggests that adsorption will seriously deplete the polymer's solution concentration as the distance from the wellbore increases. Shear degradation of the polymer may also reduce its effectiveness.

Magnetic resonance imaging of cores was used successfully to determine the oil saturation level in cores and the special distribution of oil and water inside the cores using a combination of inversion recovery ( $T_1$ ) relaxation time distribution experiments and  $T_2$  profiles. Experiments were conducted at pixel resolution sizes of  $0.47 \text{ mm}^2$ . Difficulties included broad line widths and highly variable proton relaxation times which were dependent on the core's rock type and the fact both water and oil give  $^1\text{H}$  adsorption.  $\text{D}_2\text{O}$  experiments were employed to see oil in the absence of  $\text{H}_2\text{O}$ .

Investigations using electron microscopy revealed that the indigenous microflora in North Blowhorn Creek Oil Field produce considerable quantities of polymer. In fact, this biopolymer may be the major physical cause for flow redistribution. Further, it was found that the treatment of samples for electron microscopic examinations significantly influenced the images obtained. In some cases the treatment resulted in images of polymer appearing as nannobacteria. The results demonstrated the need to prepare specimens in at least two different ways in order to obtain an accurate assessment of the microbial role in MEOR.

From this study, it was concluded that polymer flooding and MEOR are not synergistic, particularly from an economic standpoint. Evidence was obtained that microbial permeability profile modification could be made more effective by increasing the *in situ* production of polymer by the indigenous microflora.

## EXPERIMENTAL

In order to facilitate understanding of the results of this project, the detailed experimental procedures utilized are included in the RESULTS AND DISCUSSION section. Below is a brief synopsis of those procedures.

Task 1. Select, Characterize, and Test Various Polymers for Their Impact on the Microflora Indigenous to Petroleum Reservoirs in Terms of Their Inhibitory Capabilities and Their Biodegradability.

Classical chemical procedures were employed to characterize the polymers. Conventional growth studies were used to determine the ability of polymers to support growth. The disc assay procedure was used to determine the inhibitory properties of the polymer.

Task 2. Determine the Ability of Selected Polymers to Increase the Aerial Extent (Aerial Sweep Efficiency) of Stratal Material Colonized by Microorganisms in Sandpacks.

Plexiglass sandpacks 6" x 6" x 0.25" were constructed and employed in this task. <sup>56</sup>Mn was employed to trace the pathway of flow of injection water through the packs.

Task 3. Determine the Ability of Selected Polymer Flooding Protocols in Combination With Microbial Selective Plugging Techniques to Increase Oil Recovery From Berea Sandstone Core Plugs Prepared to Mimic a Depleted Oil Sand.

Berea sandstone cores 3" long by 1.5" in diameter were employed in this task. Some of the cores were subjected to analysis using magnetic resonance imaging.

Task 4. Determine the Ability of Microbial Selective Plugging Technique in Combination With Selected Polymer Flooding Protocols to Increase Oil Recovery From Live Cores Obtained From Newly Drilled Wells.

Cores from the North Blowhorn Creek Oil Field were employed in this task. Electron microscopic studies were also performed.

Task 5. Prepare a Cost/Benefit Evaluation of Adding a Polymer-Flooding Procedure to a Microbial Enhanced Oil Recovery Process Using a Selective Plugging Technique.

Data for the evaluation in this task were obtained from work performed in this study, previous studies, and the literature.

## RESULTS AND DISCUSSION

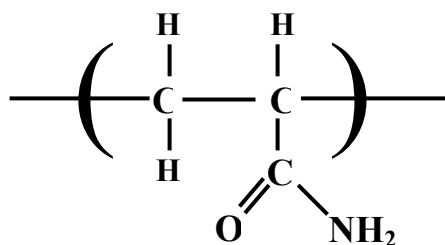
### Task 1. Select, Characterize, and Test Various Polymers for Their Impact on the Microflora Indigenous to Petroleum Reservoirs in Terms of Their Inhibitory Capabilities and Their Biodegradability.

#### Chemical Characterization

Seven different polymers have been characterized as follows:

Polymers which are soluble (linear) can serve as either gel-forming systems or related soluble polymers can exert mobility control by viscosity enhancement. The first two systems described below are gelling systems. When dissolved in water with  $\text{Cr}^{+3}$  present, slow gellation occurs after the system has been pumped into the oil-bearing stratum. This occurs slowly. The time delay allows migration of the polymer out into the oil-bearing rock prior to gellation.

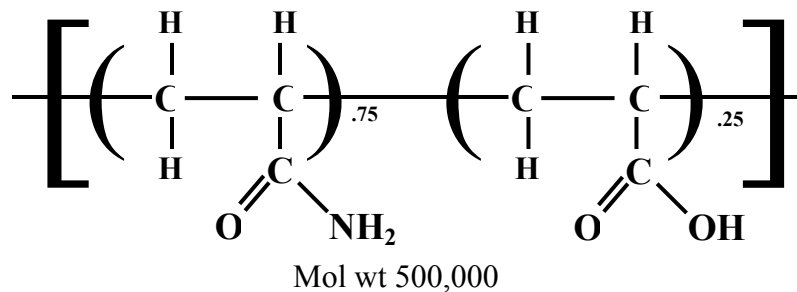
1. Alcoflood 251S This polymer is a poly(acrylamide). It is used with crosslinking agents, such as  $\text{Cr}^{+3}$  to form a gel down hole, but the polymer itself, is not crosslinked or gelled.



Mol wt above  $5 \times 10^6$

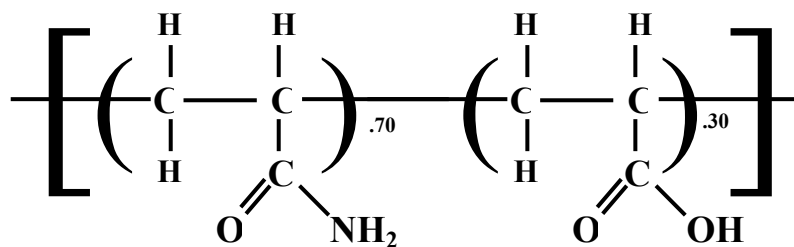
Accurate mol wt and mol wt distribution values could not be obtained because its  $\text{dn}/\text{dc}$  value was 0.1869 at  $25^\circ\text{C}$  using 632.8 nm light ( $\text{dn}/\text{dc}$  is the dependence of refractive index on polymer concentration). This value of  $\text{dn}/\text{dc}$  makes it very difficult for a refractive index detector to give strong signals. Strong signals are required for high mol wt polymers which must be employed in dilute concentrations in order to get gel permeation chromatography (gpc) measurements. Dialysis experiments confirmed the as-received polymer was free of any salts.

2. KUSP1 is a biologically produced gelling polymer obtained from Kansas State University.
3. Alcoflood 254S This is a copolymer of acrylamide (75%) and acrylic acid (25%). It produces strong durable, temperature-tolerant cross-linked gels from low viscosity solutions when treated with  $\text{Cr}^{+3}$ . It can be used to treat production wells with high fluid levels and high water/oil ratios, or for treating severe channeling problems and fractures.



<u>Gel-times</u>	Conc.	Gel Time at 80 <sup>0</sup> F
	200 ppm	23.0 h {in API Seawater}
	600 ppm	12.0 h {in API Seawater}
	359 ppm	20.0 h {60 <sup>0</sup> F API Fresh water}
	758 ppm	3.8 h {60 <sup>0</sup> F API Fresh water }
	1107 ppm	1.9 h {60 <sup>0</sup> F API Fresh water }

- 4-7. Alcofloods 1135, 1235, 1275A, and 1285 These 4 polymers are all acrylamide (70%), acrylic acid (30%) copolymers of random structure. They are anionic in water since the acrylic acid carboxyl functions are more acidic than water.



### Some Characterization Data

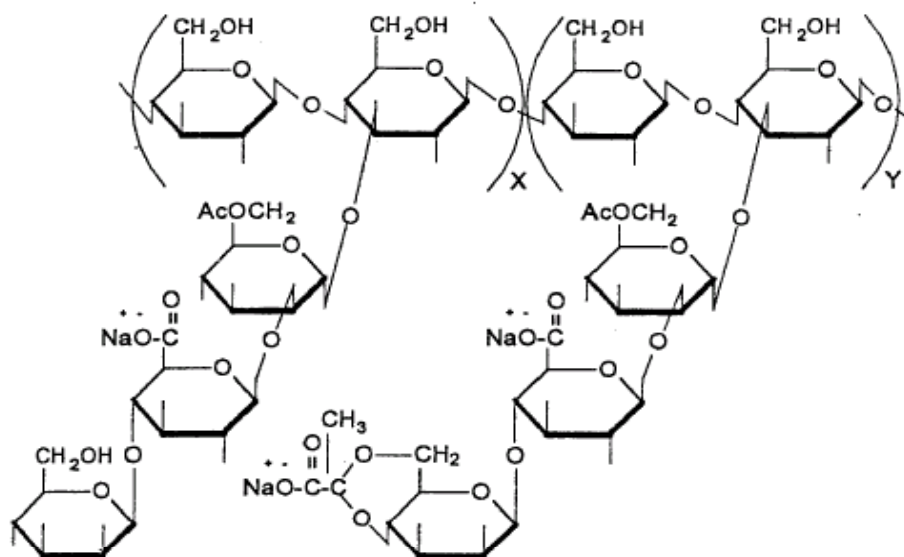
<u>Polymer Solution</u>	<u>Mol Wt</u>	<u>Ionic Character</u>	<u>pH of 1% by wt soln.</u>
1135	13,000,000	anionic	6.8-7.8
1235	~9,000,000-14,000,000	anionic	6.8-7.8
1275A	18,000,000-24,000,000	anionic	6.8-7.8
1285	~20,000,000	anionic	6.8-7.8

These polymers were free of added salt according to dialysis experiments.

### Viscosity in Water at 100<sup>0</sup> F (38<sup>0</sup> C)

Polymer (conc.) <u>(ppm)</u>	in API Fresh Water <u>(cps)</u>	in API Sea Water <u>(cps)</u>	Intrinsic Viscosity <u>(dl/g)</u>
1135 (500)	4	2.0	
(1000)	14	5.0	
1235 (500)	4	2.0	12.0
(1000)	12	3.0	
1275A (500)	14	7.0	23-26.5
(1000)	35	14.0	
1285 (500)	11	2.5	24.0
(1000)	31	5.0	

## 8. Xanthan Polymer (Flocon 4800)



**Structure of Flocon 4800**

Mol wt distribution 1,000,000 - 2,000,000

This product contains 3-5% polymer in water (as received) and >2000 ppm formaldehyde as a preservative for storage. Liquid density 0.95-1.00 g/ml.

The working viscosity is 5-40 cps. The viscosity does not change over the pH range of 5 to 12. This is not a randomly coiling polymer and a big advantage is that its solution viscosity does not vary strongly as the ionic strength varies (*e.g.*, use in brines). For example, when Flocon 4800 is used in the 150-1,000 ppm conc. range, the viscosity of its aqueous brine solutions (containing from 500 to 70,000 ppm of salts) remains in the range of 5 to 35 cps. This rod-like polymer can maintain relatively unchanged solution viscosities as the brine concentration changes. Data are shown on page 6.

Flocon 4800 solutions have proven to be pseudo-plastic. Thus, as the shear rate increases (during stirring), the viscosity decreases. This is because molecules align during shear in the direction of flow.

A proprietary polymer of microbial origin and unknown structure, KUSP1 was obtained from Kansas State University. It is described as a gelling polymer, acting by coordinating transition metal ions present in the brine during waterflooding.

<u>Conc of Polymer</u> (ppm)	<u>Shear Rate</u> (sec <sup>-1</sup> )	<u>Brookfield Viscosity</u> (cps)
1000	7.3	40
1000	50.0	14
500	9.0	9

### **Viscosity vs CaCl<sub>2</sub> Conc in Water**

<u>Flocon Conc.</u> (ppm)	<u>Viscosity</u> (cps)	<u>CaCl<sub>2</sub> Conc.</u> (ppm)
500	14.0	0
	12.5	10
	9.5	100
	8.5	1000
	9.0	10,000
	10.5	100,000

### **Microbiological Evaluation of Polymers**

Tests were conducted to determine if a polymer was (1) inhibitory to microbial cultures obtained from petroleum reservoirs or (2) would serve as a carbon and energy source for these cultures. Five cultures were selected for the testing. The cultures and some of their characteristics are as follows:

Culture #1 is a gram positive bacillus, non-acid fast, non-sporeforming, obligate anaerobe isolated from the Mabee oil field situated in Andrews Co., Tx.

Culture #3 is a gram negative bacillus, non-acid fast, non-sporeforming, microaerophile isolated from the Mabee oil field situated in Andrews Co., Tx.

Culture #10 is a gram positive coccobacillus, acid fast, obligate anaerobe isolated from the Kern river Oil field situated in Kern Co., CA.

Culture #16 is a gram positive coccobacillus, acid fast, microaerophile isolated from the Kern River Oil field situated in Kern Co., CA.

Culture #17 is a gram positive bacillus, non-acid fast, facultative anaerobe isolated from the Kern River oil field situated in Kern Co., CA.

All media employed were prepared using simulated production water in place of distilled water, and was composed of 10.9 g CaCl<sub>2</sub>, 2.71 g MgCl<sub>2</sub>, 4.57g, BaCl<sub>2</sub>, 1.84g Na<sub>2</sub>SO<sub>4</sub>, and 147.8g NaCl in 50 L of distilled water.

In preparing media, this simulated production water was supplemented with 1g NaNO<sub>3</sub> and 0.26g NaH<sub>2</sub>PO<sub>4</sub> per L and hereinafter will be referred to as PWB (production water broth).

### **Test for Inhibitory Properties of Polymers**

The protocol to determine if a polymer is inhibitory to cultures obtained from oil reservoirs was the disc assay procedure. Tests were conducted using both Bacto-Plate Count Agar (PCA) and Oil Agar (OA) prepared as follows. The crude oil employed was obtained from the North Blowhorn Creek Oil Field situated in Lamar Co., AL. PWB was saturated with oil by vigorously mixing for one h. Granulated agar (1.7%, w/v) was added to the oil-saturated PWB and dispensed in 18 ml amounts into 20 x 145 mm screw-capped test tubes. Crude oil (0.18 ml/tube) was added and the medium sterilized in the autoclave at 121C for 15 min. The PCA was prepared in 18 ml amounts in 20 x 145 mm screw-capped test tubes and sterilized as above.

A 10% suspension (w/v) of each polymer was prepared by adding 1.0 g of polymer to 9.0 ml of sterile distilled water. BBL<sup>®</sup> ½ inch paper discs were placed aseptically in the 10% polymer solution and allowed to remain for 24 h. The discs then were taken out of the suspension and allowed to air dry. Under anaerobic conditions, 0.2 ml of the test microbial culture was added to 18 ml of melted and cooled (45 C) OA and mixed. Approximately 3.5 ml of the inoculated agar was poured into 20, 35x10 mm plastic petri dishes. After the agar solidified, a polymer-saturated disc was placed on the surface of the agar. Duplicates were done for each polymer. Plates of inoculated PCA were prepared using cultures #3, 10, 16, and 17. Plates prepared as above but without polymer-saturated discs were employed as controls.

The petri plates were incubated in BBL<sup>®</sup> anaerobic chambers for 20 d at 30 C. After incubation, plates were examined for zones of inhibition around the discs indicating inhibition of the culture by the polymer.

The following eight polymers have been tested and shown not to be inhibitory to the microbial cultures –Alcoflood 251S, KUSP1, Alcoflood 254S, Alcoflood 1135, Alcoflood 1235, Alcoflood 1275A, Alcoflood 1285, and Flocon 4800.

In addition to the eight polymers cited above, Dr. Hester (University of Southern Mississippi) has supplied us with a polymer solution of a polymer (DOE/NPTO grant), which exhibits very large extensional viscosities relative to their shear-based viscosities.

Tests have shown that the polymer is not toxic to any of the aerobic or anaerobic organisms nor is it degraded by them.

### **Tests for the Ability of Polymers to Support Microbial Growth**

Tests of the ability of microbial cultures from oil reservoirs to grow on polymer and/or degrade the polymer are being conducted using three different media - (1) polymer in PWB, (2) polymer in PWB supplemented with 1% (v/v) oil, and (3) polymer in PWB supplemented with 1% (v/v) molasses were sterilized by autoclaving for 15 min at 121C. A 1.8% polymer suspension (w/v) was prepared by placing 1.8 g of polymer in 100 ml of distilled water. One ml of the 1.8% polymer suspension was added to 18 ml of each of the three media listed above to make a 0.1% polymer medium. Under anaerobic conditions, 10 µl of each of the five microbial cultures were added to two tubes of each of the three media. Controls were prepared with no cells added to medium plus polymer and with only media with no cells and no polymer. All of the tubes were allowed to incubate at 30C and monitored weekly for growth or alterations in the polymer.

Growth was observed in cultures containing molasses plus polymer (Alcoflood 1135, Alcoflood 1235, Alcoflood 1275A, Alcoflood 1285, and 254S) after three wks of incubation. One of the five cultures showed slight growth in the molasses plus polymer KUSP1. Also, after three wks, Culture #16 grew slightly in oil medium plus polymer (Alcoflood 1135, Alcoflood 1275A, Alcoflood 1285, and KUSP1). These results indicate the lack of inhibitory properties of the polymers. No growth was obtained in samples containing polymer as the sole source of carbon and energy even after 45 d and therefore their destruction by microorganisms present in the reservoir does not seem to be a problem. All of the above tests have been repeated and identical results obtained.

## **Task 2. Determine the Ability of Selected Polymers to Increase the Aerial Extent (Aerial Sweep Efficiency) of Stratal Material Colonized by Microorganisms in Sandpacks.**

### **Description of Sandpacks**

Each Plexiglas sandpack is 6" x 6" by 0.25" and has a total internal volume of 41.49 ml. The sandpacks are fitted with a No.17 hypodermic needle in each of two opposite corners to serve as a means of introducing liquids into the sandpacks and collecting the effluent. A 1" diameter plug was glued onto a 1 1/2" x 1 1/2" Plexiglas base plate to close the sandpack (secured using methylene chloride) following filling with formation materials.

Originally, the protocol for studies using sandpacks involved tracing the pathway of the flow of injection water through the sandpack using  $^{36}\text{Cl}$  as the tracer. After consultation with nuclear engineers at Mississippi State University, it was decided that the flow of injection water through the pack could be adequately achieved using  $^{56}\text{Mn}$ . This switch from  $^{36}\text{Cl}$  to  $^{56}\text{Mn}$  offered a number of advantages. In the first place, the half-life of the  $^{56}\text{Mn}$  is 2 h vs. 301,000 y for  $^{36}\text{Cl}$ , thus reducing problems associated with the collection and storage of spent injection water. Also, the amounts of  $^{56}\text{Mn}$  required for a given experiment can be generated on site, obviating the need to purchase and store  $^{36}\text{Cl}$ . Most importantly, however, since different gamma emitters, emit at different wavelengths, studies with multiple tracers is possible. For example, the use of  $^{51}\text{Cr}$  as a cross-linker for a polymer would enable us to track the movement and location of the polymer *per se* while following the flow of the injection water using soluble  $^{56}\text{Mn}$  ions.

Much difficulty was encountered in formulating the packing material in the sandpacks. The chosen composition of the packing material is 95 g crushed Berea sandstone, 5 g clay, 11 g oil-microorganism mixture, and 8 ml simulated injection water.

Figure 1 is a photograph of completed sandpack ready for use. Figure 2 is a diagrammatic sketch of the sandpack showing dimensions. Prior to use in an experiment, simulated injection water (hereinafter referred to as water) is allowed to flow through the sandpack to establish a flow path. The water is allowed to flow through the pack using only the pressure achieved by having the water reservoir situated three ft above the pack as illustrated in Figure 3.



Figure 1. Photograph of a completely assembled sandpack.

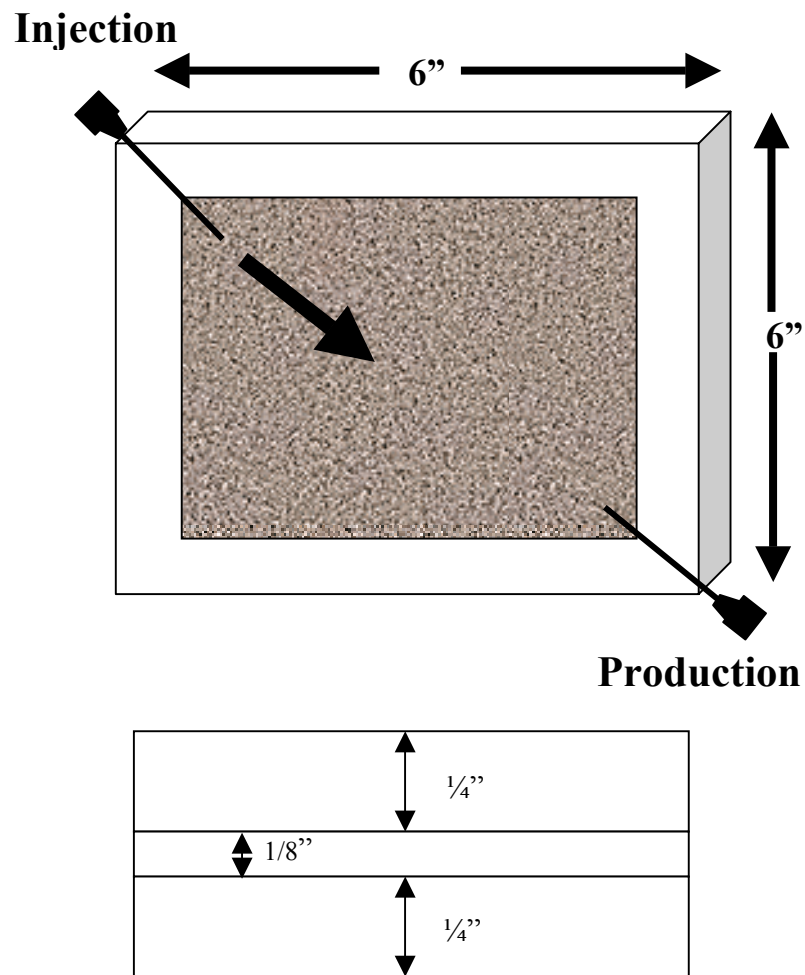


Figure 2. Schematic of sandpack.



**Figure 3. Photograph of the setup for waterflooding the sandpacks.**

### **Results of Sandpack Experiments**

The injection water employed to track the path of the water through the pack was prepared as follows. The following ingredients were dissolved separately in 2 L of distilled water: 10.9 g of  $\text{CaCl}_2$ , 2.71g of  $\text{MgCl}_2$ , 4.57g of  $\text{BaCl}_2$ , 1.84 g of  $\text{Na}_2\text{SO}_4$ , and 147.8 g of  $\text{NaCl}$ . Once dissolved, the solutions were mixed in a 50 L carboy. The volume of this solution was adjusted to 50 L using distilled water. The pH of the injection water was adjusted to 7.0 using a 10%  $\text{HCl}$  solution (v/v).

After the path of the water through the pack had been established, a polymer solution was injected and the path of the injection water again determined using the  $^{56}\text{Mn}$  solution described above. Representative data are shown in Figure 4, and as may be seen, the path of the injection water was altered to some degree by the injection of the polymer solution. In other experiments, the polymer solution drastically altered the flow path of

the injection water (see Figure 5). Polymer Alcoflood 1285 was employed in the above tests.

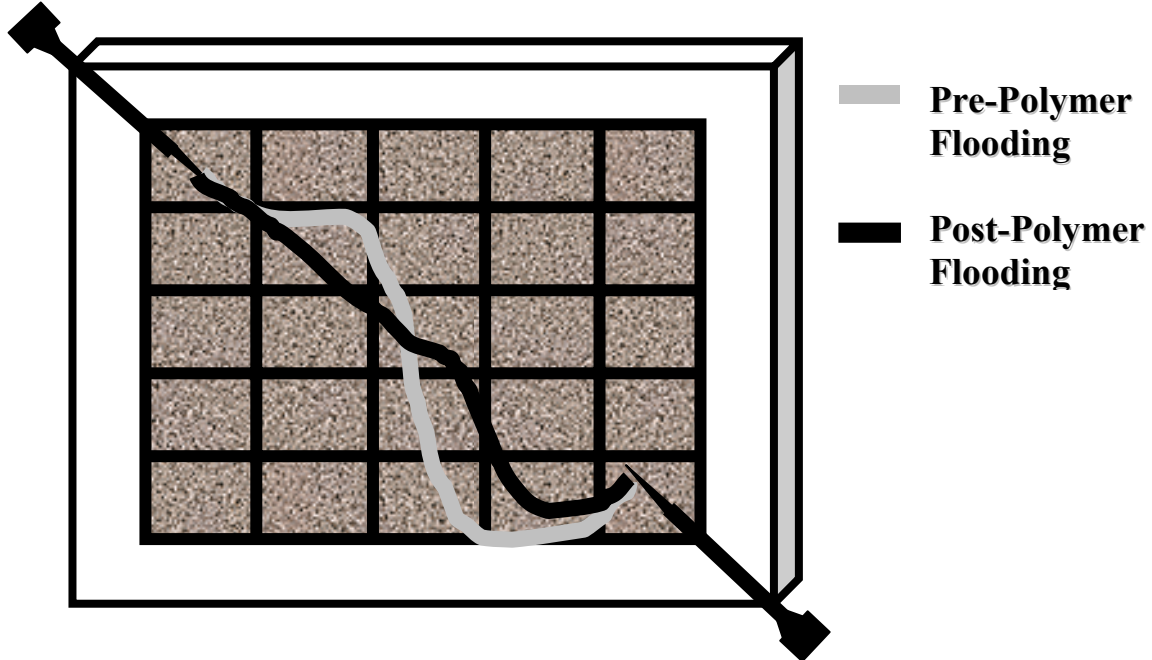


Figure 4. Test using Alcoflood 1285 showing only a slight impact of polymer flooding on the pathway of injection water through the sandpack.

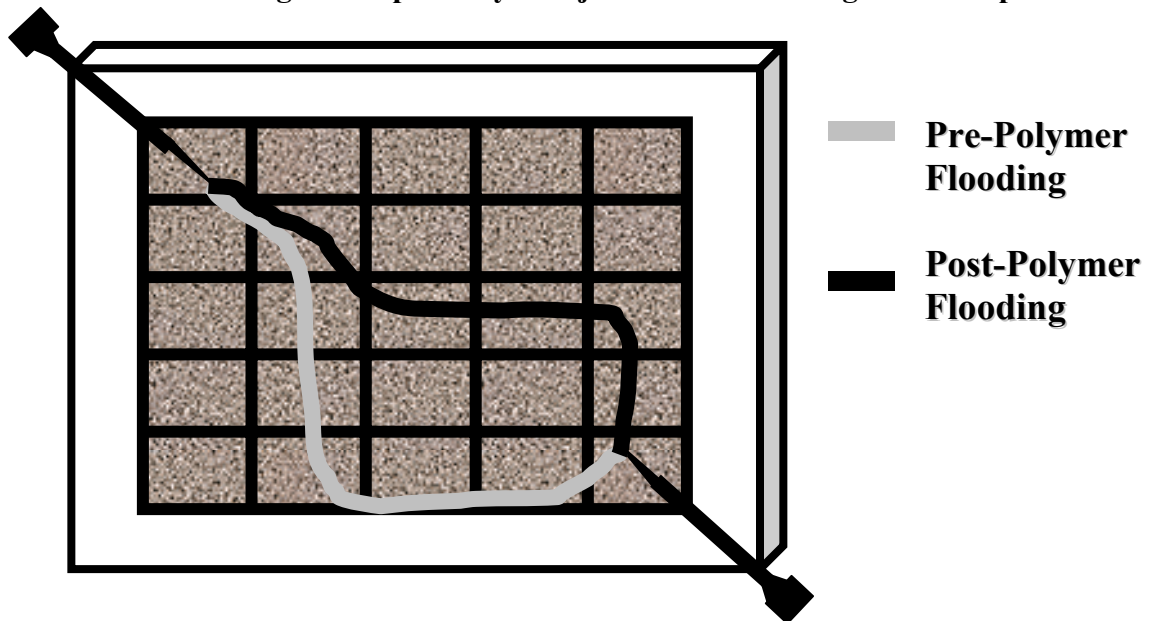


Figure 5. Test using Alcoflood 1285 showing diversion of the pathway of injection water through the sandpack caused by the injection of polymer.



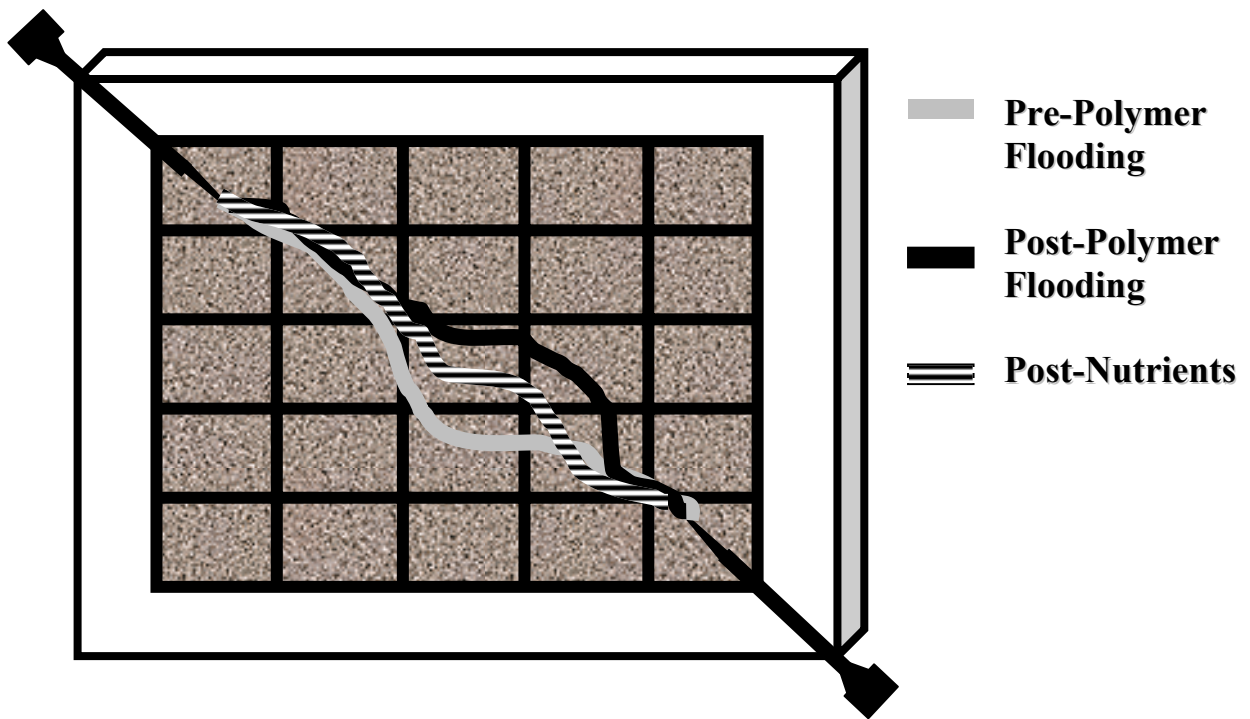


Figure 7. Test using crosslinking polymer Alcoflood 254S showing impact of polymer flooding followed by nutrient additions.

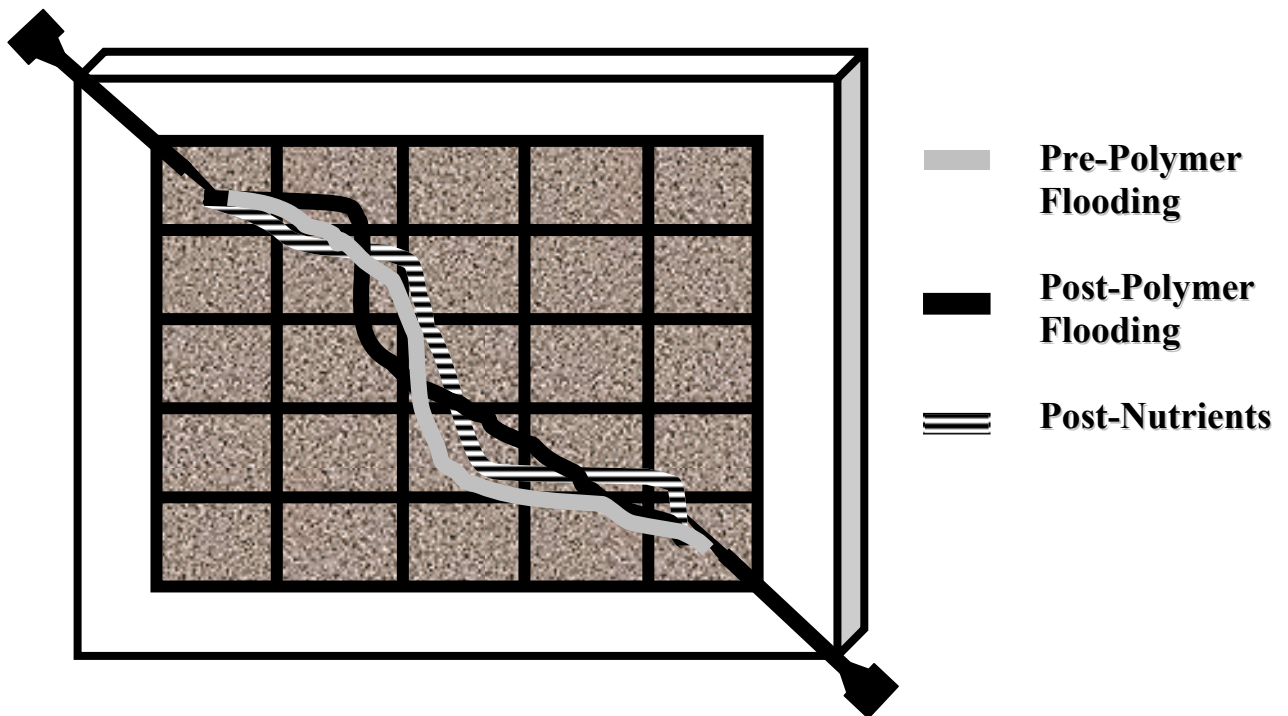


Figure 8. Test using Flocon 4800 showing impact of polymer flooding followed by nutrient additions.

### **Task 3. Determine the Ability of Selected Polymer Flooding Protocols in Combination With Microbial Selective Plugging Techniques to Increase Oil Recovery From Berea Sandstone Core Plugs Prepared to Mimic a Depleted Oil Sand.**

#### **Studies of Alcoflood 1285 (Mol wt~20,000,000) Water Solutions in Berea Cores.**

Alcoflood 1285 (an acrylamide polymer with 25% of the monomer units hydrolyzed to carboxyl salt groups) was used to assist oil recovery from oil depleted cores and evaluate its effect on MEOR. First, it was necessary to demonstrate if this polymer was (1) adsorbed by Berea cores or (2) if it undergoes shear degradation which lowers the molecular weight while passing through narrow pores in the core.

Viscosity monitoring was employed. Since Alcoflood is used in such a dilute solution (0.3mg to 2mg per L of water), it is impossible to use polymer recovery experiments after pumping solutions through cores to measure weight losses. Therefore, viscosity studies were required.

Standard brine solutions were made and their viscosities were measured. Then 0.75mg polymer/L of solution polymer concentrations were made. The polymer solution was taken up into an evacuated Berea core with an initial pore volume of about 17-20 ml. After sitting submerged for several h, the core was rigged for pumping the same polymer/water solution through it. Then several liters of polymer solution were pumped through the core at a constant rate. The rate was controlled by the pressure differential between the reservoir (head) pressure and the backpressure regulator at the outlet end of the system.

The viscosity of the brine solution was compared to that of the starting polymer/brine solution, the viscosity of the first 25 ml of polymer/brine solution to be pumped out of the core, and the viscosity of polymer/brine solutions after more extended amounts were pumped through the core. This same experiment was then repeated a second time at higher flow rates (higher shear conditions). These results are presented in Table I where the viscosities are simply represented as the time for a standard amount of solution to flow through the Cannon Ubbelohde Viscometer. The longer the flow time, the higher the viscosity.

**Table I: Viscosities of Brine and Polymer Solutions and Viscosities of Polymer Solutions After Pumping Through a Berea Core.**

	Exp. 1 Flow Rate = 0.034 ml/sec	Exp.2 Flow Rate = 0.213 ml/sec
Brine Solution: ( $\eta_0$ sec)	99	99
Brine/Polymer (starting solution)	130.9	125.7
First 25 ml from core	98.5	124.7
Middle Sample		
(at 2455 ml pumped)	114.0	
(at 850 ml pumped)		116.0
Final Sample		
(at 3226 ml pumped)	115.3	
(at 1700 ml pumped)		113.3

\* In both experiments a polymer concentration of 0.75 mg of Alcoflood 1285 per liter of brine was used.

When the core is first filled with polymer solution, essentially all of the polymer is adsorbed on the internal Berea core surfaces. This can be seen by comparing the viscosity of the first ~1.5 core vol of solution to be pumped out (25 ml vs ~17 ml pore vol). The initial polymer solution viscosity of 130.9 cp has dropped to 98.5 cp, which is essentially the same as that of pure brine solution (99 sec). Thus, the polymer present in that volume of solution has been adsorbed. After pumping 2455 ml through (e.g. 144 core pore volumes), the viscosity of the exiting polymer was 114 cp. This remained the same after 3226 ml (190 core void volumes) were pumped through (e.g. 115.3 cp). Thus, all the internal pore volume surfaces have reached equilibrium-coating levels. The difference in viscosity between the original polymer solution and that pumped out much later (130.9 cp – 114 cp = 16.9 cp) must then be due to shear degradation.

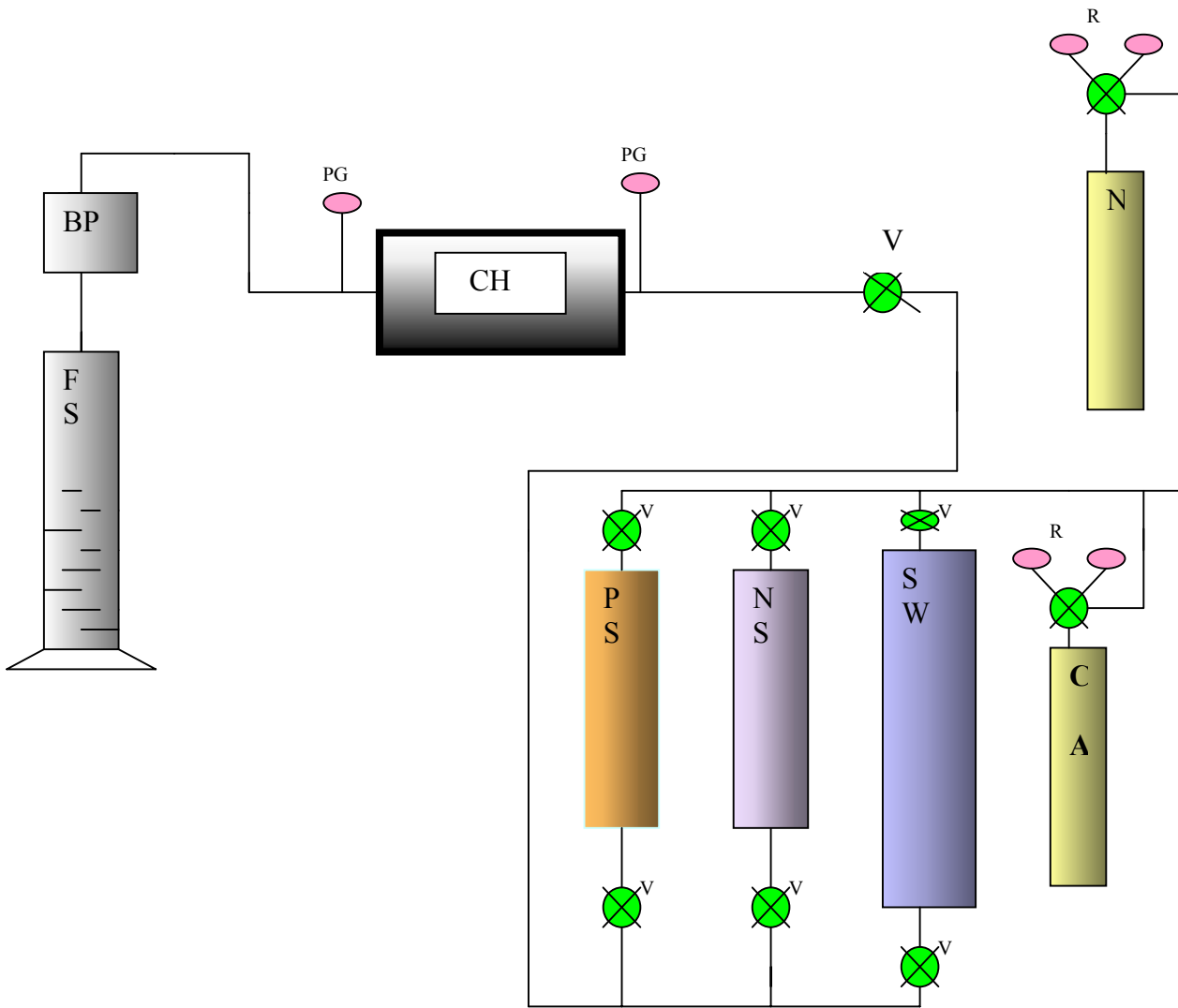
In the second experiment, the first 1.5 core void volumes of liquid pumped out of the core had the same viscosity as that of the initially made polymer solution (125.7 cp and 124.7 cp, respectively). This contrasts sharply with the first experiment but is completely logical. In the first experiment, the core surfaces had never previously been exposed to polymer. This same core, however, was used in the second experiment. By that time it had had 3226 ml of polymer solution pumped through it (e.g. 2.42 mg of polymer solution had been pumped into the core before experiment 2 had started). Thus,

when experiment 2 began, the core surfaces had already adsorbed all the polymer they could hold. After 850 ml and 1700 ml of polymer solution had been pumped through (experiment 2) the viscosities (115 cp and 113.3 cp) were the same as those seen at the middle and end of experiment one (114.0 cp and 115.3 cp, respectively). Thus, we suggest shear degradation during flow through the core probably accounted for the difference in the viscosity between the initial polymer solution and that pumped through the core. However, if shear degradation accounts for this drop, the amount of shear degradation in the two experiments was essentially the same despite the fact the flow rate in the second experiment was about 6.3 times greater.

### **Core Flood Experiments**

The assembly prepared to test polymer flooding and microbial growth is shown in Figure 9 and several cores prepared to mimic a depleted oil sand. A core was placed in a vacuum chamber, evacuated, and filled with injection water. The water-saturated core was placed in the core flood assembly and injection water flowed through the core. Crude oil from the North Blowhorn Oil Field (Lamar Co., AL) then was pumped through the core until no more water was present in the effluent. Injection water was again pumped through the core until no more oil was present in the effluent injection water. At this point, the core is considered equivalent to a depleted oil sand.

The cores as prepared above were employed in experiments to determine the effects of microbial activity combined with polymer flooding on the flow rate of injection water through these cores. When microbial activity is encouraged through the addition of  $\text{KNO}_3$  and  $\text{Na}_2\text{HPO}_4$  and then followed by an application of polymer, the flow rate is greatly reduced by the microbial growth and little more plugging seems to have taken place because of the polymer addition (see Figure 10). This suggests that the flow paths established prior to the start of the investigation were beginning to become plugged. Further evidence that established flow paths were being plugged and new flow paths were being established was shown by the presence of oil 61 d after treatment began. The impact on flow rates, as shown in Figure 11, was more pronounced initially when the core was treated first with polymer. Increases in flow rate occurred even after the nutrient additions began and it was only after 45 d that the flow rate decreased. The flow rate



**BP:** Back Pressure regulator  
**CA:** Compressed Air  
**CH:** Core Holder  
**FS:** Fluid Separator  
**PS:** Polymer System  
**N:** Nitrogen  
**NS:** Nutrient Solution  
**PG:** Pressure Gauge  
**R:** Regulator  
**SW:** Simulated production Water  
**V:** Valve

**Figure 9. Diagrammatic sketch of the core testing assembly.**

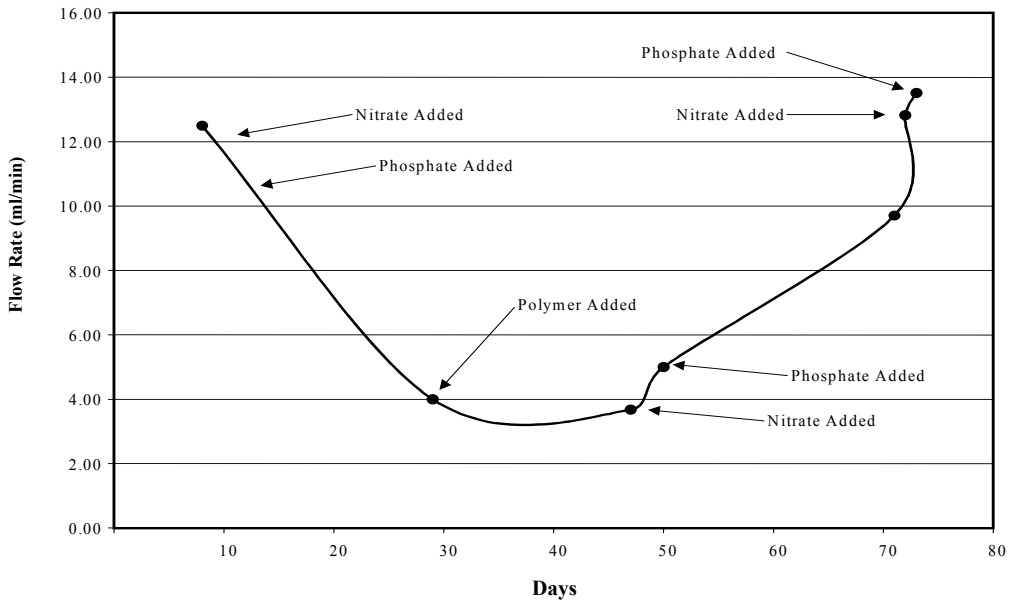


**Figure 10. Flow rate for Berea sandstone core when nutrients are added before polymer.**

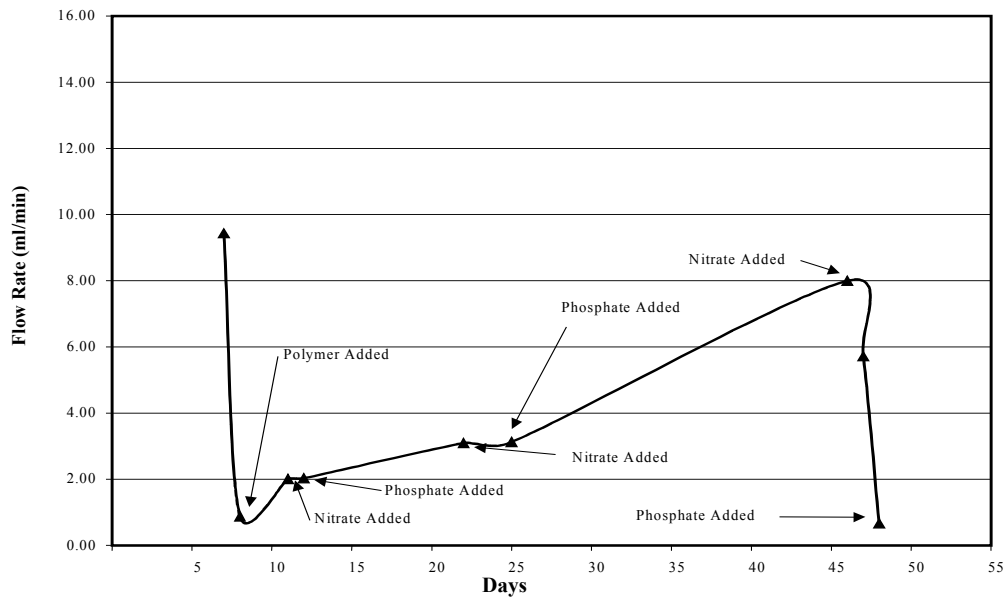


**Figure 11. Flow rate for Berea sandstone core when polymer is added before nutrients.**

decreased from 8.0 ml/min to 0.8 ml/min with the addition of the polymer solution. The flow rates slowly increased to 8.0 ml/min with the addition of the nutrient solutions suggesting that the polymer was being removed from the flow paths. The flow rate was decreased again 5 d later suggesting that microbial growth was responsible for the decrease.

Evidence for the plugging of the established flow paths and the establishment of new flow paths was shown by the presence of oil 37 d after treatment began. In this experiment, the addition of polymer caused a large decrease in flow rate, but this was followed by an increase in flow rate. These data suggest that very little growth of the microflora was occurring until the polymer had been flushed from the core.

It is interesting to note that after 20 d of nutrient feeding, the flow rate had been reduced 69% while the flow rate after polymer flooding dropped 89% initially but was reduced only 66% after 20 d.

Other experiments demonstrated that the injection of a polymer solutions (Alcofloods 1235, 1275A, 1285, and Flocon 4800) through the core resulted in the recovery of additional oil from the core. Similarly, when the injection water was supplemented with microbial nutrients (potassium nitrate and disodium hydrogen phosphate) additional oil was observed in the effluent several days after the injections.

### **Initial Magnetic Resonance Imaging Studies Using Berea Sandstone Cores**

The original plan was to alternate the polymer and nutrient injections in the search for synergy with the main criterion for success being the recovery of oil from the cores. However, at the contractor's meeting held in Denver in June 2000 Gary Walker (DOE) suggested several individuals for us to contact in regard to techniques being used by others to increase the amount of information we can obtain in our core experiments. Discussions of NMR imaging experiments were held with Dr. Ted Watson of Texas A&M. He then conducted a preliminary magnetic resonance imaging (MRI) experiments as described below.

Initial attempts were made to image oil-depleted Berea sandstone core by NMR using a GE2-Tesla CSI-II imager/spectrometer with a 31 cm magnet bore. This spectrometer was equipped with a 20G/cm shielded gradient-coil set and a birdcage RF coil. The work was performed at Texas A&M University by Professor Ted Watson (also

a DOE/NPTO grant holder). The key question was: can regions of H<sub>2</sub>O versus regions of oil clearly be imaged using <sup>1</sup>H NMR? If successful, the three-dimensional images would permit us to directly observe (to high resolution) the locations of oil versus water throughout the core and follow these as a function of both polymer/waterflooding and waterflooding after microbial growth. Thus, a direct observation between patterns of water flow and oil removal would be obtained upon, (a) polymer flooding, (b) MEOR experiments, or (c) synergism between polymer flooding and MEOR.

The following suite of experiments were performed on two Berea sandstone cores (about 3.5 in long and 1.25 in dia.).

Core 1. A core was prepared as described above using oil from the North Blowhorn Creek Oil Field/Lamar Co. AL (API gravity 28-35.2) .

Core 2. This core was identical to Core 1 except that it was subsequently treated with a polymer flood where 255 ml (12-14 core void volumes) of a polymer solution (Alcoflood 1285, mol wt ~ 20,000,000: 75 mg per L of standard brine solution) was pumped through the core.

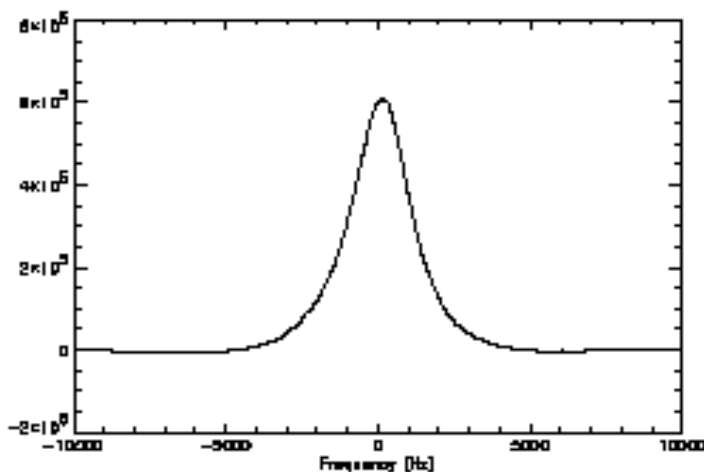
The cores were:

- (a) Profile imaged along longitudinal axis,
- (b) Two-dimensional images were made (horizontal slices of 5 mm thickness taken),
- (c) Inversion recovery (T<sub>1</sub>) experiments were done,
- (d) NMR <sup>1</sup>H spectra were taken. Also, inversion recovery experiments were done on both oil and water.

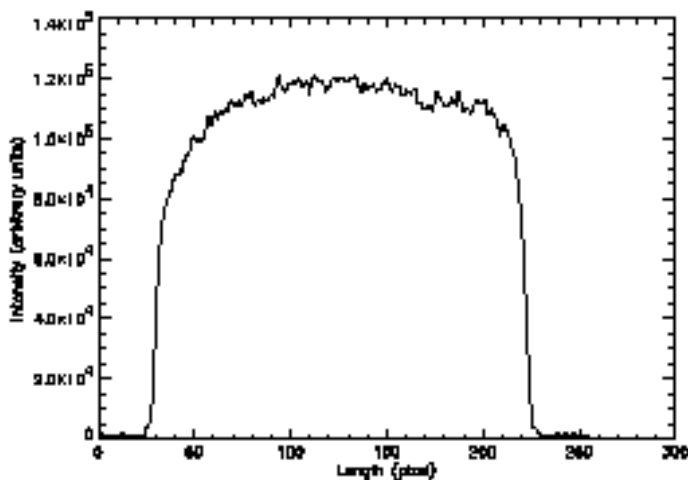
Unfortunately, these experiments proved unable to distinguish between the oil and water regions of the cores due to severe NMR line-broadening associated with the Berea sandstone. This can be seen in Figure 12 where a broad <sup>1</sup>H line width of ~2000 Hz was obtained. This width is much larger than the 300 Hz (at 85 MHz) chemical shift difference between the protons in oil (*e.g.* C-H) and the protons in water (*e.g.* O-H). This means it was necessary to reduce the line broadening. Berea sandstone is particularly bad in this respect but, it was hoped that the use of cores from the North Blowhorn Creek Oil Field would reduce this problem.

Figure 13 shows a one-dimensional profile of the <sup>1</sup>H signal intensity across the length of the Core 1 at a pixel size of 0.47 mm. A similar profile of Core 2 shows some

fluid loss from one end of the polymer-flooded sample (Figure 14). Two-dimensional images are shown in Figures 15 and 16 for Cores 1 and 2, respectively. These images are of 5 mm thick slices taken directly down the center of the cores' long axes. The brightened areas indicate greater concentrations of  $^1\text{H}$  nuclei (*e.g.* oil and water). The dark areas are rock. If resonances for oil and water regions could be resolved, visualization of oil and water distributions would be possible on scale similar to that shown in these images. Inversion-recovery experiments are shown for the oil sample and for Cores 1 and 2 in Figure 17.



**Figure 12. NMR spectrum of oil-depleted Berea Core 1 containing residual North Blowhorn Creek Oil (API gravity 28-35.2).**



**Figure 13. 1-D profile of oil-depleted Berea Core 1 containing residual North Blowhorn Creek Oil (API gravity 28-35.2). The pixel size is 0.47 mm.**

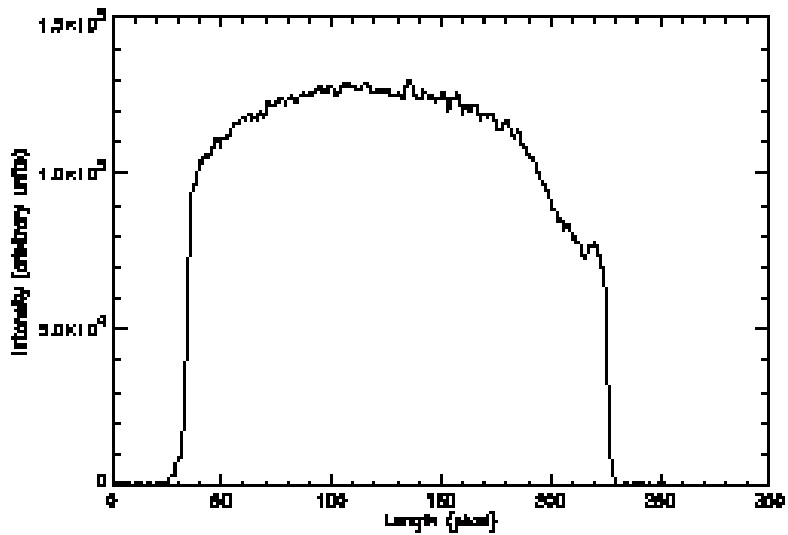


**Figure 14.** 1-D profile of oil-depleted Berea Core 2 containing residual North Blowhorn Creek Oil (API gravity 28-35.2) after an aqueous polymer flooding treatment with Alcoflood 1285. The pixel size is 0.47 mm.

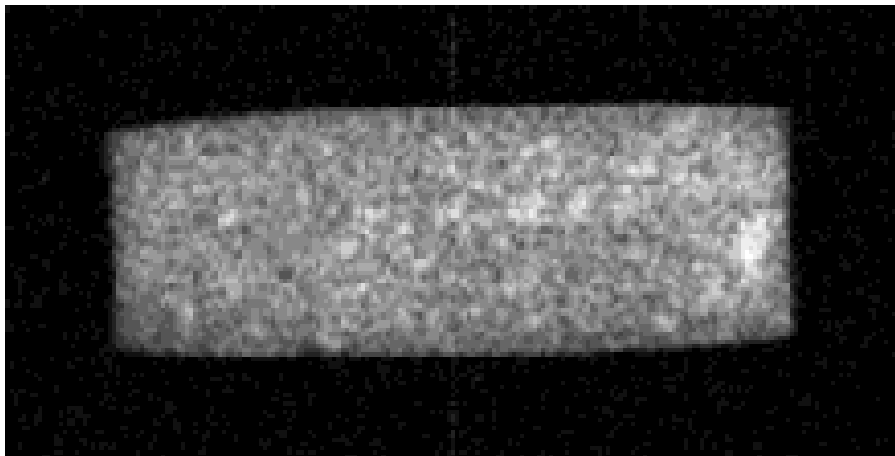


**Figure 15.** 2-D image of oil-depleted Berea Core 1 containing residual North Blowhorn Creek Oil (API gravity 28-35.2).

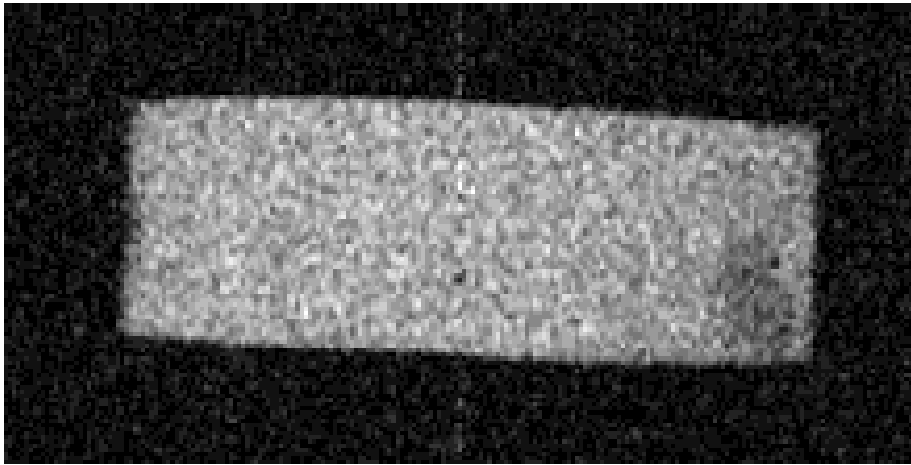


**Figure 16. 2-D image of oil-depleted Berea Core 2 containing residual North Blowhorn Creek Oil (API gravity 28-35.2) after an aqueous polymer flooding treatment with Alcoflood 1285.**

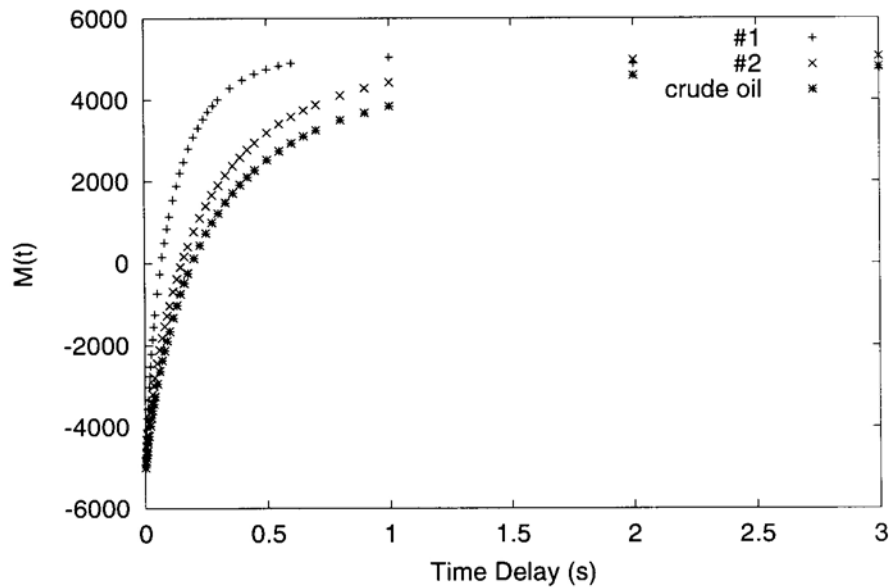


**Figure 17. Inversion-recovery  $T_1$  data for the core samples and oil.**

Oil signal relaxation occurs at a different rate in the core versus in bulk. This observation may simply reflect that the signal in the core represents both oil and water. The relaxation characteristics of Cores 1 and 2 differed. The calculated relaxation

distributions are shown in Figure 18. The tall peak in Core 1 belongs to water and the less intense peak belongs to oil. The interpretation of the relaxation times for Core 2 is more difficult. Clearly two peaks exist. The taller is assigned to water and the shorter (fast relaxation ) is assigned to oil.

Several experiments were attempted to get reasonable oil/water contrast in order to clearly follow changes in water and oil distributions in cores as a function of treatments.

1. Use  $D_2O$  instead of  $H_2O$ . Thus, only the oil protons will be seen and oil distribution would be clearly imaged.
2. Use different rock samples. For example carbonate rocks have narrow line-widths, which would give more accurate determinations of the relative amounts of each fluid phase. Bentheimer sandstone (line-widths of 300-275 Hz) could be used. In live core experiments, the rock from the North Blowhorn Creek Field should be better than using Berea cores.
3. Image water using Na-23 (a large amount of Na is present in the brine solution used so water location, independent of oil, could be followed).
4. Add tiny amounts of EDTA to the water used so that the water relaxation time is changed.

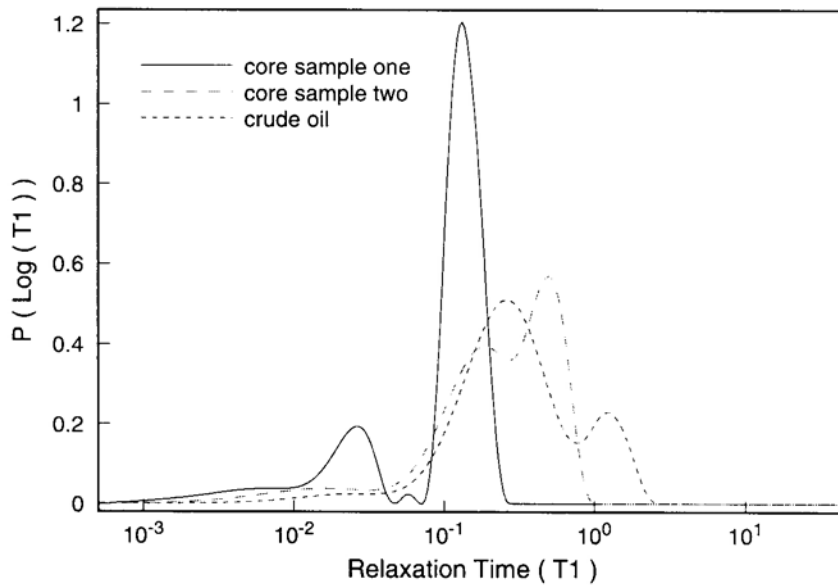


**Figure 18.  $T_1$  distributions for the core samples and oil.**

## **Further Nuclear Magnetic Resonance Imaging Analysis of Berea Sandstone Cores and North Blowhorn Creek Cores**

In light of the above results, NMR-imaging was next applied to observe water flow patterns and oil recovery from cores. In order to differentiate water from oil in the cores, the following four cores were prepared as described below.

- Core 1 was a Berea core, initially filled with injection water containing 1.2% wt EDTA as the manganese salt. This was added to speed up the relaxation times and, hopefully, increase the water/oil contrast. Crude oil was pressurized into the core followed by flushing with water (containing EDTA) until no more oil came out.
- Core 2 was a Berea core that was first filled with D<sub>2</sub>O, followed by adding oil and then flushing with more D<sub>2</sub>O until no more oil emerged. Since only trace amounts of water protons would be present, this experiment was intended to observe only the oil and thus the water's location would be obvious by default.
- Core 3 was treated the same as core 2 but 80% D<sub>2</sub>O/20% H<sub>2</sub>O was used.
- Core 4 was taken from the North Blowhorn Creek Oil Field. It was removed from a section of the field which had already undergone waterflooding. It was not further treated.

The samples were studied in a GE 2-Tesla CS I-II imager having a 31cm magnet bore, equipped with a 20 G/cm shielded gradient-coil set and birdcage RF coil. Two-dimensional slice images were generated. They provided information on the spatial distribution of the oil. Quantitative one-dimensional images also were obtained and the fluid present was obtained as a function of the longitudinal direction. Finally, inversion-recovery experiments gave a distribution of T<sub>1</sub> relaxation times in the sample.

### **Results of NMR Imaging Experiments**

Relatively little signal was obtained from Core 4 from North Blowhorn Creek. In contrast, considerable oil was present in Berea cores 1-3. The oil saturation levels for the four cores were: Core 1, 21.4%; Core 2, 21.9%; Core 3, 24.7% and Core 4, 4.87%. This latter value was actually about 3.7% upon correcting for the lower porosity of the North Blowhorn Creek's core rock. Since Berea Core 2 only can give <sup>1</sup>H absorption resonances

for the oil (since D<sub>2</sub>O was used instead of H<sub>2</sub>O), the agreement among Cores 1-3 was excellent, clearly demonstrating that the North Blowhorn Creek Core (#4) had much less oil present due to its very low porosity.

T<sub>1</sub> inversion-recovery experiments demonstrated that Cores 2-4 were quite similar and further supported oil quantitation by this method as being reasonably accurate. The relaxation time in Berea Core 1 was shorter than 0.1 sec. showing that EDTA did, indeed, lower relaxation times.

The level of image resolution was approximately 0.47mm. Example images of these cores can be seen in Figure 19.

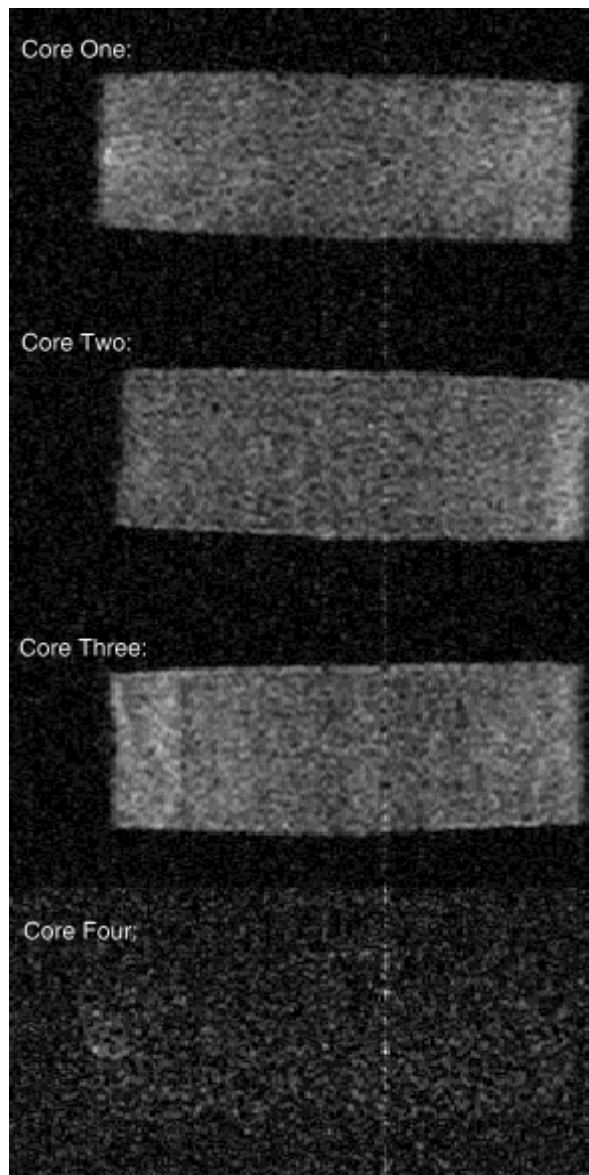


**Figure 19. NMR images of four cores.**

The dark areas represent rock and the light areas may be attributed to H<sub>2</sub>O or oil (in the case of Berea Core 2 only oil would be observed because D<sub>2</sub>O was used in place of H<sub>2</sub>O). Examination quickly revealed there were no large water channels through which the water is passing without generally permeating through the cores. Therefore, when waterflooding is no longer removing any more oil, the passages through which the water is passing must be generally substantially smaller than 0.4mm in diameter. Thus, water is flowing through small pores which are likely coated with oil on the sides. Many other pores may be completely blocked by oil.

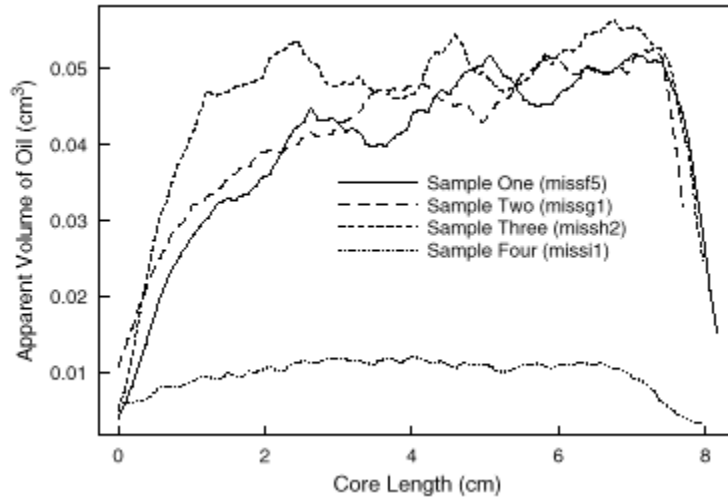
The one-dimensional T<sub>2</sub> profiles for the four cores are shown in Figure 20. These are presented in a format that gives the volume of oil detected per sample length along the length of the cores. Clearly North Blowhorn Creek Core 4 has far less oil than the other three cores. The reason is that the North Blowhorn Creek core has a substantially lower porosity and permeability than the Berea cores. Another obvious feature observed in this figure is the greater oil depletion at the front end of Cores 1-3 versus the oil present at the back end. The flow of water may have moved some of the oil away from the front end toward the rear. However, this core had been producing only water as pumping continued (*e.g.* no more oil emerged as waterflooding continued).

Figure 21 also exhibits the inversion recovery (T<sub>1</sub>) relaxation distributions of Core 1 and Core 4. Both of these cores contain water and oil but Core 1 also has EDTA/Mn salt to lower the relaxation time.

Two new depleted cores were obtained from the North Blowhorn Creek Oil Field. These were previously waterflooded until no more oil was obtained. Then one core (Core D4, Cut 8, Sleeve 1) was treated with the nutrients KNO<sub>3</sub> and Na<sub>2</sub>HPO<sub>4</sub>, which were added with injection water. The second core (Core D4, Cut 8, Sleeve 2) was treated with aqueous solutions of Alcoflood 1285 (25% hydrolyzed polyacrylamide, mol wt ~ 22 x 10<sup>6</sup>). In both cases further oil was recovered from these cores. The subsequent effects on the flow rates are given in Figure 22 for Core D4 Cut #8 Sleeve 1 and Figure 23 for Core D4 Cut #8 Sleeve 2.

The samples were analyzed using a GE 2T CSI-II imager/spectrometer with 31 cm magnet bore and 20 G/cm shielded gradient-coil set and a bird cage RF coil. Three

kinds of experiments were performed on the two samples. (1) Two-dimensional images, which correspond to a horizontal slice 5 mm thick along the longitudinal axis, were obtained. These provide qualitative measures of the spatial distribution of the hydrogen nuclei. (2) One-dimensional images were taken. These are quantitative measures of the amount of hydrogen nuclei corresponding to slices orthogonal to the longitudinal axis.



**Figure 20. One-dimensional  $T_2$  Profile: apparent oil volume per sample length.**

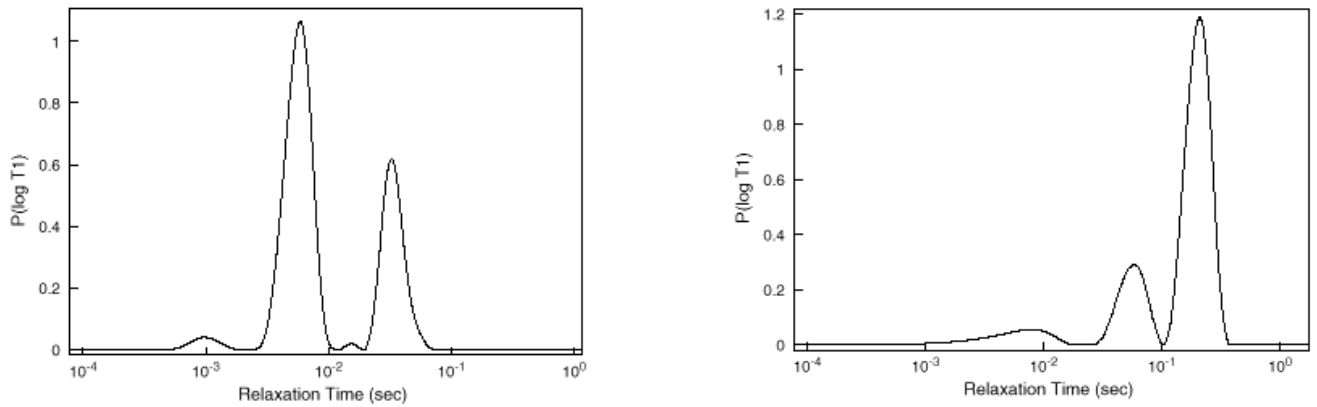


**Figure 21. Core 1 and Core 4 relaxation distribution figures.**

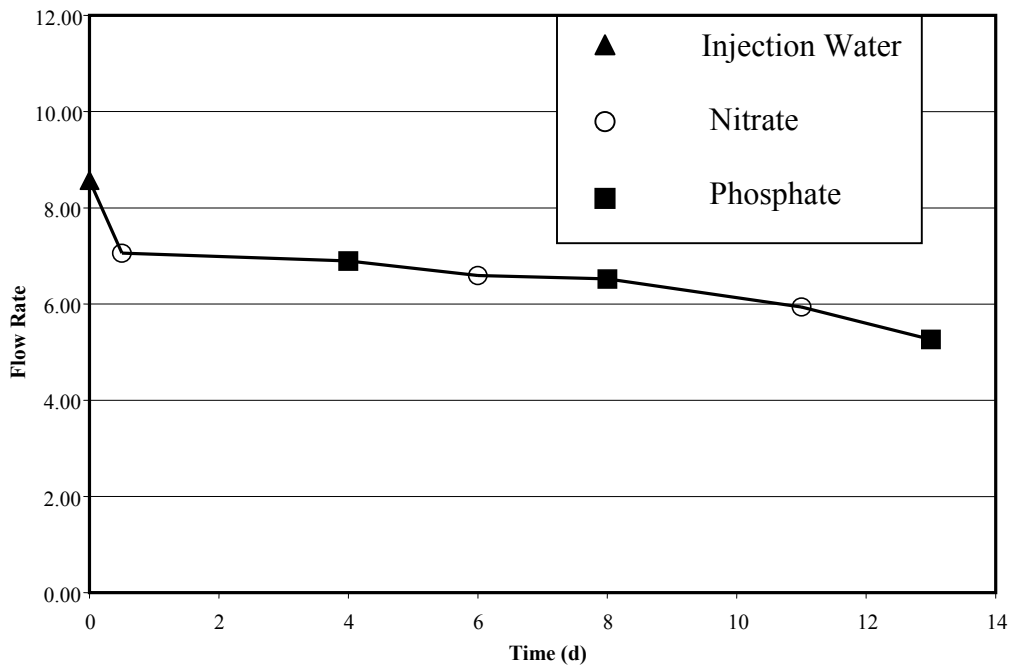


**Figure 22. The effects of microbial activity on flow rates for D4 Cut #8 Sleeve 1 over time. This was a depleted oil core from the North Blownhorn Creek Oil Field that was treated with  $KNO_3$  and  $Na_2HPO_4$  in the injection water.**

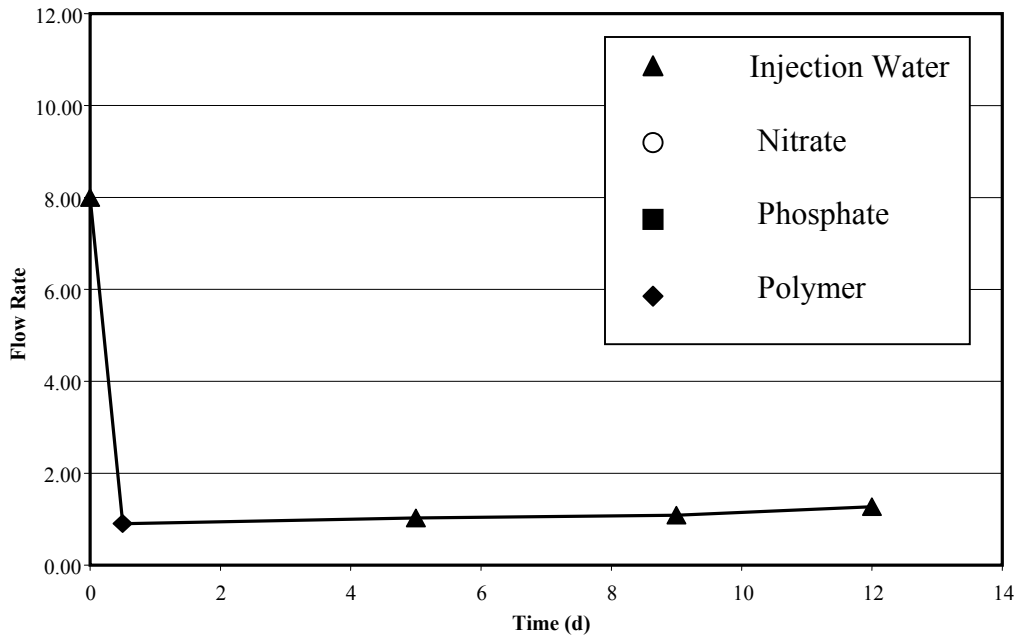


**Figure 23. The effects of Alcoflood 1285 treatment on flow rates over time. D4 cut #8 Sleeve 2 was used.**

(3) Inversion recovery experiments were run. These provide the distribution of  $T_1$  relaxation times, which gives us information about the fluids within the samples.

Figures 24 and 25 show the two-dimensional slice imaging experiments. The images are taken on a 5 mm slice of central transverse layer. The field of view is 120 mm x 60 mm. This domain corresponds to 128 x 56 blocks with a pixel size of 0.47 mm x 0.47 mm. In each slice selective imaging gives the magnitude of the magnetization, which is proportional to the amount of hydrogen nuclei. The signal is represented on a gray scale. The brighter areas indicate greater amounts of hydrogen nuclei. The signals from oil versus those from water cannot be differentiated in these images because of the broad lines associated with the spectroscopic signals.

The two-dimensional image of Sleeve One indicates that there is a relatively large signal in the center of the sample on the right-hand side of the sample. Sleeve Two appears to have considerably less fluid, and the fluid appears to be more evenly distributed.

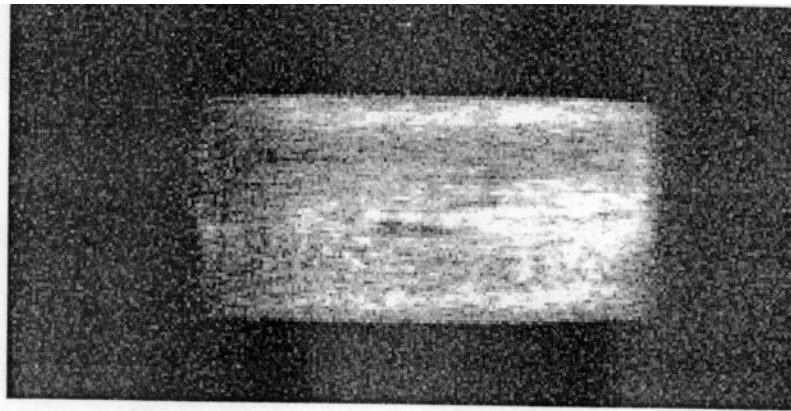


**Figure 24. Sleeve One: Two-dimensional profiles.**

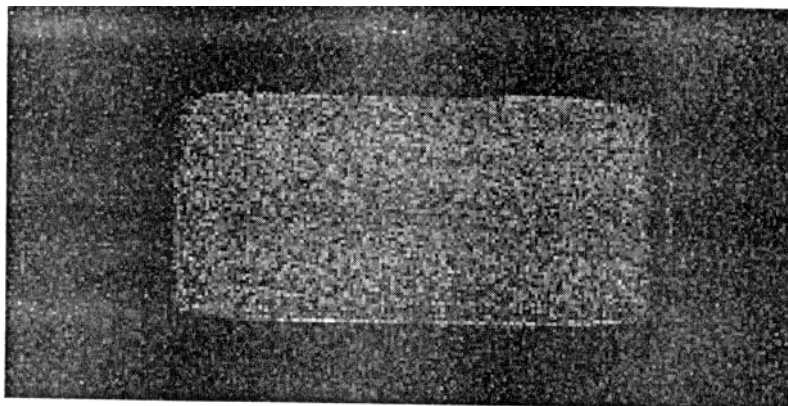


**Figure. 25. Sleeve Two: Two-dimensional profiles.**

These results are supported by the one-dimensional profiles shown in Figure 26. At a given position along the longitudinal axis, the graph is proportional to the number of hydrogen nuclei corresponding to a unit length along the longitude axis. The actual volume of fluid per length is calculated based on the supposition that the hydrogen nuclei density of the observed fluid is that of water, and is thus called the ‘apparent’ volume of water. However, the reader is reminded that oil and water have not been discriminated in these signals so this does not actually represent the amount of water, unless water is the only liquid present. Figure 26 shows that Sleeve One has considerably more liquid than Sleeve Two. It also shows that there is more fluid in the right-hand side of Sleeve Two. These observations are consistent with those made with the two-dimensional images described above.

Figure 27 shows the  $T_1$  distributions obtained from the inversion-recovery experiments. The integral under any segment of the graph is proportional to the amount of hydrogen nuclei corresponding to that range of relaxation time. Based on our earlier work, we believe that the taller peak to the right represents water.

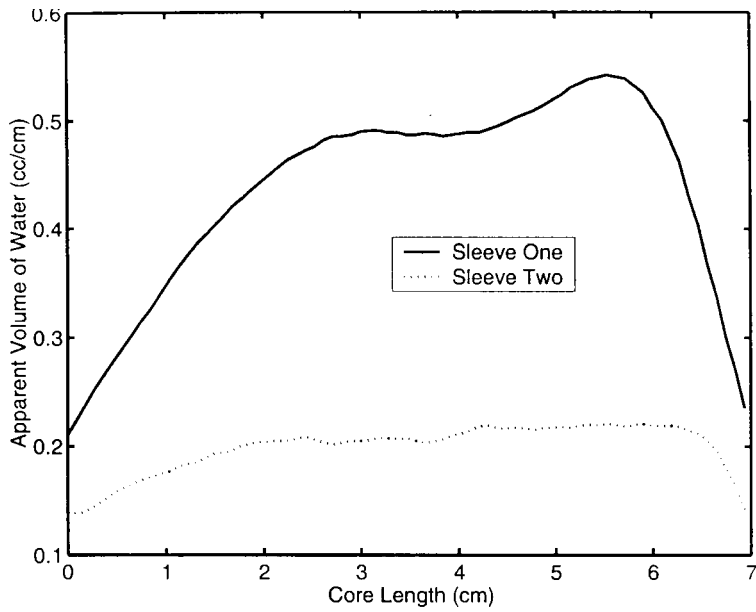


**Figure 26. One-dimensional profiles.**

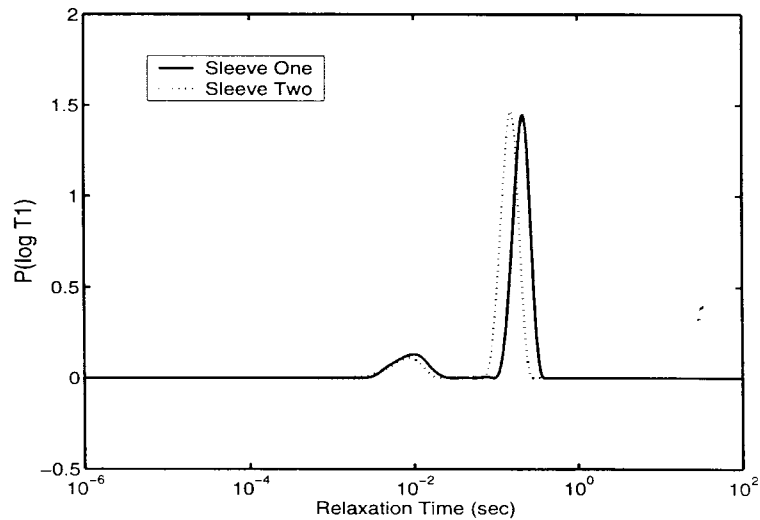


**Figure 27. Inversion recovery:  $T_1$  relaxation distributions.**

The larger relaxation times belong to water and the shorter times belong to oil. These measurements suggest that the ratio of water to other liquids is about the same for both samples, and that the samples contain mostly water. The actual fractions of water and oil are provided in Table II. Clearly far more water than oil remains in each of these samples.

**Table II: The Relative Amount of Fluids in the Samples.**

	Oil	Water
Sleeve One	0.15%	0.85%
Sleeve Two	0.12%	0.88%

#### **Task 4. Determine the Ability of Microbial Selective Plugging Technique in Combination With Selected Polymer Flooding Protocols to Increase Oil Recovery From Live Cores Obtained From Newly Drilled Wells.**

##### **Coreflood Experiments Using Live Cores**

Attempts to obtain new cores from recently drilled wells have not been successful and cores from previously drilled wells are unsatisfactory due to the method of storage since being obtained. This potential problem was foreseen and contingency plans put in place earlier. Cores obtained from the last DOE project which had been preserved under nitrogen, were employed for the live core experiments. These cores were in as close to their original state as possible and did contain indigenous microorganisms in their native state.

The cores employed in this study were from an area in the North Blowhorn Creek Oil Field which had undergone waterflooding. The objective of this study was to determine the effects of polymer flooding and microbial activity on the flow rates of simulated injection water through live cores. Additionally, the experiments were designed to determine if there was any synergism between these enhanced oil-recovery methods.

Experiments were conducted in Hassler sleeves at 30 C. Core D4 Cut #15 Core 1 was injected with injection water containing 0.24%  $\text{NaNO}_3$  followed by 2 separate injections of injection water with 0.06%  $\text{Na}_2\text{HPO}_4$  with this treatment regime being repeated over a period of 40 d. The results of these experiments are given in Figure 28 and showed a steady decline in flow rate of 0.111 ml/min/d. The effect of polymer addition followed by nutrient additions was determined using Core D4 Cut #15 Core 2. The core was injected with polymer Alcoflood 1285 followed by injection water containing 0.24%  $\text{NaNO}_3$  followed by 2 separate injections of injection water with 0.06%  $\text{Na}_2\text{HPO}_4$  with treatments of  $\text{NaNO}_3$  and  $\text{Na}_2\text{HPO}_4$  being repeated over a period of 40 d. The results of this experiment are given in Figure 29. As expected, the flow rate in the core was immediately decreased as a result of polymer treatment. However, the flow rate began returning to normal once the polymer had passed through the core. Following nutrient additions in Core D4 Cut #15 Core 2, the flow rate began to decline at a rate of 0.266 ml/min/d. These results show that the addition of nutrients increased

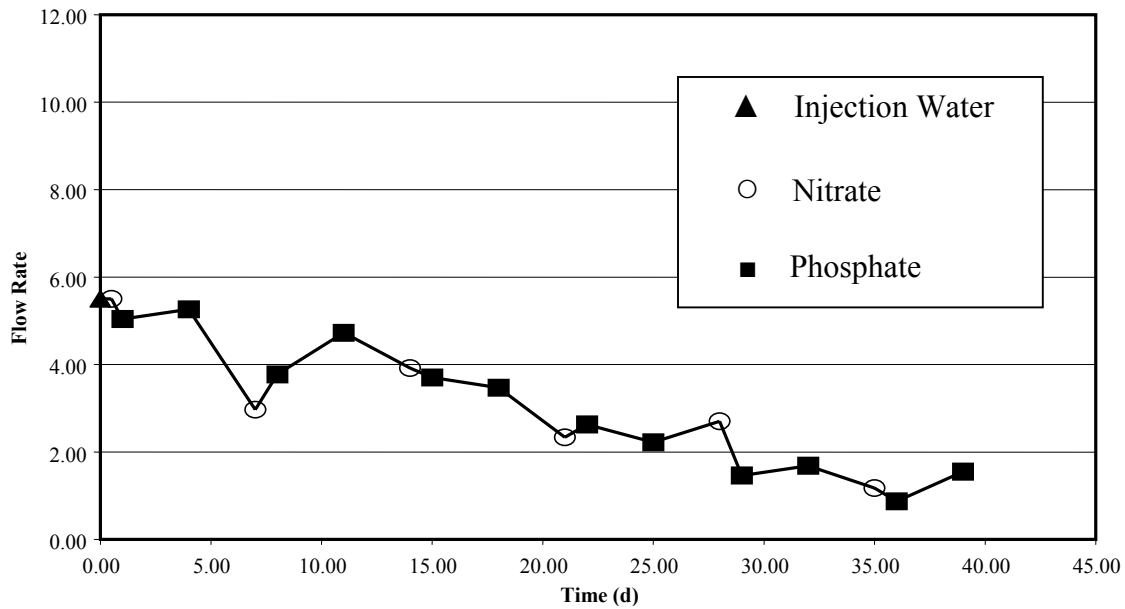


**Figure 28. The effects of microbial activity on the flow rate using Core D4 Cut #15 Core 1.**

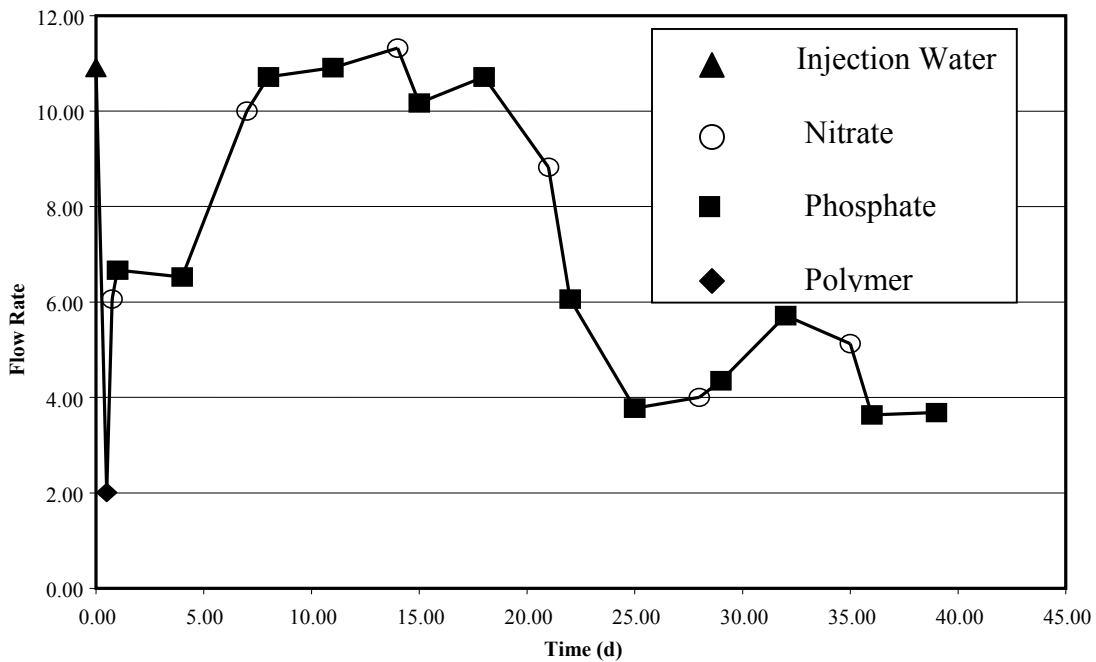


**Figure 29. The effects of polymer flooding (Alcoflood 1285) on the flow rate using Core D4 Cut #15 Core 2.**

microbial activity resulting in significant decreases in the flow rate and the benefits of the polymer initially are short lived. As plugging of flow paths through microbial activity occurs, injection water should begin to infiltrate unswept areas of the core.

The previous experiment was repeated using two cores from D4 Cut #10 and was conducted in Hassler sleeves at 30 C. Core D4 Cut #10 Core 1 was treated as described above for Core D4 Cut #15 Core 1 except that treatment was stopped after 30 d.

The results of this experiment are given in Figure 30 and showed a steady decline in flow rate of 0.025 ml/min/d which amounts to a 73% decrease over 30 d. The effect of polymer addition followed by nutrient additions was determined using Core D4 Cut #10 Core 2 and received the same treatment as Core D4 Cut #15 Core 2, described above except that treatment was stopped after 30 d. As expected, the flow rate in the core was immediately decreased (84%) as a result of polymer treatment (as shown in Figure 31). However, the flow rate began to increase once the polymer had passed through the core and continued to increase even after some nutrient treatments had occurred. These results suggest that either the number of microorganisms in the core plug was low or the polymer interfered with the nutrients reaching the microbes. The latter might take place if some polymer was adsorbed on the microorganism's surfaces slowing their response to nutrient treatment. Thus, the benefits of this polymer are short lived and may actually be deleterious to microbial growth. The plugging of flow paths through microbial activity (as shown in Figures 28 and 29) did result in the infiltration of injection water into unswept areas of the core.

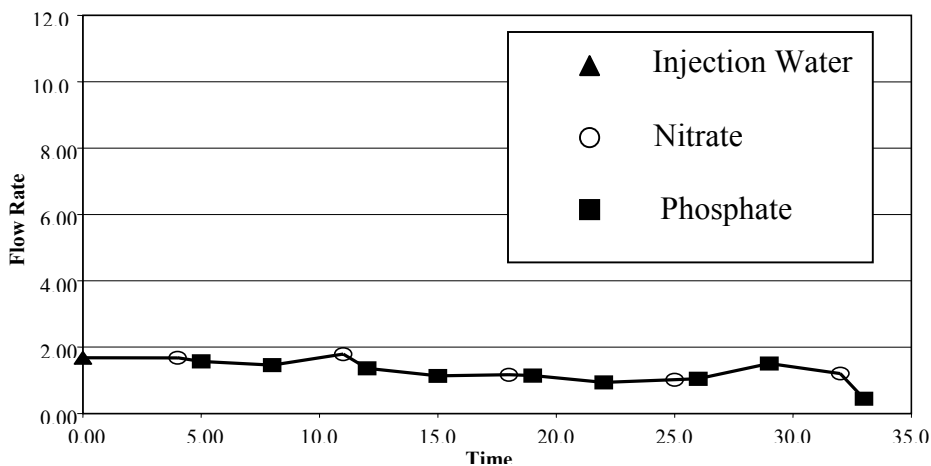


**Figure 30. The effects of microbial activity on the flow rate of injection water through Core D4 Cut #10 Core 1 over time.**

Another polymer, Flocon 4800 polymer (Xanthan,) was tested sequentially with microbial activity for its synergistic effect on the flow rate of fluid through Core D4 Cut #9 Core 1 (Figure 32). The results from this core were compared to the effects of microbial activity only on flow rate of fluid through Core D4 Cut #9 Core 2 (Figure 33). When polymer was employed, the flow rate was initially reduced by 30% but then made a quick recovery back to normal in approximately 5 d. Therefore, the Flocon 4800 would have to be added regularly to maintain any positive effects.

The results showed that the Flocon 4800 polymer was not as effective as the Alcoflood 1285 polymer in the initial reduction of flow rates (30% as compared to 84%). There was a 0.026 ml/min/d decrease in the flow rate observed for Core D4 Cut #9 Core 2 which only received nutrients.

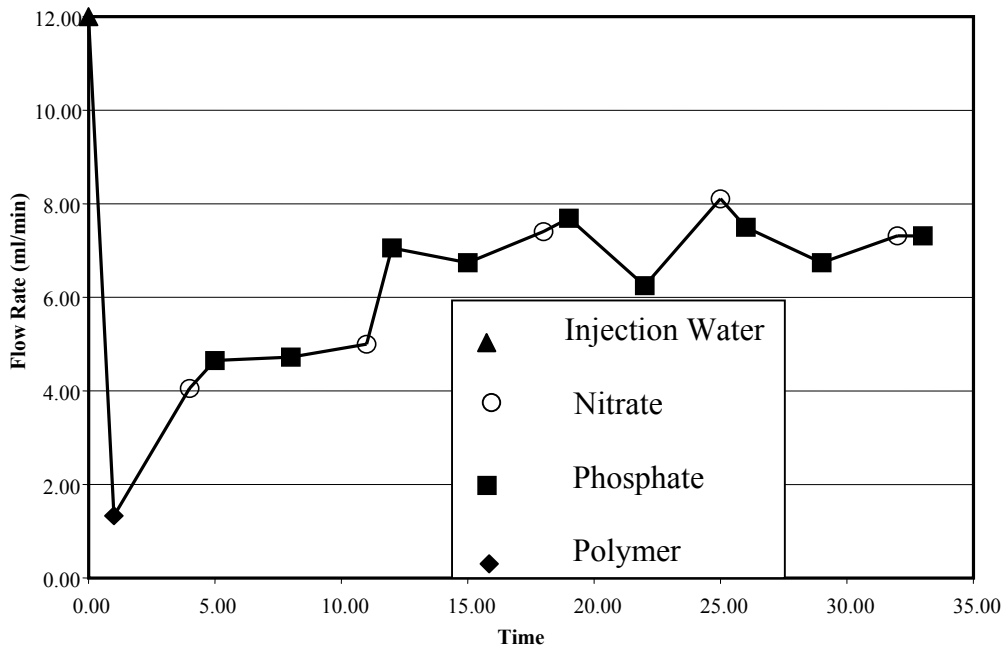


**Figure 31. The effects of Alcoflood 1285 treatment and microbial activity on the flow rate of injection water through Core D4 Cut #10 Core 2 over time.**

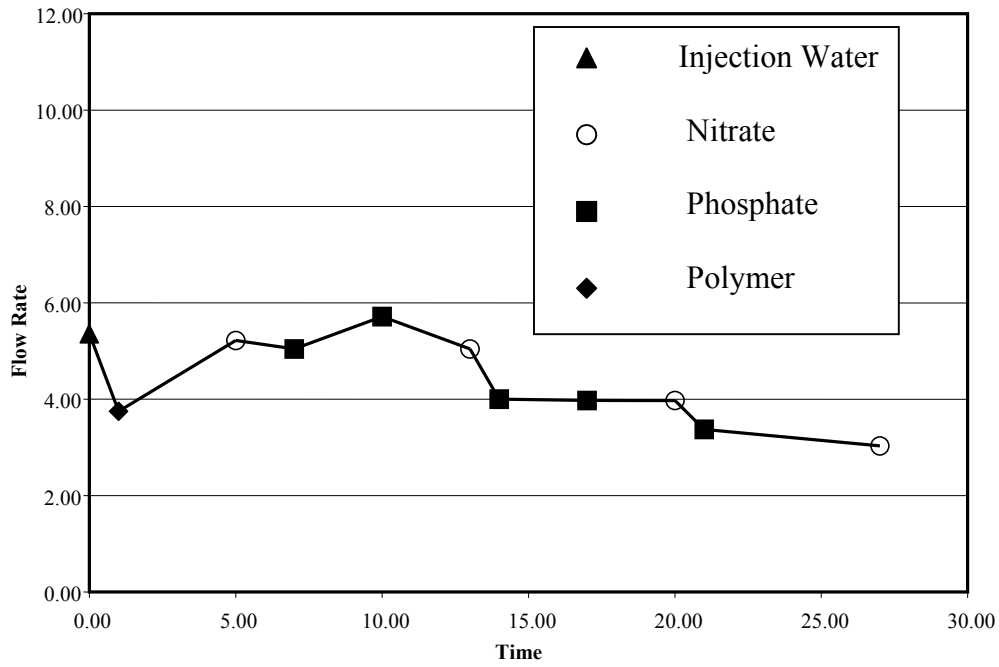


**Figure 32. The effects of Flocon 4800 treatment and microbial activity on the flow rate of injection water through Core D4 Cut #9 Core 1 over time.**

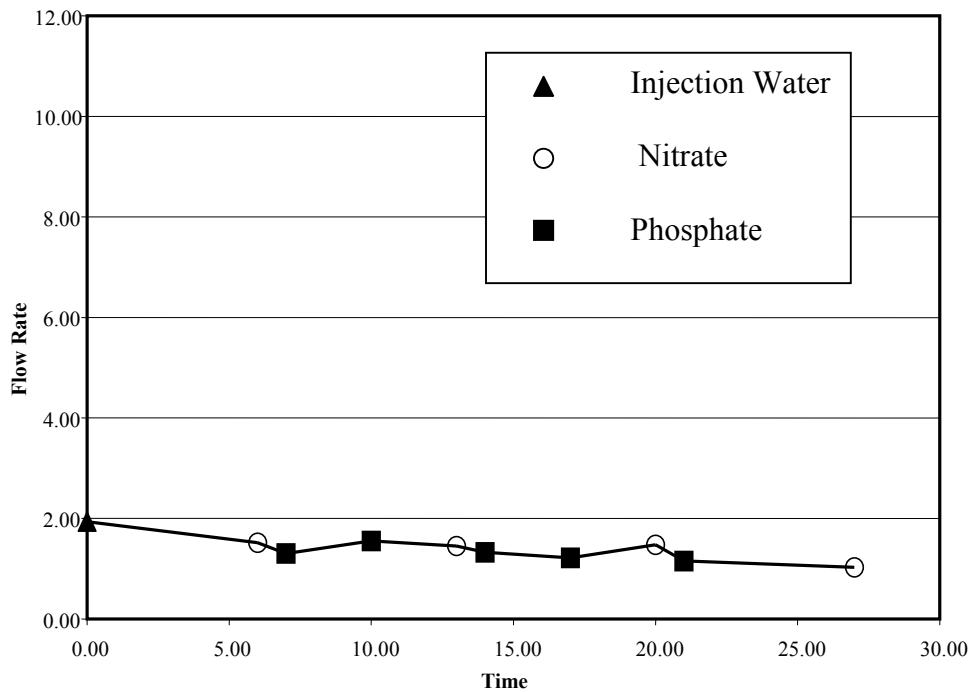


**Figure 33. The effects of microbial activity on the flow rate of injection water through Core D4 Cut #9 Core 2 over time.**

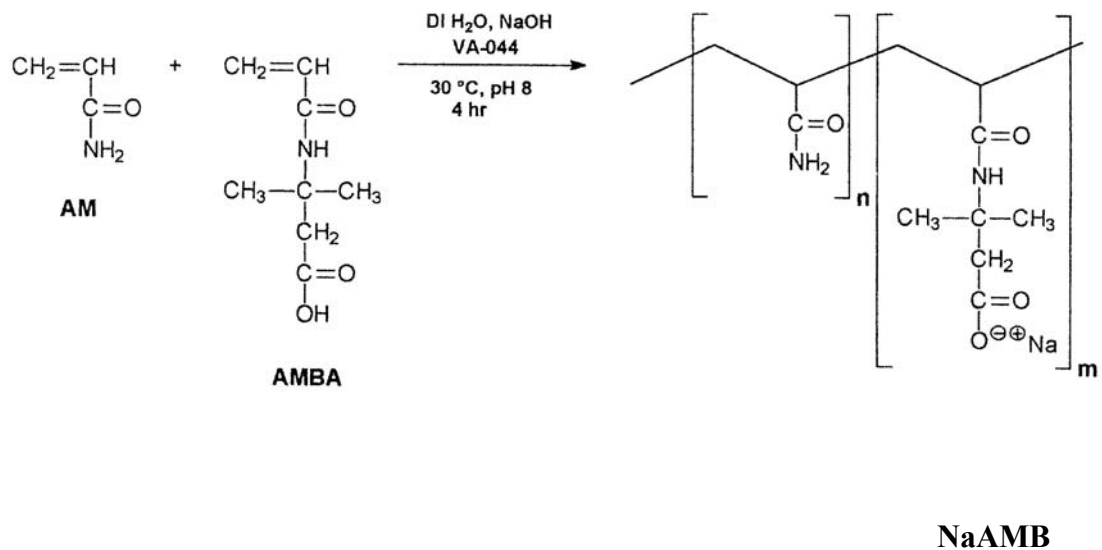
It was observed that permeability had very little effect on the ability of microorganisms to reduce the flow rate with the cores from D4 Cut #15 and the cores from D4 Cut #9. Core 2 from D4 Cut #15 was 2.0X more permeable than core 1 from D4 Cut #15 and yet the microbial activity in both cores resulted in 65% and 63% reduction, respectively. Similarly, Core 2 from D4 Cut #9 was 2.8X more permeable than Core 1 from D4 Cut #9 and microbial activity reduced flow rates 47% and 44%, respectively. In regard to Core D4 Cut #10 Core 2, the lack of change of flow rate after the addition of nutrients was probably due to either a lack of a sufficient microbial population or the nutrients were not getting to them.

### **Investigation of the Polymer (NaAMB)**

A polymer, NaAMB, was synthesized at the University of Southern Mississippi by Professor Roger Hester by the copolymerization of acrylamide and N-acryloyl-3-amino-3-methylbutanoic acid. This polymer (designated NaAMP) has a low molecular weight for a flow control polymer with a  $MW = 1.25 \cdot 10^6$ . (See Figure 34). However, it has been chemically designed to have a high extensional viscosity (described more in the following section).

The viscosity behavior of NaAMB was studied in the standard injection water. These data are summarized in the Table III. The purpose of these data are, not only to characterize this polymer but also, to eventually see if the polymer adsorbs to the core and to determine if shear degradation of NaAMB occurs when it is pumped through Berea cores. Less shear degradation should occur since its molecular weight and coil hydrodynamic volume is much lower than other mobility control polymers we have studied. However, these measurements have not yet been made. Viscosity measurements were made after pumping a polymer solution through a Berea core to establish whether or not adsorption is occurring and to look for shear degradation at high and low flow rates through the core.

NaAMB also was tested by pumping it through cores which had been flooded with simulated injection water until no more oil would come out. The NaAMB polymer effectively removed more oil. This is a significant result given the low molecular weight



- Synthetic parameters:
  - $[M]_{\text{total}} = 0.40 \text{ M}$
  - $[M]:[I] = 2000$  (0.05 mol% based on  $[M]_{\text{total}}$ )
  - NaAMB-10-2: 10 mol% AMBA in feed
  - Mol wt 1.25 MM (e.g.  $1.25 \times 10^6$ )

**Figure 34. Synthetic equation.**

**Table III: Viscosity Measurements on NaAMB (Mol wt  $1.25 \cdot 10^6$ ) Determined at 30.3°C in Standard Injection Brine Solutions.**

Concentration (g/100cc)	$t_0$ (sec.)	$t_{\text{(soln)}}$ (sec.)	$t/t_0$	$n_{\text{sp}}^a$	$n_{\text{inh}}^a$	$n_r^a$
0.1000	101.6	350.5	3.45	2.45	0.896	2.45
0.0833	101.6	338.4	3.33	2.33	1.016	2.80
0.0714	101.6	295.5	2.91	1.91	0.906	2.67
0.0625	101.6	260.8	2.57	1.57	0.720	2.51
0.0556	101.6	238.8	2.35	1.35	0.541	2.43
0.0500	101.6	227.1	2.24	1.24	0.423	2.47

<sup>a</sup> $n_{\text{sp}} = t/t_0 - 1$ ;  $n_{\text{inh}} = (1/c)\ln(t/t_0)$ ;  $n_r = n_{\text{sp}}/\text{conc.}$

of this polymer which was also used at a low (500 ppm) concentration. Low molecular weight polymers give only modest enhancements in the shear viscosity. This suggests that the critical extension viscosity of NaAMB may have played a role in the removal of more oil from the core.

Core A This core was saturated with oil (while water wet) at a pressure drop of 190psi (250psi inlet with 60psi back pressure). Eighteen ml of water was taken up in the core. Then 395 ml of injection water was pumped through at an inlet pressure of 200psi and a back pressure of 60psi. Nine ml of oil was collected before no more oil could be removed. Thus, waterflooding removed 9 of the 18ml of oil in the core. Subsequent flooding with 385 ml of a 500ppm solution of NaAMB, at an injection pressure of 300psi and back pressure of 60psi, removed an additional 2 ml of oil (> 20% recovery of the remaining oil). The flow rate of injection water vs 500ppm of NaAMB in injection water through the core is instructive. The polymer did not slow down the flow through the core appreciably (6.67 ml/min for injection water vs. 5.17 ml/min for injection water plus 500 ppm of NaAMB) is shown in Table IV.

**Table IV: Flow Rates and Pressure Drops over Core A During Injection Water/Water NaAMB/Injection Waterflooding.**

	$\Delta P$	FLOW RATE
Injection Water (start)	140psi	2.54 ml/min
500ppm RH-1 injection water	240psi	5.17 ml/min
Injection Water (after)	40psi	6.67 ml/min

Another core was treated in a similar fashion. Water flooding alone removed 9 ml of oil and polymer flooding (500ppm NaAMB) 1ml more of oil. This core only took up 11 to 12 ml of oil initially. The polymer flow rate was 0.81 ml/min ( $\Delta P=290$ psi) while the injection water flow rate was 1.05 ml/min ( $\Delta P=290$ psi).

**Extensional Viscosity Studies**

Initial studies were performed to determine the extensional viscosities of polymers used for flow control. The calculation of the approximate extension rate,  $\epsilon$ , for a fluid which is being forced through a porous medium (strata or core) is a very important

consideration. When the fluid's extension rate equals the critical extension rate of the polymer coil,  $\epsilon_c$ , the polymer coil will rapidly unfold or unwind and extend in the direction of flow. This event causes energy to be absorbed. Therefore, when the polymer coil rapidly extends, the fluid flow resistance through the porous media will go up sharply. When this occurs flow control will increase. In other words, at the critical extension rate the fluid's effective viscosity goes up thereby helping divert the fluid in another flow direction where the rate of flow is slower.

Since polymer 1285 from Alcoflood was used in previous experiments, its critical extensional velocity was studied along with NaAMB (from R. Hester). The structure of NaAMB has been designed to give a large extension effect. Solutions of these polymers were pumped at various flow rates through well characterized Berea cores (known porosity,  $\Phi$  from the uptake experiments and permeability which was determined according to  $k=QL\mu/S\Delta P$  where  $Q$ =volumetric flow rate through a porous media of length  $L$  and cross sectional area  $S$  of a Newtonian fluid having a shear viscosity of  $\mu$ , where  $\Delta P$  is the pressure drop across length  $L$ ). The intrinsic viscosities in the standard injection solution was determined by dilution viscometry. The polymer solutions of a known concentration were pumped through cores at a series of different pressure drops (*e.g.* a series of flow rates). Plots of the flow rate versus  $\Delta P$  were made. These plots should be linear up to the point the fluid's extension velocity reaches the polymer's critical extension velocity. A change in slope could indicate the point where  $\epsilon = \epsilon_c$ .

The viscosity behavior of polymer RH-1 was studied in the standard injection water. These data are summarized in the Table V below. The purpose of these data are, not only to characterize this polymer but also, to eventually see if the polymer adsorbs to

**Table V: Viscosity Measurements on RH-1 (Mol wt  $1.25 \cdot 10^6$ ) Determined at 30.3°C in Standard Injection Brine Solutions.**

Concentration (g/100cc)	$t_o$ (sec.)	$t_{(soln)}$ (sec.)	$t/t_o$	$n_{sp}^a$	$n_{inh}^a$	$n_r^a$
0.1000	101.6	350.5	3.45	2.45	0.896	2.45
0.0833	101.6	338.4	3.33	2.33	1.016	2.80
0.0714	101.6	295.5	2.91	1.91	0.906	2.67
0.0625	101.6	260.8	2.57	1.57	0.720	2.51
0.0556	101.6	238.8	2.35	1.35	0.541	2.43
0.0500	101.6	227.1	2.24	1.24	0.423	2.47

<sup>a</sup> $n_{sp} = t/t_o - 1$ ;  $n_{inh} = (1/c)\ln(t/t_o)$ ;  $n_r = n_{sp}/conc.$

the core and to determine if shear degradation of RH-1 occurs when it is pumped through Berea cores. Less shear degradation was expected since its molecular weight and coil hydrodynamic volume is much lower than other mobility control polymers studied.

### **Role of Extensional Viscosity in Polymer Flooding for Mobility Control**

Polymer flooding increases water viscosity relative to that of other reservoir fluids, thereby reducing water mobility and lowering the amount of water flooding “fingering” through oil. It also lowers the flow through higher permeability channels. Microbial growth would also redirect more flooding water resulting in improved recovery efficiency. In essence, microbial biomass and exocellular polymers produced by growing microbes would then act like gel-forming polymers by forming blockages which, in turn, force more water through low permeability regions to recover more oil.

Another often neglected point is that viscosity has both shear and extension components. Shear viscosity operates at all shearing rates and a fluid’s shear viscosity may be Newtonian or non-Newtonian. Extensional viscosity is the increase in viscosity which occurs at the critical flow rate at which the randomly coiled polymer chains rapidly extend in the direction of flow. In this process the random coil and its entrained solvent are deformed into an ellipsoid-like volume with the long axis along the flow direction. The critical extension velocity is the flow rate at which this coil distortion takes place. Each polymer has a critical extension rate (velocity) designated as  $\epsilon_c$ . At the critical extension velocity, a sudden increase in resistance to flow will occur because the polymer coils (plus entrained solvent) deform and this causes an absorption of energy. Thus, at the critical extension rate, the flow resistance will increase.

The critical extension rate,  $\epsilon_c$ , for a polymer is given by equation (1) (Durst and Hass,1981):

$$\epsilon_c = \frac{6\pi^2 RT}{25 \bar{M}_w |\eta| \mu} \quad (1)$$

where  $R$  is the gas law constant,  $T$  is absolute temperature,  $|\eta|$  is the intrinsic viscosity of the polymer in the solvent being used and  $\mu$  is the shear viscosity of the solvent (not of the polymer solution).

Any liquid being pumped through a porous medium exhibits what is termed extension rate (velocity). The liquid's extension velocity (*e.g.* extension rate) depends on its volumetric flow rate and characteristics of the porous rock through which it flows. The liquid extension rate,  $\varepsilon_c$ , is defined by equation (2) (Durst and Hass, 1981):

$$\varepsilon = 2^{1/2}(V) / \phi d \quad (2)$$

where  $\phi$  is the rock porosity,  $d$  = the rock's effective particle size diameter and  $V$  is the velocity at which the liquid flows through the porous media (calculated by volume of liquid pumped per unit time divided by the cross sectional area of the porous media).

When the fluid's extension rate becomes equal to the polymer's critical extension rate (*e.g.* when  $\varepsilon = \varepsilon_c$ ), the polymer coils elongate and an increase in flow resistance occurs. This flow resistance can manifest itself over and over if the rock permeability, pore structure, and flow rates are of the correct magnitude. When a steadily advancing front of a water-polymer solution enters a pore (see Figure 35), the flow rate must speed up since the open volume decreases. If the velocity in this pore throat reaches the point where  $\varepsilon = \varepsilon_c$ , a sharp increase in viscosity (resistance to flow) occurs causing the fluid which is directly behind to seek alternate flow channels (*e.g.* be redirected). As the solution emerges from the pore into a more open area, its velocity decreases and the extended polymer now recoils into random coils. Hence, this fluid region can later experience increased flow resistance again if its velocity accelerates upon encountering another pore.

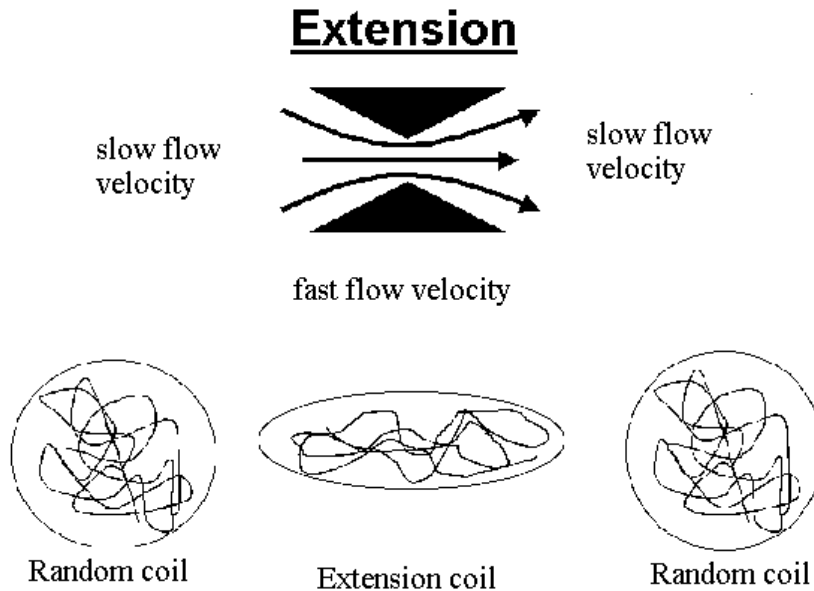


**Figure 35. Onset of extensional viscosity.**

Two polymers are being used for mobility control: Alcoflood 1285, a 30% hydrolyzed polyacrylamide with a molecular weight of about 20,000,000 and NaAMB which is a copolymer with acrylamide (AM) and AMBA (shown below) with a molecular weight of  $12.5 \times 10^6$ . A key goal of this work is to determine the flow rate ranges through reservoir rock and Berea sandstone where the extensional viscosity of these two polymers will become important. This task is exceedingly difficult to achieve because the rock media is fractal in nature. Furthermore, the  $\epsilon_c$  values of these two viscosity enhancing polymers are not known. Professor Roger Hester, a DOE contractor at the University of Southern Mississippi, is investigating this question. We have cooperated with him in taking his basic research a step closer to practical application by investigating the extensional viscosity problems in rock cores.



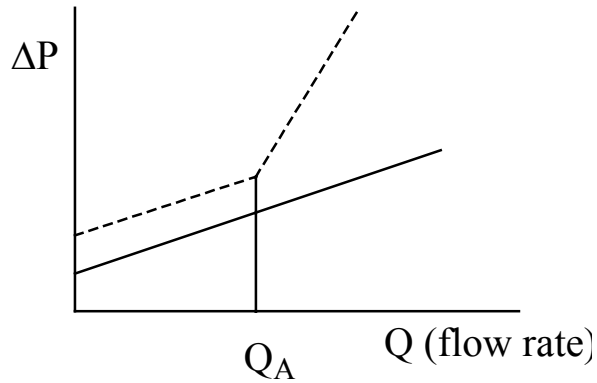


**Figure 36. Determining the flow rate at which the extensional viscosity begins to contribute.**

In our own work, rock media are being used (Berea and North Blowhorn Creek cores). Thus, we don't have a defined geometry media. Therefore, the volumetric fluid flow rate,  $Q$  is related to the pressure drop  $\Delta P$  through equation (3) (Collins, 1976) where the permeability of the medium must be known.

$$Q = \frac{k S \Delta p}{L \mu} \quad (3)$$

$Q$  = volumetric flow rate

$L$  = length

$S$  = cross sectional area

$\mu$  = the shear viscosity of a fluid employed in permeability measurements of that specific rock..

Note, the shear viscosity of our standard brine solution can be obtained from the literature value of  $\mu_w$  for water by multiplying  $\mu_w$  by the measured  $(\eta_{\text{brine}}/\eta_w)$  which is available from simple viscosity measurements.

By measuring  $Q$  vs  $\Delta P$  one gets  $Q_A$ . Then at  $Q_A$  the critical extension velocity  $V_A$  (e.g.  $\epsilon_c$ ) is obtained by knowing the rock porosity. This value of  $V_A$  ( $\epsilon_c$ ) is what is needed for substitution into equation (2) resulting in equation (4) (Durst and Hass, 1981).

$$\varepsilon = \varepsilon_c = 2^{1/2}(V) / \phi d \quad (4)$$

Now all terms are known except  $d$ , so the equation can be solved for  $d$ . The value of  $d$  accounts for all the geometrical parameters which exist within the fractal rock structure. Thus, this approach requires a knowledge of  $\varepsilon_c$  of the polymer, measurements of  $Q$  vs  $\Delta P$  on the core and a determination of  $d$  from a combination of these measurements.

The  $\varepsilon_c$  values for Alcoflood 1285 and NaAMB were not known. Thus, experiments concentrated on obtaining  $Q$  vs  $\Delta P$  measurements when pumping polymer brine solutions through Berea cores and then searching for sharp changes in slope. A major problem exists. The range of flow rates employed in core measurements may be too high (or too low) to be in the  $Q_A$  range where the extensional viscosity effects to kick in (e.g. where the  $\Delta P$  vs  $Q$  slope will change). Equipment limitations did not permit us to accurately measure the low  $\Delta P$  values that would be needed to achieve low values of the volumetric flow rate,  $Q$ , through our cores (those values which correspond to fluid flow through an oil field at a few feet per day or lower). A second consideration is the rock permeability,  $k$ . The lower the permeability becomes, and the greater the  $\Delta P$  must be at any constant flow rate. Thus, if  $k$  is very low, a  $\Delta P$  in an easily measured range can be used and still obtain a low flow rate. If the value  $Q_A$  for a given polymer solution and rock combination is low this is an advantage. However, the Berea cores have porosity,  $\phi$ , values about 0.2 (20%) and the grain sizes in the rock are large enough, so that the Berea sandstone permeability is high. This means that low  $\Delta P$  values will give relatively high  $Q$  values, perhaps higher than the magnitude of  $Q_A$ . If this is true,  $Q$  values versus  $\Delta P$  plots would not be able to locate the point where a change of slope occurs (e.g.  $Q_A$  or from the value  $\varepsilon_c$ ).

One approximation method should be mentioned. If sandstone is considered to be compressed sand grains and spherical shapes are assumed, then the value  $d$  (now the effective diameter of a sand sphere) as obtained from equation (5) (Scheidegger, 1974)

$$d = \frac{1-\phi}{\phi} \left( \frac{180 k}{\phi} \right) \quad (5)$$

where  $k$  is the permeability (measured with the brine solution employed) and  $\phi$  is the porosity. By measuring  $k$  and  $\phi$  for the cores and employing equation (5), an approximation of  $d$  can be obtained. This value of  $d$  could be used in equation (2) to give the fluid extension rate at any velocity (*e.g.* volumetric flow rate).

The standard brine solution used had the following composition.

10.9g  $\text{CaCl}_2$

2.71g  $\text{MgCl}_2$

4.57g  $\text{BaCl}_2$

1.84g  $\text{Na}_2\text{SO}_4$

147.8g  $\text{NaCl}$

All these salts are dissolved in 50 L distilled water.

Viscosity measurements were done in Cannon Ubbelohde dilution viscometers. Using a  $75\mu\text{m}$  capillary diameter the following measurements were obtained on the 1285 and NaAMB polymers (See Figures 37 and 38). Shear effects make accurate measurements of the  $|\eta|$  values impossible in this equipment.

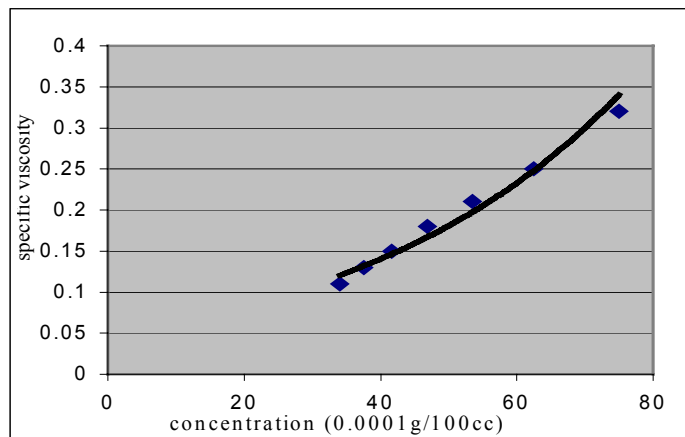


**Figure 37. Specific viscosity vs. concentration for polymer Alcoflood 1285 in standard brine solution.**

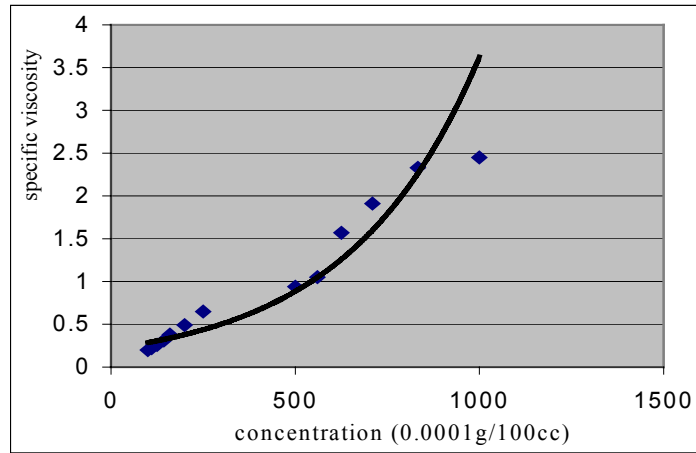


**Figure 38. Specific viscosity vs. concentration of the polymer NaAMB in standard brine solution.**

The cores were subjected to a long term (10 or more core volume equivalents passed through) prepumping period where polymer-brine solutions are passed through the core to allow the adsorption of polymer on the core internal surface to come to equilibrium. Thus, in the  $\Delta P$  versus  $Q$  experiments, no change in polymer concentration within the flood solution can take place as the solution passes through the core. The prepumping treatment was monitored by comparing the starting viscosity of the polymer solution with the viscosity of the effluent polymer solution. A lowering of viscosity occurs due to (a) adsorption on rock surface and (b) shear degradation of the molecular weight. When the viscosity of the effluent becomes constant with time, then no more adsorption is occurring. These data are omitted for brevity.

Core porosities were measured by weighing the dry core ( $w_1$ ) and then putting it under vacuum followed by submerging in the brine solution. The weight ( $w_2$ ) after submersion was obtained and the porosity calculated from the change in weight, the densities of the brine and the overall core volume.

Flow rate versus  $\Delta P$  measurements were performed on cylindrical Berea cores 9.0 cm in length and 3.8 cm in diameter.

### **Experiments on the Polymer NaAMB**

The plots below show experimental values of  $\Delta P$  versus flow rate of NaAMB polymer/brine solutions when pumping through a Berea core with a porosity of 20.72%

(Figures 39-44). This experiment illustrates that the core undergoes internal changes leading to a higher permeability with time. Note the flow rates in Figure 38 are higher than the initial experiments at 5.0ppm, as shown in Figure 39.

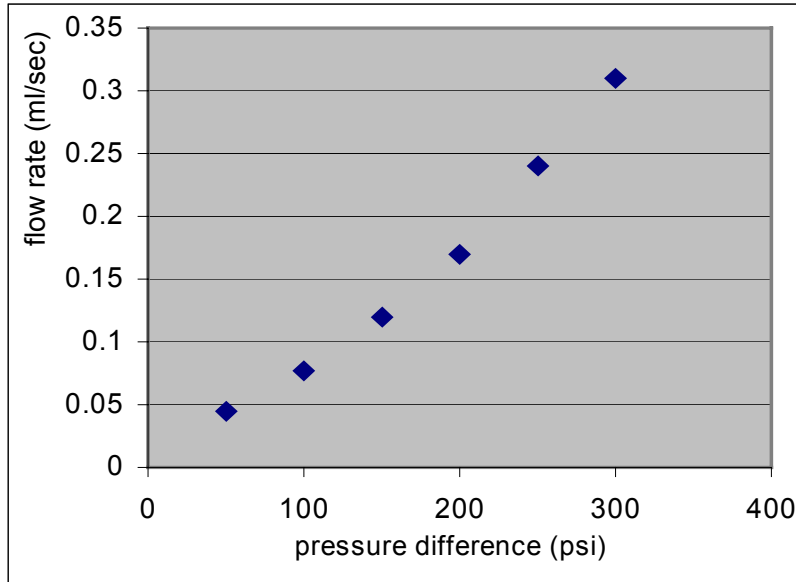


**Figure 39. NaAMB (5 ppm) without prepumping.**

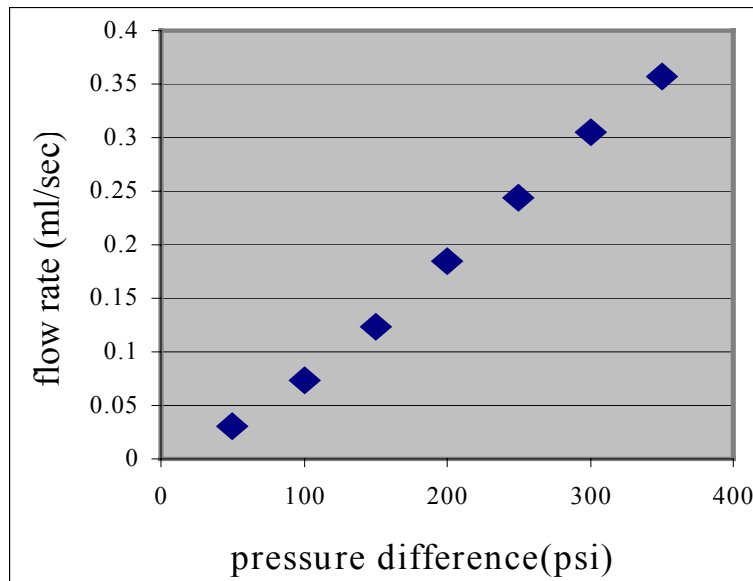


**Figure 40. NaAMB (5 ppm) after prepumping of 10 core volumes of polymer solution through core.**

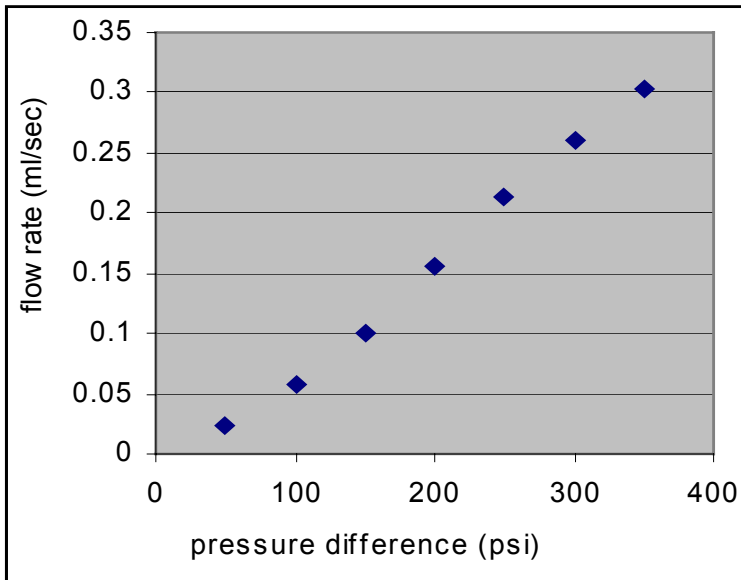


**Figure 41. NaAMB (2.5 ppm) after prepumping.**

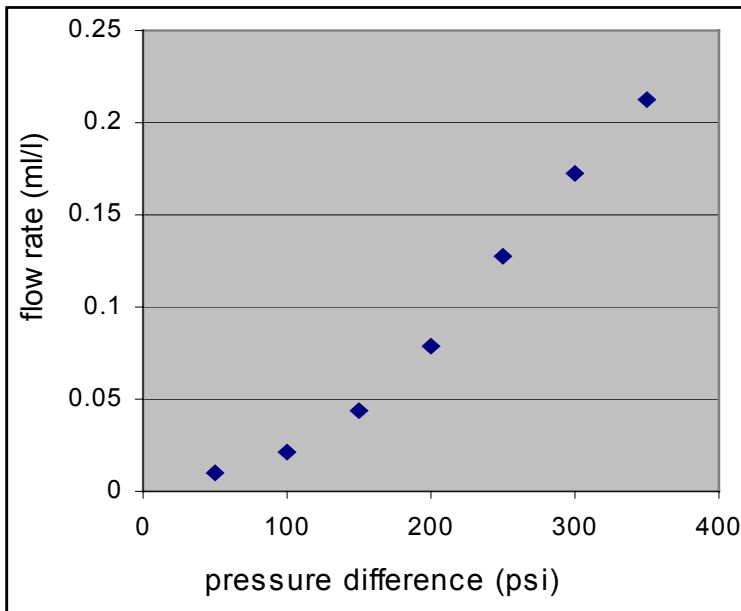


**Figure 42. NaAMB (1.0 ppm) after prepumping.**

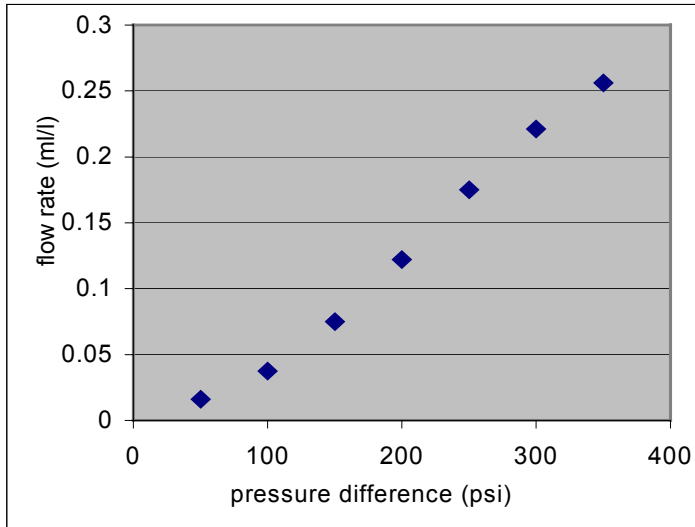


**Figure 43. NaAMB (0.5 ppm) after prepumping.**

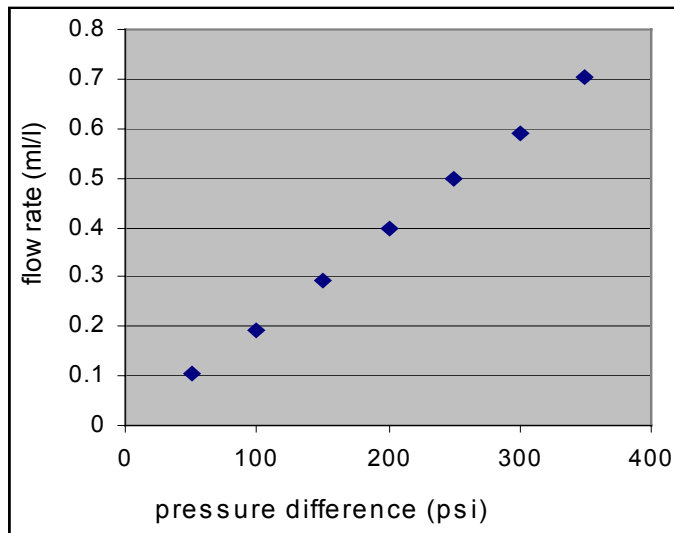


**Figure 44. NaAMB (5 ppm) after prepumping after all the above experiments had been done on the same core.**

A significantly higher concentration of NaAMB was then used. After prepumping 10 core volumes of 50ppm NaAMB solution through the core, the Q vs.  $\Delta P$  plot was obtained. This is shown in Figure 45.

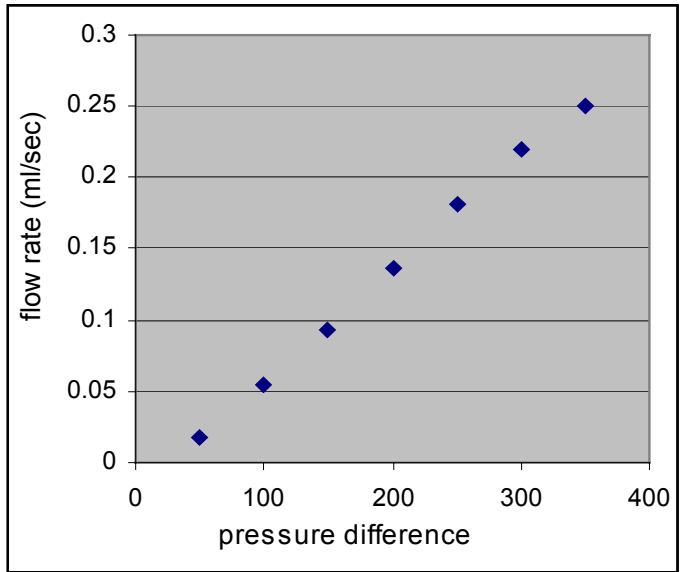


**Figure 45. NaAMB (50 ppm) after prepumping Alcoflood 1285 polymer.**

The plots below show experimental values of  $\Delta P$  versus flow rate for the 1285 polymer/brine solution when pumped through a Berea core with a porosity of 19.41%. Pure brine solution was first used and this was followed by various concentrations of Alcoflood 1285 as shown in Figures 46-48.

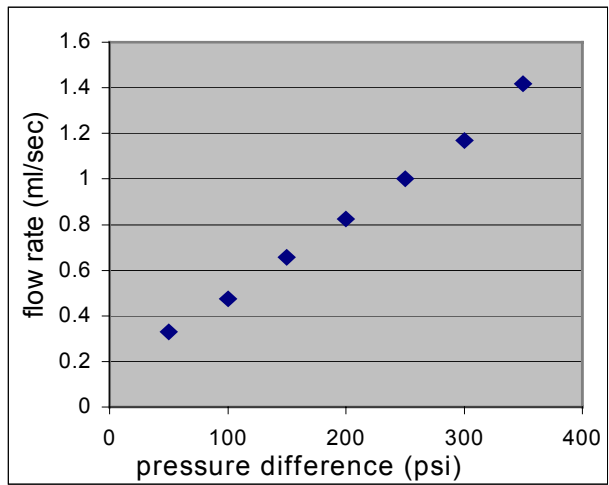


**Figure 46. Pure brine solution after prepumping.**

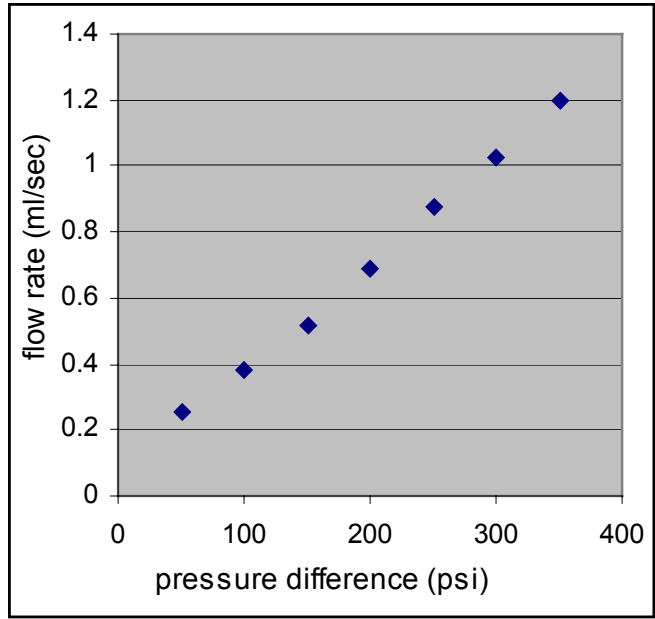


Figure 47. Alcoflood 1285 (15 ppm) after prepumping.

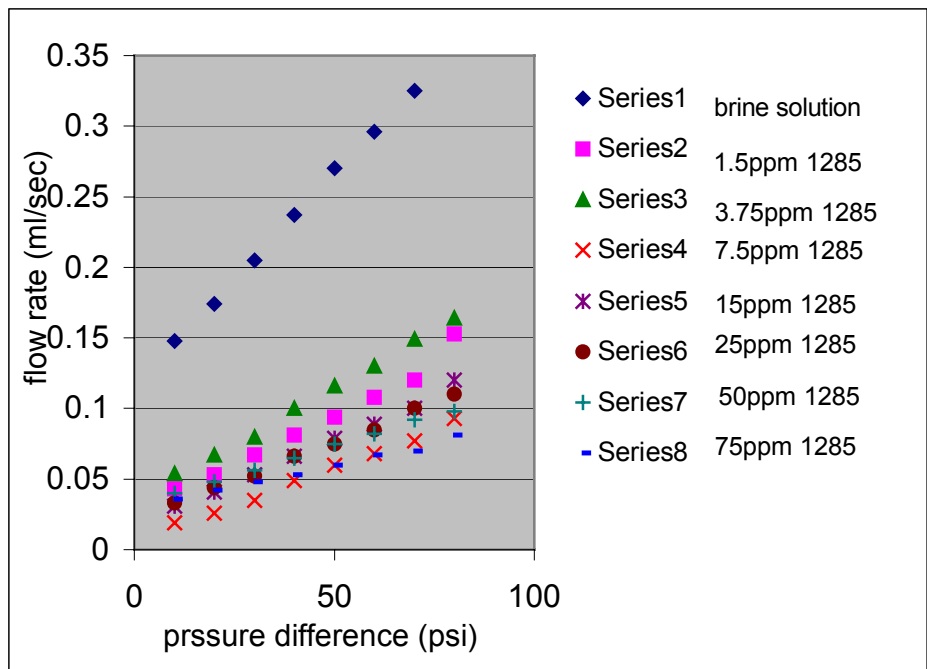


Figure 48. Different concentrations of Alcoflood 1285 polymer solutions.

## **Studies Using the Electron Microscope**

An understanding of the spatial relationships between organic matter (bacteria and biofilm) and the mineral matrix and porosity in a rock is necessary to fully perceive the MEOR process. Five widely used sample preparation and imaging procedures for scanning electron microscope (SEM) study of organic-rich samples were investigated. The purpose of these experiments was to contrast and evaluate these techniques in order to determine which procedure(s) best preserves the *in situ* bacterial and biofilm textures and the relationships between these organic materials and the porosity and rock. The techniques tested were ethanol dehydration with hexamethyldisilazane (HMDS), which is the most commonly applied technique for study of biological samples; ethanol dehydration with critical point drying; ethanol/acetone dehydration with critical point drying, which is a procedure often used in medical research; 10% glutaraldehyde fixation; and simple air drying.

Details of the protocols tested are: A) Glutaraldehyde fixation and ethanol dehydration (Step 1. Fix specimens in 2.5% glutaraldehyde for 2 h; Step 2. Dehydrate in ethanol, 10-15 min per step: 35%, 50%, 70%, and 95% ethanol; Step 3. Continue dehydration: 100% ethanol (4 changes) for one h; Step 4. Change to HMDS (hexamethyldisilazane), 2 changes, 10 min each; Step 5. Air dry sample.); B) Glutaraldehyde fixation, ethanol dehydration, and critical-point drying (Steps 1-3 from A; Step 4. Five CO<sub>2</sub> flushes in critical-point drier); C) Glutaraldehyde fixation, ethanol dehydration, acetone dehydration, and critical-point drying (Steps 1-3 from A; Step 4. Dehydrate in acetone, 10-15 min per step: 35%, 50%, 70%, and 95% acetone; Step 5. Five CO<sub>2</sub> flushes in critical-point drier); D) Glutaraldehyde fixation (Fix sample in 10% glutaraldehyde for 2 h); E) Air-dry. In the first set of experiments sandstone and limestone samples were inoculated with bacteria and fed, and were then prepared for SEM using each of the techniques detailed above.

The results of these experiments showed that no tested protocol correctly maintains the *in situ* textures of both the bacteria and the biofilms. Exopolysaccharide slime (EPS) biofilm occurred as a more or less smooth continuous coating over both rock and bacteria in air-dried or glutaraldehyde fixed samples (Figure 49). Slight to moderate curling of the edges of the biofilm was sometimes observed, especially in air-dried

samples. In these samples, it was uncommon to observe bacteria completely uncovered by EPS biofilm. Individual or colonies of bacteria most commonly occurred as lumps and bumps beneath the slime or as partially emergent bodies. The bacterial bodies themselves were deformed to varying degree in both procedures (Figure 50).

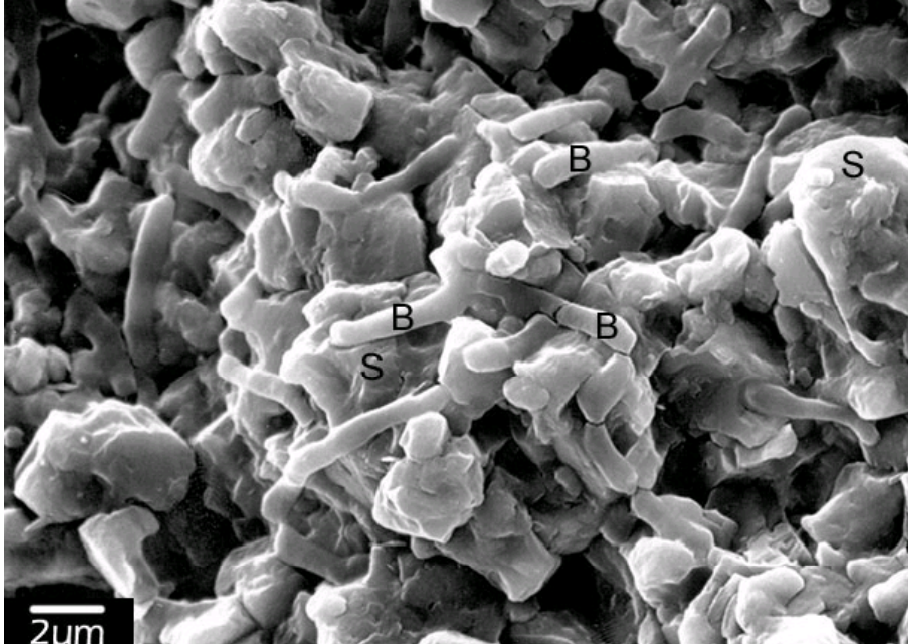


**Figure 49. EPS biofilm slime covers both rock matrix and the deformed cylindrical bacteria in air-dried sample.**

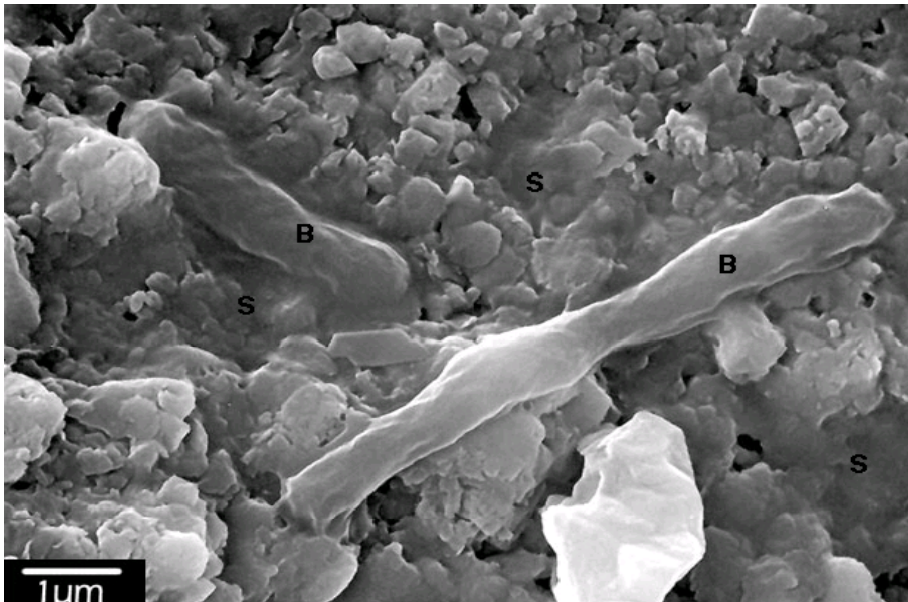


**Figure 50. EPS biofilm slime (S) occurs as a more or less continuous coat over both rock and distorted bacteria (B). Sample fixed in 10% glutaraldehyde.**

Bacterial shape was well preserved in the dehydration and drying procedures, however, these techniques greatly changed the morphology of the EPS biofilm from a continuous coat to curled, desiccated, and tattered remnant sheets and strings. Tangled nests of vermicelli-shaped bacteria were commonly observed and were frequently completely devoid of slime (Figure 51). Biofilm fragments also occurred as small (<100 nm) spheres, ovoids, and beaded chains (Figure 52). It was concluded that an accurate investigation of organic material in rocks requires two samples, one preserved by glutaraldehyde fixation for characterization of the EPS biofilm, and one by ethanol dehydration for examination of the bacterial bodies themselves.

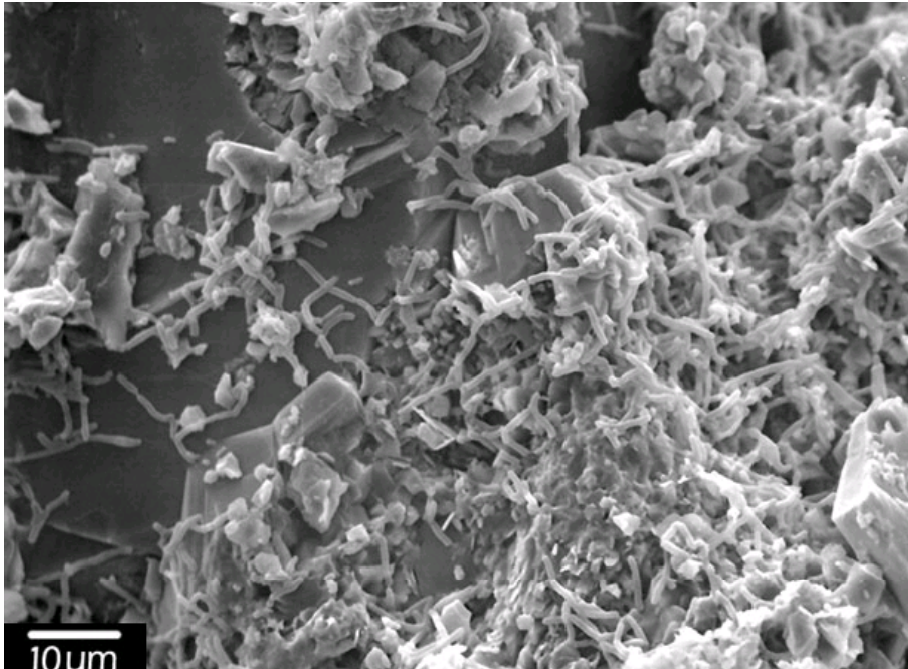


**Figure 51. Abundant undeformed bacteria devoid of EPS slime. Ethanol and HMDS dehydration sample.**

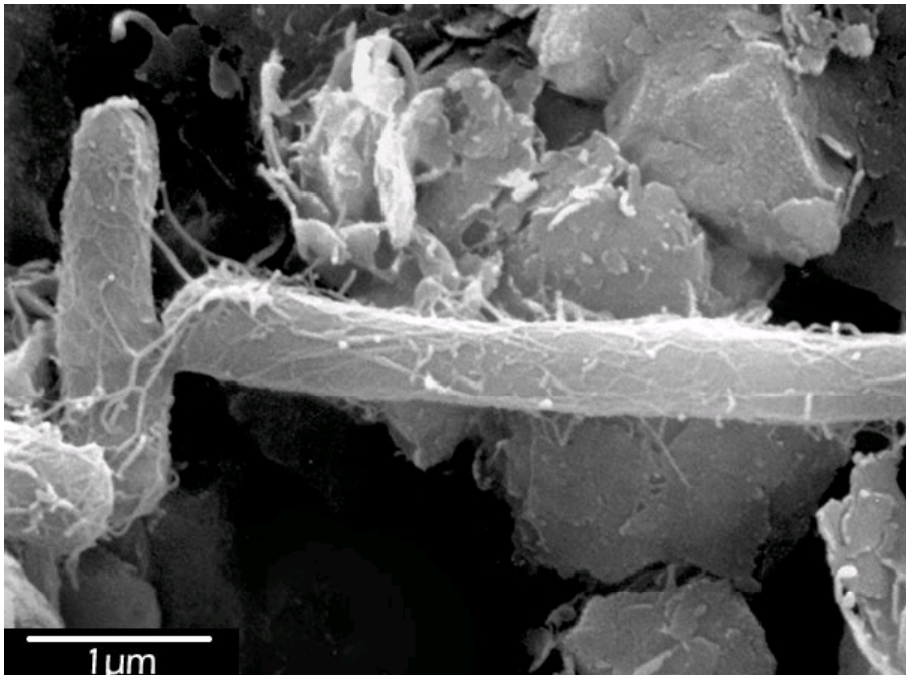


**Figure 52. Well-preserved bacterial body covered with tattered remnant-strings of EPS. Gluteraldehyde fixation, ethanol and acetone dehydration, and critical point dried sample.**

Several experiments were performed on NBCU bacteria and rocks. In the first experiment, sandstone samples were inoculated with indigenous NBCU bacteria from a laboratory culture and incubated for two wks. SEM examination of the samples showed an EPS slime layer forming an irregular but continuous sheet that draped across sand grains and stretched across pore throats and crevices. Bacteria were uncommon and randomly distributed throughout the samples. In places, two different morphologies of EPS biofilm were present: a beaded, globular layer overlain by a smooth, sheetlike layer (Figure 53).

In another experiment small pieces of live NBCU core were fed with nitrogen- and phosphorus-rich nutrients on the same schedule as the NBCU cores that have been flow tested. After two wks, SEM analysis showed that the sandstone core pieces were so completely covered with biofilm that the entire mineral surface was obscured (Figure 54). Fewer bacteria were observed in this experiment than in the experiments using cultured bacteria.

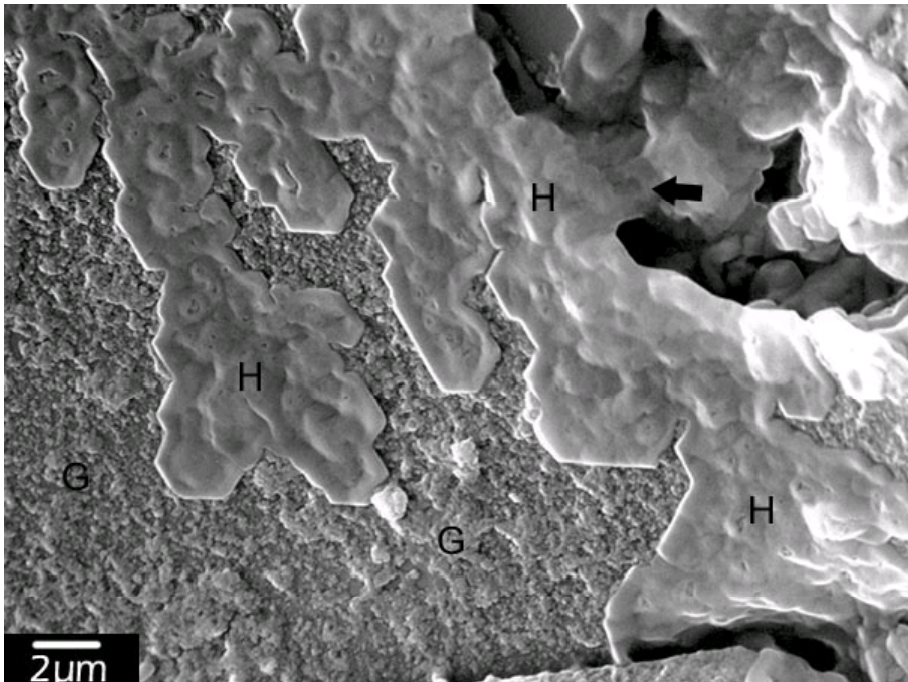


**Figure 53. Grain-coating morphologies of EPS biofilm.**

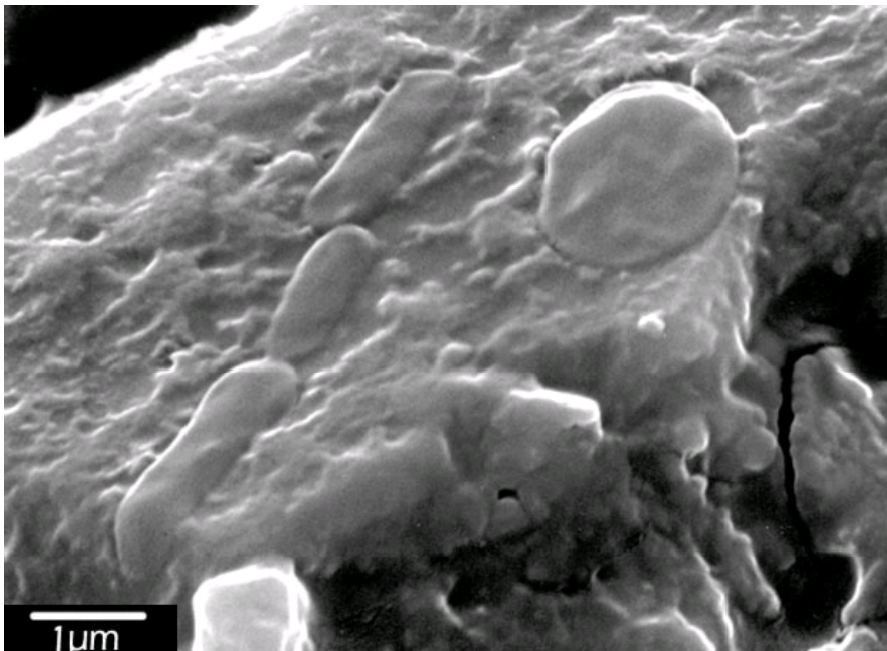


**Figure 54. EPS biofilm completely covering bacterial bodies and mineral grains.**

It has been debated whether the efficacy of MEOR is due to pore blockage by bacterial bodies or by EPS capsule. These experiments suggest that it is the EPS biofilm

that is almost entirely responsible for the plugging of sandstone pores and that this is accomplished (at least at first) not by completely filling the pore spaces but by stretching across pore throats in a meniscus or web-like morphology (Figures 54-56).

The growth of the *in situ* bacteria and the pore-occluding biofilm was studied in a series of timed experiments in which live NBCU core plugs were fed nitrogen- and phosphorus-rich nutrients in the flow test apparatus weekly for four wks. The cores were sampled and imaged on the SEM every three or four d.

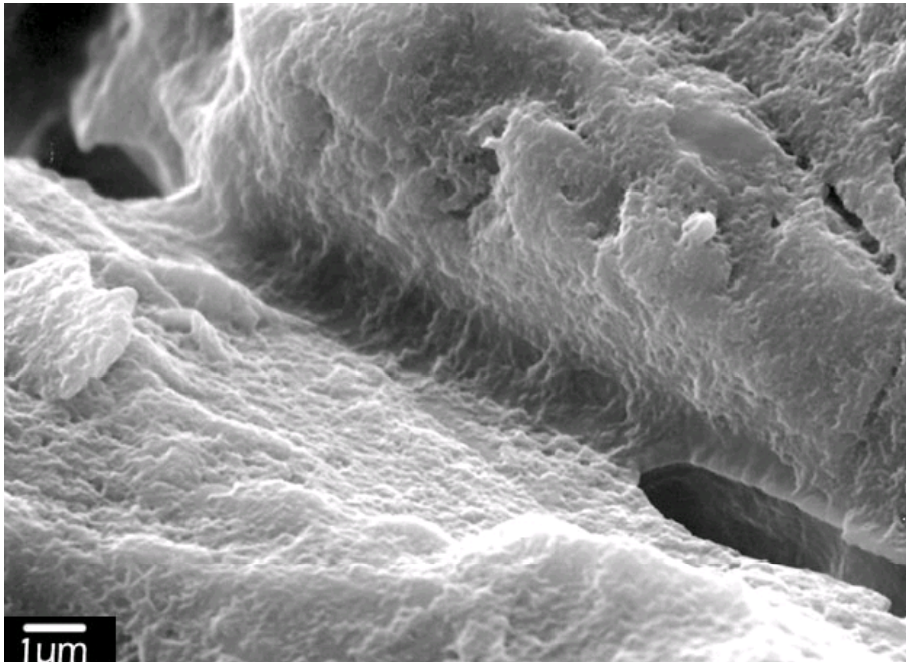


**Figure 55. EPS slime meniscus partially occluding porosity.**

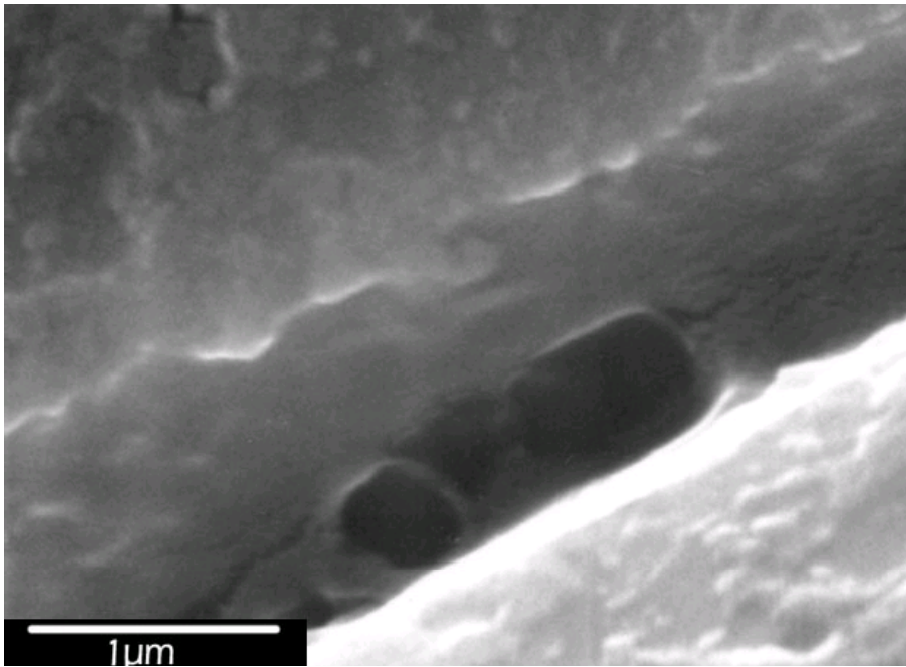


**Figure 56. Sandstone porosity partially filled with EPS biofilm.**

In unfed control samples bacteria were extremely scarce to completely absent and there was no evidence of organic grain-coats or biofilm. After only a few days feeding bacteria ranging in size from  $< 1 \mu\text{m}$  to several  $\mu\text{m}$  in size were obvious in the samples (Figure 57). The bacteria and nearby mineral grains were often covered with an exceedingly thin sheath of EPS (Figure 58). In the following wks this proto-biofilm became thicker and more widespread and often had a clotted or even ropy texture (Figure 59). At the same time full-size bacteria became more abundant and the small  $<1 \mu\text{m}$  varieties became uncommon. After three wks the EPS biofilm covered most mineral surfaces and completely occluded porosity (Figure 60).

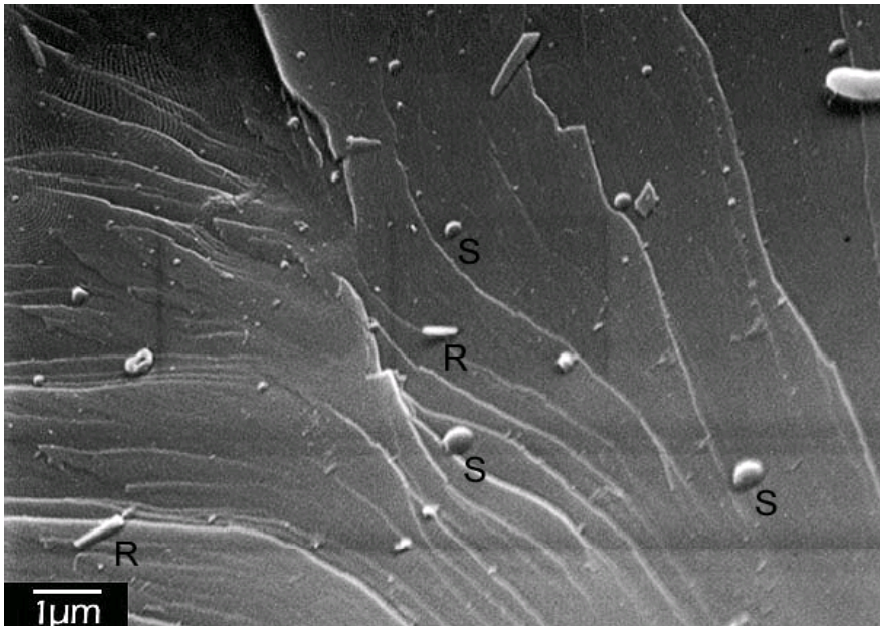


**Figure 57. Large ( $> 1 \mu\text{m}$ ) and small ( $< 1 \mu\text{m}$ ) ovoid and spherical bacteria and bacterial textures grown in less than one wk.**



**Figure 58. Bacterium surrounded by thin “halo” of EPS.**

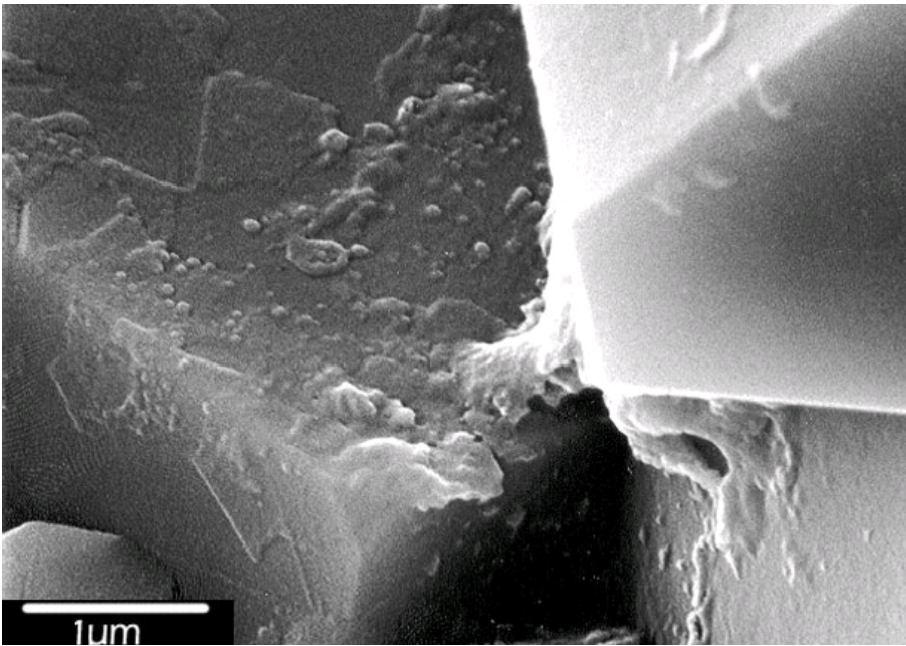


**Figure 59. Thick and clotted EPS biofilm developed in two wk growth.**

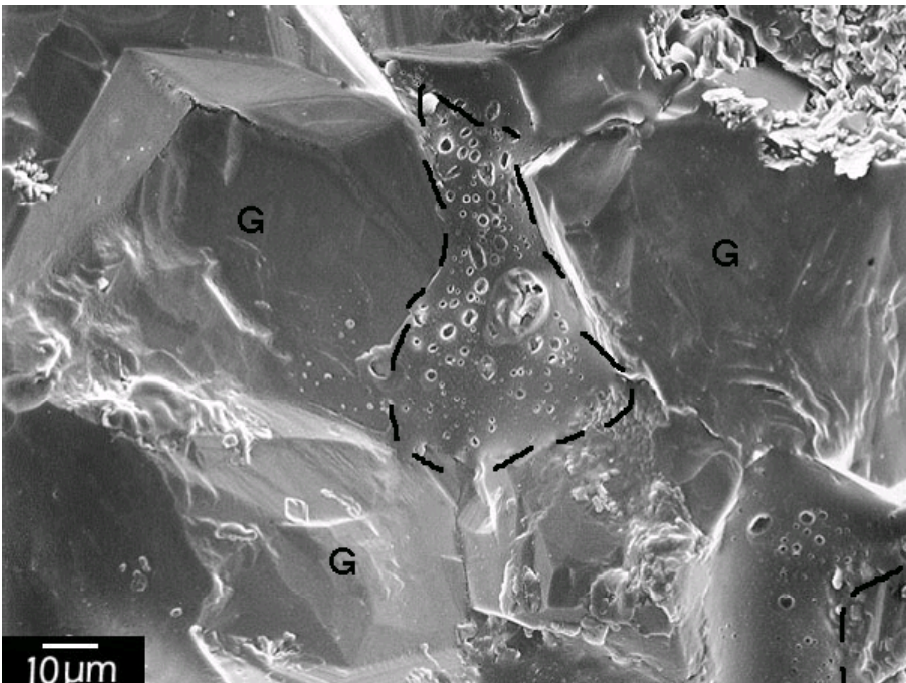


**Figure 60. EPS slime (outlined) completely filling porosity between sandstone grains (G).**

The sub-micron ovoids and spheres observed in the early stages of the timed experiments (Figure 54) are similar in size to dwarf-form bacteria, ultramicrobacteria (UMB), or nanobacteria. “Nannobacteria” are 25-300 nm ovoid shapes that are observed during high-magnification SEM research and may represent a third major species of organic material, along with bacteria and humus (or kerogen), present in soils and rocks. Because of their general resemblance to eubacterial cocci or bacilli, and because of their tendency to occur in chains or clusters, they have been interpreted as extremely small (therefore “nano”) bacteria (Figures 61 and 62). They have been implicated in the formation of mineral deposits in terrestrial and extraterrestrial samples, and in the development of arterial plaque in the human body (Folk, 1993; McKay *et al.*, 1996; Folk and Lynch, 1997, 1998, 2001; Kirkland *et al.*, 1999; Folk *et al.*, 2001).

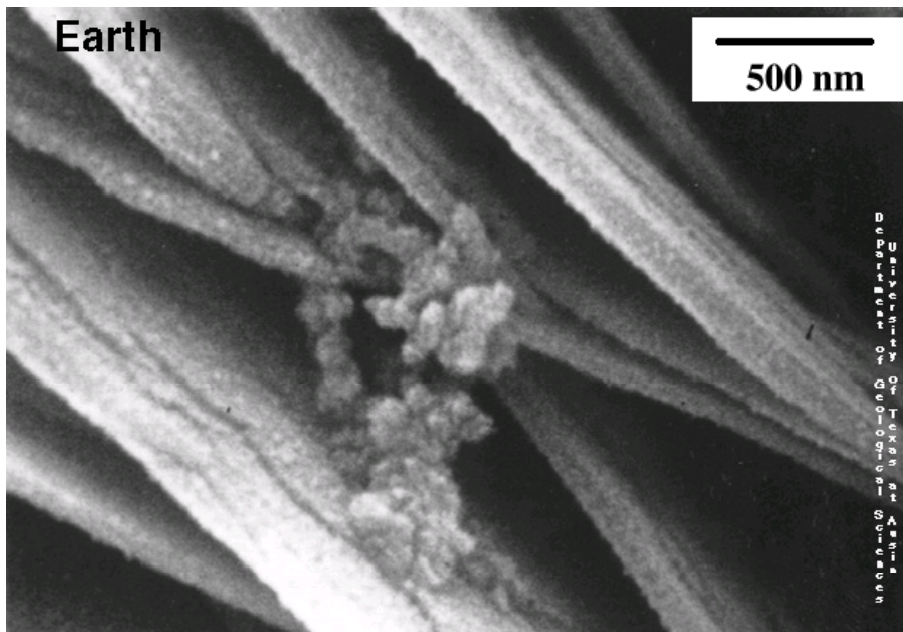


**Figure 61. Purported nanobacteria drape between mineral crystal grains in weathered rock from Italy.**

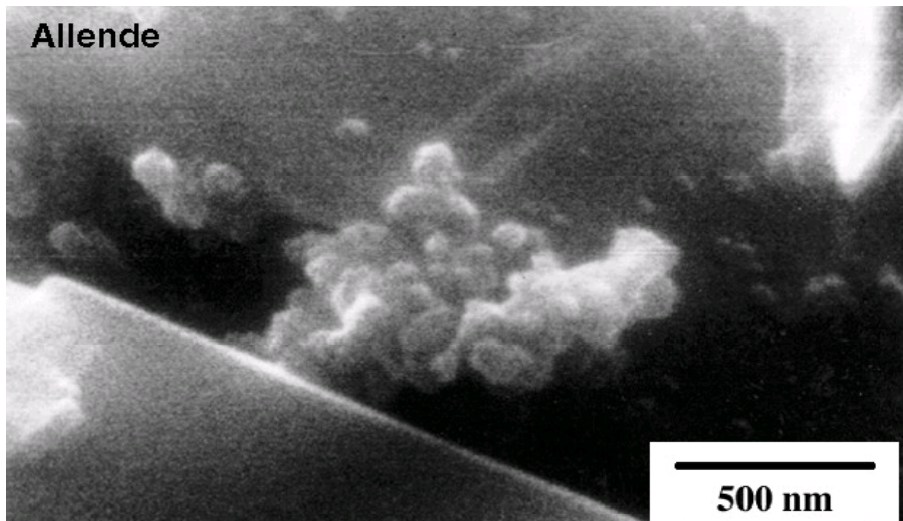


**Figure 62. Nanobacteria on mineral surfaces in the Allende Meteorite, which fell to Earth in 1968. (Photo by Lynch, Department of Geological Sciences, University of Texas at Austin.)**

It would be difficult to find a more contentious geologic or biologic topic than the existence or non-existence of these nanobacteria. Critical attention from the microbiology community has been focused on the small size of the nanobacteria, which are often 1/1000<sup>th</sup> the volume of typical bacteria. Nonetheless, confirmation of the biological affinity of some of these features, especially the larger ones, has been made using molecular biology techniques (Spark *et al.*, 2000). However, laboratory experiments have shown that the suspect textures that can be formed by mineral precipitation in an organic-rich, though abiotic, environment (Kirkland *et al.*, 1999). Current research also shows that textures very similar to the purported nanobacteria can be produced by dehydration of polysaccharide capsule or biofilm (Figures 63 and 64; Fratesi and Lynch, 2001). The relationship between the textures, different minerals, and different organic compounds requires further research.

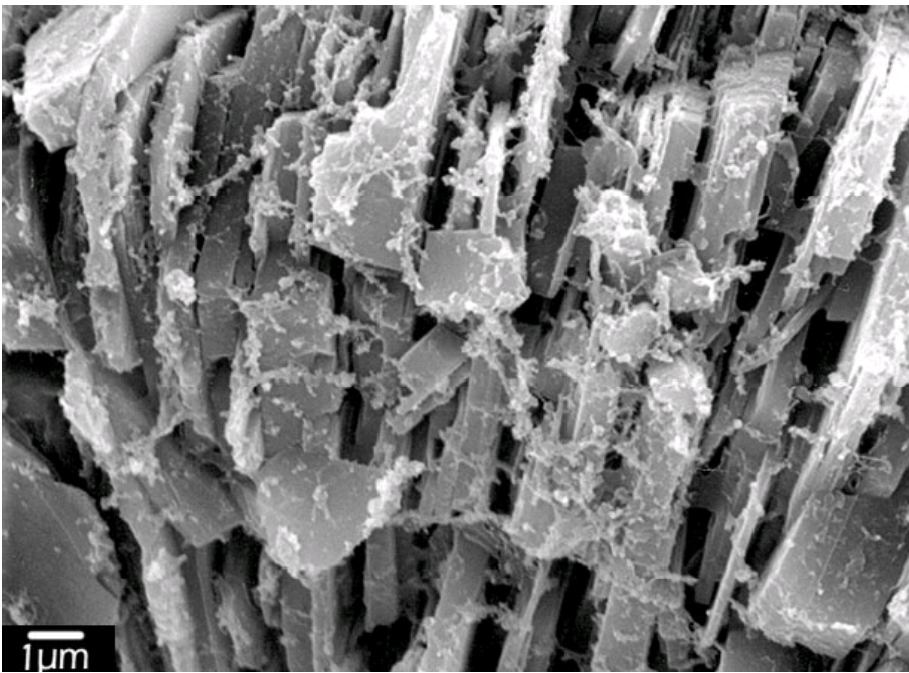


**Figure 63. Chain and filament-like morphology of EPS slime produced by dehydration preservation resembles purported nannobacteria.**

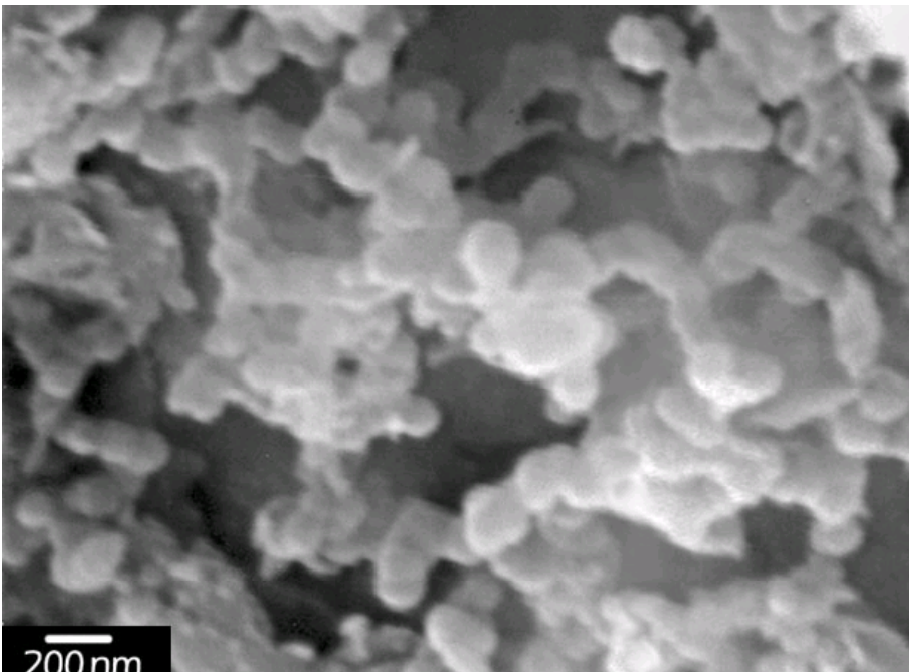


**Figure 64. High-magnification image of “nannobacterial textures” produced by dehydration of EPS biofilm.**

## **Task 5. Prepare a Cost/Benefit Evaluation of Adding a Polymer-Flooding Procedure to a Microbial Enhanced Oil Recovery Process Using a Selective Plugging Technique.**

### **The Economic Aspects of MEOR and Polymer-MEOR**

Oil and natural gas are finite commodities and sooner or later their ever-increasing production (demand) will have to peak. Their discoveries, particularly mammoth and gigantic reservoirs, have already done so. In 1998, 90% of total global energy came from fossil fuel (oil and natural gas). At some point in time, production will peak and new discoveries will decrease. It is believed that the mammoth and gigantic reservoirs have already been discovered and the world's energy needs will have to rely on a greater recovery of known reserves.

The world demand for oil is presently about 22 billion barrels per year and the US presently imports 10,847,000 barrels of crude oil and products daily. This is about 60% of total demand (consumption). The US demand for crude oil is expected to have a moderate growth rate of 2% per year.

The US economy is very sensitive and heavily depended on oil and oil prices. Recent severe fluctuations of gas prices at the pump have clearly shown that cuts in world oil production, even by one million barrels, will adversely effect the US economy.

The Estimated Ultimate Recovery (EUR) for the world oil reserves is estimated to be somewhere between 1,800-2,200 billion barrels. The total proven world oil reserves is about 1,000 billion barrels of which 2/3 of it located in the most unstable and unpredictable part of the world, the Middle East.

It is therefore clear that the US economy is vulnerable to the lack of reliable oil reserves as well as control over the location of much of the world proven oil reserves. Consequently, the only reliable sources of crude oil are the ones within the US territory. A total of 41,000 reservoirs have been discovered in the US and a good majority of them are mature and have passed their primary phase of their production. Many of these reserves are in danger of being abandoned, although 1/2 to 2/3 of Original Oil In Place (OOIP) is left behind. Contrary to the common view, when producing wells in an active oil field are prematurely abandoned it is, practically speaking, almost impossible to bring them back to their previous production level. Some of the major reasons for these natural

phenomena are much higher cost of drilling, problems with lease stipulation, problems with producing facilities including wellbore and wellbore area (skin) in the reservoirs, water and/or gas encroachment in the reservoirs, heavy cost of implementation of new technological tools and equipment, higher cost of labor, and last but not least, consideration of new local, state, and federal laws, particularly environmental laws.

Considering all other options, it seems in-field "RESERVE GROWTH" is the most economically prudent alternative to accessing and securing new resources for the economical recovery of these valuable crude oil reserves.

In field "Reserve Growth" may come from the following sources:

- By-passed oil
- Incompletely drained reservoirs
- Untapped reservoirs compartments
- Deeper pool potentials
- Extension of known pools
- Horizontal drilling
- Development and implementation of more efficient and sophisticated reservoir characterization, simulation, and data handling. And finally the most important one of all,
- EOR, Implementation of the most economically and technically suitable Enhanced Oil Recovery

As stated above, by the time reservoir production is through the primary production phase, (producing under reservoir's own energy), some 1/2 to 2/3 of OOIP is left behind. Waterflooding, as the sole means of secondary oil recovery is presently responsible for over 50 percent of all oil recoveries in world oil fields. Even then, substantial amounts of OOIP will be left behind. Tertiary oil recovery, where feasible, can be implemented to recover some of these vastly untapped oil resources.

Tertiary oil recovery includes:

- Steam injection
- *In-situ* combustion
- Miscible and immiscible gas injection

- Polymer flooding
- Surfactant flooding
- Microbial methods

Tertiary oil recovery, mostly thermal miscible and immiscible gas injection, is responsible for 748,000 barrels of oil daily, which amounts to 12 per cent of total US daily oil production. Unfortunately, tertiary oil recovery in general, and microbial recovery in particular, has not been implemented to its full potential mainly due to economics and lack of documented successes.

The use of microorganisms to enhance oil recovery (MEOR) was proposed some 50 years ago, but unfortunately, to date, field trials for commercial exploitation of this method have been very few. Using microorganisms indigenous to oil reservoirs could aid in oil recovery in a number of ways including, the production of acids, solvents, gases, emulsifiers, and polymers. In particular, using microbially produced polymers and microbial biomass, the more porous channels of reservoir rocks can be selectively plugged, and consequently injection water will be forced to flow into tighter and untapped new channels, thereby increasing the sweep efficiency of waterflooding operation in the entire reservoir and, not just around the injection wells.

Manipulating the *in-situ* microflora to alter the natural permeability setting of the reservoir rock has been termed MPPM (microbial permeability profile modification). Laboratory experiments on live cores, as well as field implementation of MPPM, have shown the economic viability and technical superiority of this MPPM method over all other EOR methods, as a tertiary method in enhancing oil recovery (Table VI).

Implementation of any of the methods shown in Table VI, except MPPM, require substantial initial capital, costly maintenance and will interfere with the normal day-to-day production operation, which significantly reduces profit. On the other hand, MPPM requires minimal initial capital outlay, minimal operation maintenance, and will not interfere with day-to-day normal field operation and its related income.

**Table VI: Comparison of MEOR Methods.**

<b>Methods</b>	<b>Additional Expenses Per Produced Barrel of Oil, in \$</b>	<b>Major Problems</b>	<b>Environmental Concern</b>
Steam Injection	3-5	High cost of operation	Not friendly
In-situ Combustion	5-10	Lack of control	Possible
Miscible/Immiscible gas Injection	2-8	Limited resources, not feasible everywhere	No major problem reported
Polymer Flooding	5-10	Expensive, short life	Possible
Surfactant Injection	8-12	Expensive, inefficient	Not friendly
MPPM (MEOR)	1-2	None	Friendly

Because of the similarities in the mode of operation of MPPM and polymer flooding for the purpose of enhancing oil recovery, it was reasoned that coupling these two technologies might result in a synergy that is not only cost effective, but also more efficient in oil recovery. Keep in mind that polymer flooding is expensive and has a short-term effectiveness in the complex reservoir environment. On the other hand, manipulating the indigenous microflora takes a longer period of time but lasts for a prolonged period of time. Introduction of polymers along with nitrate and phosphate into the reservoir could bring about a unique solution to problems encountered with polymer flooding and microbial selective plugging by providing fast and long lasting permeability profile modification.

Amongst scores of polymers, a few with superior potential for polymer flooding were chosen and run in Berea sandpacks followed by experiments using live cores in the following experimental designs:

- Microbial nutrient flooding alone
- Selected polymer flooding alone
- Microbial nutrient flooding in advance of polymer flooding, and
- Polymer flooding in advance of microbial nutrient flooding

The results of these experiments showed that while polymers may increase the plugging of the reservoir pore channels initially, the short lifespan of their effectiveness

in the complex reservoir environment was not followed rapidly enough by microbial growth and accompanying biopolymer production to achieve the synergy desired.

Treatment with polymers in advance of microbial treatment did not help to increase the effectiveness of microbial plugging. Keep in mind that polymer flooding will increase the cost of the MEOR-Polymer process by orders of magnitude, while increasing polymer production by the microflora can be achieved with only a minimal increase in MEOR cost.

This research project did demonstrate that the indigenous microflora produce copious quantities of polymers when fed with proper nutrients. This important finding led to the conclusion that the production of polymer by the indigenous microflora will result in sufficient plugging and additional plugging by the way of polymer flooding would not be cost effective. So far as the nature of reservoir microflora is known, a suitable feed and feeding regime will bring about *in-situ* production of copious amount of polymers to plug the wider channels and direct the water flow into untapped channels. Furthermore, this process unlike polymer flooding, will not be restricted to the wellbore area, but will take place throughout the reservoir in areas where the injection water carrying the microbial nutrient reaches.

In short, the United States economy is highly dependent on crude oil resources at a reasonable price. As the exploration and production of crude oil approaches its inevitable peak, the US has no other choice but to look for secure and reliable new crude oil resources. The best source of securing the required oil resources are the billions of barrels of oil left behind in the U.S. waiting for a cost effective technology to bring them up. As a vital means of tertiary oil recovery, microbial permeability profile modification by the *in-situ* microbial population is indeed superior to all other known methods of enhancing oil recovery today. It is the cheapest, it is efficient, practically speaking it will work in every types of reservoir rock and structure, it requires minimal initial capital for operation and maintenance, it will not interfere with day to day normal field production operation, it will receive the highest tax credit, and finally it is environmentally friendly. Substantiated and extensive laboratory works along with active field application attest to this claim.

## CONCLUSIONS

Nine polymers (two  $\text{Cr}^{3+}$  gelling partially hydrolyzed poly(acrylamides), five viscosity enhancing 25% hydrolyzed poly(acrylamides) of high molecular weight, one xanthan polymer and a special polymer of moderate molecular weight designed to have a high critical extension viscosity) were characterized (molecular weight, viscosities in water and brine solutions, intrinsic viscosities). None of these polymers inhibited the growth of five different oil-degrading cultures obtained from petroleum reservoirs. Further, they were not able to serve as a carbon and energy source for these cultures.

Experiments were conducted in sandpacks to determine if polymers and/or microbes would alter the pathway of water flowing through the pack. Originally,  $^{36}\text{Cl}$  was to be employed in tracking the water path through the sandpack but it was decided that since  $^{56}\text{Mn}$  could be produced in our laboratory there would be no need to purchase the  $^{36}\text{Cl}$ . Also, since the half-life of  $^{56}\text{Mn}$  is only 2.58 hrs vs 301,000 yrs for  $^{36}\text{Cl}$ , disposal of the radioactive waste did not pose a problem. Polymer flooding was shown to increase aerial sweep efficiency in crushed Berea sandstone/clay/oil sandpacks using simulated injection water containing  $^{56}\text{Mn}$  as the radioactive tracer. Phosphate and nitrate additions also altered sweep pathways by stimulating microbial growth, which facilitated local plugging.

In studies using Berea sandstone cores, high molecular weight 25% hydrolyzed poly(acrylamides) adsorbed on the internal surfaces of Berea cores until an equilibrium layer had formed and further polymer traversed the cores without further adsorption. Shear degradation of these polymers occurred during flow through the cores according to viscosity studies. Both polymer flooding and treatment with microbial nutrients caused changes in the flow of injection water through the cores. No synergy between polymer flooding and MEOR was observed.

Other studies were conducted using live cores obtained from the North Blowhorn Creek Oil Field. Neither polymer flooding nor treatment of the cores with microbial nutrients produced evidence of a polymer flooding/MEOR synergy to produce more oil recovery from cores. While polymer flooding slows the flow rate through cores and redistributes water flow in cores, its effect is short lived. As soon as the polymer pulse

passes through the core, the flow rate again increases. The period required for effective MEOR is much longer. Thus, microbial growth and its modification of sweep efficiency requires a long timeframe and this does not match that of polymer flood pulses. Only continuous polymer flooding or a very long (hence expensive) polymer pulse could match up these timeframes, but this would require greater polymer consumption. Furthermore, evidence of polymer adsorption within cores suggests that adsorption will seriously deplete the polymer's solution concentration as the distance from the wellbore increases.

Magnetic resonance imaging of cores was used successfully to determine the oil saturation level in cores and the special distribution of oil and water inside the cores using a combination of inversion recovery ( $T_1$ ), relaxation time distribution experiments, and  $T_2$  profiles. Experiments were conducted at pixel resolution sizes of  $0.47 \text{ mm}^2$ . Difficulties included broad line widths and substantial variations in proton relaxation times which were dependent on the core's rock type and the fact that both water and oil give  $^1\text{H}$  adsorption.  $\text{D}_2\text{O}$  experiments were employed to see oil in the presence of  $\text{H}_2\text{O}$ .

Investigations using electron microscopy revealed that the indigenous microflora produce considerable quantities of polymer when supplied with nitrate and phosphate. One might conclude that this biopolymer is the major physical contribution to the redistribution of water flow. Further, it was found that the treatment of samples for electron microscopic examinations significantly influenced the images obtained. In some cases the treatment resulted in images of polymer appearing as nannobacteria. The results demonstrated the need to prepare specimens in at least two different ways in order to obtain an accurate assessment of the microbial role in MEOR.

After the successful demonstration of microbial permeability profile modification (MPPM) in the North Blowhorn Creek Oil Field, the question arose as to how much of the alterations of the flow path of injection water was caused by the microbial cells *per se* as contrasted to that caused by polymer produced by the indigenous microflora. While there was no answer to the question at the time, results from this project suggest that much of the diversion of water flow from the high permeability zones to lower permeability zones was caused by polymer produced by the microflora. This finding suggests that increasing the microbial nutrient levels in the injection water will enhance the impact of MPPM by increasing the microbial polymer production.

## REFERENCES

- Brown, L.R., A.A. Vadie, and J.O. Stephens, 2002, Slowing Production Decline and Extending the Economic Life of an Oil Field. *New MEOR Technology: SPE Reservoir Evaluation and Engineering*; Feb. 2002, 33-41.
- Collins, R.E., 1976, *Flow of Fluids Through Porous Media*, Petroleum Pub. Co., Tulsa, OK.
- Durst, F. and R. Hass, 1981, Dehnströmungen mit verdünnten Polymer lösungen: Ein theoretisches Modell und seine experimentelle Verifikation, *Rheol. Acta*, 20,179-92.
- Folk, R. L., 1993, SEM Imaging of bacteria and nannobacteria in carbonate sediments and rocks: *Journal of Sedimentary Petrology*, 63, 990-999.
- Folk, R. L., and Lynch, F. L., 1997, Nannobacteria are alive on Earth as well as Mars: *Proceedings of the International Symposium on Optical Science, Engineering, and Instrumentation (SPIE)*, 3111, 406-419.
- Folk, R. L., and Lynch, F. L., 1998, Morphology of nannobacterial cells in the Allende carbonaceous chondrite, in Hoover, R. B., ed., *Instruments, methods, and missions for astrobiology: Proceedings of the Society of Photo-optical Instrumentation Engineers*, 3441, 112-122.
- Folk, R. L., and Lynch, F. L., 2001, Organic matter, putative nannobacteria, and the formation of ooids and hardgrounds: *Sedimentology*, 48, 215-229.
- Folk, R. L., Kirkland, B. L., Rodgers, J. C., Rodgers, G. P., Rasmussen, T. E., Lieske, C., Charlesworth, J. E., Severson, S. R., and Miller, V. M., 2001, Precipitation of minerals in human arterial plaque: the potential role of nannobacteria: *Geological Society of America annual meeting, abstracts with programs*, A-189.
- Fratesi, S. E., and Lynch, F. L., 2001, Comparison of organic matter preservation techniques for SEM study of geologic samples: *Geological Society of America annual meeting, abstracts with programs*, A-296.
- Kirkland, B. L., Lynch, F. L., Rahnis, M. A., Folk, R. L., Molineux, I. J., and McLean, R. J. C., 1999, Alternative origins for nannobacteria-like objects in calcite: *Geology*, 27, 347-350.

- McKay, D. S., Gibson, E. K., Thomas-Keprta, K. L., Vali, L. H., Romanek, C. S., Clemett, S. J., Chilliier, Z. D. F., Maechling, C. R., and Zare, R. N., 1996, Search for past life on Mars: Possible relic biogenic activity in Martian meteorite ALH84001: *Science*, 273, 924.
- Scheidegger, A.E., 1974, *The Physics of Flow Through Porous Media*, 3<sup>rd</sup> Ed., University of Toronto Press, Toronto, Canada.
- Spark, I., Patey, I., Duncan, B., Hamilton, A, Devine, C, and McGovern-Traa, C. 2000. The effects of indigenous and introduced microbes on deeply buried hydrocarbon reservoirs, North Sea: *Clay Minerals*, 35, 5-12.

## **ACKNOWLEDGEMENTS**

The authors wish to express their sincere appreciation to John E. Parker for his efforts in the coreflood studies and to Dr. Charles A. Sparrow for his assistance in the experiments involving radioisotopes.

The SEM analyses were facilitated and assisted by Richard Kuklinski, Kay Nevels Milam, and Bill Monroe, of the Electron Microscope Center at MSU.

Dr. Shahpoor Vosooghi in the Chemical Engineering Department of Kansas State University provided the KUSP1 polymer.

The contributions of the following students is acknowledged with thanks Magan Green and Karen Thompson in Biological Sciences, Zhuguang (Judy) Liu in Chemistry, Beth Fratesi in Geosciences, and Ali Hemmatabadi in Management and Information Systems.